UNDERSTANDING THE SOLUTION-PHASE BIOPHYSICS AND CONFORMATIONAL DYNAMICS OF VIRUS CAPSIDS

by

Vamseedhar Rayaprolu

A dissertation submitted in partial fulfillment
of the requirements for the degree

of

Doctor of Philosophy

in

Biochemistry

MONTANA STATE UNIVERSITY
Bozeman, Montana

May, 2013

©COPYRIGHT

by

Vamseedhar Rayaprolu

2013

All Rights Reserved

APPROVAL

of a dissertation submitted by

Vamseedhar Rayaprolu

This dissertation has been read by each member of the dissertation committee and has been found to be satisfactory regarding content, English usage, format, citation, bibliographic style, and consistency and is ready for submission to The Graduate School.

Dr. Brian Bothner

Approved for the Department of Chemistry and Biochemistry

Dr. Mary Cloninger

Approved for The Graduate School

Dr. Ronald W. Larsen

STATEMENT OF PERMISSION TO USE

In presenting this dissertation in partial fulfillment of the requirements for a doctoral degree at Montana State University, I agree that the Library shall make it available to borrowers under rules of the Library. I further agree that copying of this dissertation is allowable only for scholarly purposes, consistent with "fair use" as prescribed in the U.S. Copyright Law. Requests for extensive copying or reproduction of this dissertation should be referred to ProQuest Information and Learning, 300 North Zeeb Road, Ann Arbor, Michigan 48106, to whom I have granted "the exclusive right to reproduce and distribute my dissertation in and from microform along with the non-exclusive right to reproduce and distribute my abstract in any format in whole or in part."

Vamseedhar Rayaprolu

May, 2013

DEDICATION

I dedicate this dissertation to my parents for their infinite patience and support.

ACKNOWLEDGEMENTS

I would like to thank Dr. Brian Bothner, for showing me new avenues in viral dynamics and biophysics. I am blessed to have him as my mentor. He has been instrumental in teaching me the intricate details of not just science but life in general. I would also like to thank all the faculty, staff, and students of Montana State University with whom I have worked during my time here. I have learned a lot from all of them and am very grateful to them for furthering my scientific and worldly knowledge.

TABLE OF CONTENTS

1. INTRODUCTION 1

Key Themes in Protein Dynamics 2
Flexibility 3
Stability 5
Virus Capsids are Active Nucleo-Protein Complexes 9
Large-Scale Quaternary Transitions in a T7 Icosahedral Virus Maturation 11
Tetravirus Maturation Involves a Cleavage Event 13
Dynamic Breathing Motion of the Human Rhinovirus (HRV14) 14
Local Rigid Body Movements Govern Capsid Conformational Changes of a Plant Virus 15
Solution Based Approaches to Studying Virus Capsid Dynamics 16
Summary 18
Literature Cited 19

2. VIRUS PARTICLES AS ACTIVE NANOMATERIALS THAT CAN RAPIDLY CHANGE THEIR VISCOELASTIC PROPERTIES IN RESPONSE TO DILUTE SOLUTIONS 24
Contribution of Authors and Co-Authors 24
Manuscript Information Page 25
Abstract 26
Introduction 26
Results and Discussion 28
Conclusions 34
Literature Cited 35

3. COMPARATIVE ANALYSIS OF ADENO ASSOCIATED VIRUS CAPSID STABILITY AND DYNAMICS 37

Contribution of Authors and Co-Authors 37
Manuscript Information Page 39
Abstract 40
Introduction 41
Materials and Methods 46
Virus-like Particle Production and Purification 46
Differential Scanning Fluorescence (DSF) Stability Assay 47
Differential Scanning Calorimetry (DSC) 48
Electron Microscopy 48
Proteolysis and Peptide Mapping 49
Results 49

TABLE OF CONTENTS - CONTINUED

Stability of AAV Capsids....49
Capsid Protein Dynamics....54
Discussion....59
Acknowledgements....65
Literature Cited....66

4. LEARNING NEW TRICKS FROM AN OLD DOG; STUDIES OF CCMV CAPSID SWELLING....75

Contribution of Authors and Co-Authors....75
Manuscript Information Page....77
Abstract....78
Introduction....79
Materials and Methods....83
Virus Purification....83
Differential Scanning Fluorescence (DSF) Stability Assay....84
Size-exclusion Chromatography....84
Hydrogen-Deuterium Exchange Mass Spectrometry....85
Limited Proteolysis....85
Results....86
Thermal Stability Measurements Show Distinct Differences....86
High Resolution Analysis of Capsid Hydrodynamic Radii....88
Intact Protein HDX-MS Differentiates Between Swollen and Pseudo-Closed forms....89
Deterministic Trends Seen in Proteolytic Profiles of SS-CCMV....90
Discussion....92
Abbreviations Used....99
Literature Cited....100

5. CONCLUDING REMARKS....102

LITERATURE CITED....103

APPENDICES....120

APPENDIX A: Supporting Information for Chapter 2....121
APPENDIX B: Supporting Information for Chapter 3....128

LIST OF TABLES

Table Page

1. Timescales and Range of Internal Motion in Proteins that Describe Flexibility 4

2. Frequencies and Dissipations of CCMV....31

2. Subunit Contact Energies of AAV as Calculated by VIPER....53

3. Cleaved Residues in AAV Capsids....57

4. Subunit Contact Energies of CCMV as Calculated by VIPER....95

LIST OF FIGURES

Figure Page

1. Schematic Illustration of Dynamics in Proteins....9

2. Global and Local Quaternary Conformational and Structural Transitions Seen in Four Icosahedral Viruses....12

2. Closed and Swollen Forms of CCMV....29

3. QCM-D Analysis of CCMV....32

4. Structure and Conservation of Adeno-Associated Viruses....45

5. Temperature Dependence of Fluorescent Dye Binding....50

6. Thermal Stability of AAV Particles after Heating....52

7. Proteolysis of AAV Serotypes Monitored Using SDS-PAGE....55

8. The Top and Side Views of 3 Subunits of AAV2 VP3 with Proteolytic Residues of Each Subunit Marked with a Different Color....58

9. Closed Form of the CCMV Capsid....81

10. DSF Profiles of WT and SS Conformations....87

11. Size-Exclusion Profiles of the Conformations of the WT and SS Capsids....88

12. HDX-MS Profile of the WT and SS Pseudo-Closed and Swollen Forms....90

13. Proteolysis Profile of WTPC, SSPC, WTS, SSS....92

ABSTRACT

Viruses are the most abundant form of life on the planet. Many forms are pathogenic and represent a major threat to human health, but viruses recently have been used as nanoscale tools for gene therapy, drug delivery and enzyme nanoreactors. Viruses have historically been viewed as static and rigid delivery vehicles, but over the last few decades they have been recognized as flexible structures. Their structural dynamics are a crucial element of their functionality. Characterizing the biophysical properties of these viruses is both challenging and exciting. We have developed and used a multidimensional approach to tackle this task. Our techniques include Differential Scanning Fluorimetry, which probes the melting temperatures of virus capsids by the use of a fluorescent dye and Hydrogen-Deuterium Mass Spectrometry, which investigates the flexibility of the virus capsid protein by following the change in mass when Hydrogen is exchanged with Deuterium. Flexible regions exchange more. The above techniques are well complemented by the use of size-exclusion chromatography, which differentiates virus capsids based on their hydrodynamic radius and Limited proteolysis which again probes dynamic regions of the capsids up to the amino acid level. We have studied two different systems, Cowpea chlorotic mottle virus (CCMV) and Adeno-associated virus (AAV) using these methodologies. The sum result of these assays indicate that, in case of CCMV, capsids can undergo structural transitions due to very subtle pH and cation concentrations and the capsid protein is capable of rigid body transitions which affect the stability, while maintaining most of the secondary structure. In the case of AAV, the inherent sequence differences explains only partially the differences in stability and proteolytic susceptibility.

CHAPTER 1

INTRODUCTION - UNDERSTANDING THE SOLUTION-PHASE BIOPHYSICS AND CONFORMATIONAL DYNAMICS OF VIRUS CAPSIDS

Introduction

Viruses are the most abundant biological entities on earth and infect practically all organisms. There are an estimated 10^{32} virus particles, comprising 94% of the nucleic-acid containing entities in the oceans (1). Reproduction and proliferation of viruses relies entirely on their ability to hijack the cellular machinery of the host. Viral fitness and adaptability is greatly enhanced by their ability to incorporate precise genetic elements into their genomes and has been a key to their evolutionary success. Most viral genomes are severely limited in the amount of genetic material that is encoded. This is due largely to size limits based on the dimensions of the particle. Nowhere is the size limitation more severe than in the small nonenveloped, icosahedral viruses. These virions are nothing more than a noncovalent association of protein subunits assembled to form a capsid that surrounds and protects the genetic material which may be DNA or RNA.

The first virus structure ever to be determined was that of Tomato Bushy Stunt Virus by Stephen Harrison in 1978 at a 16Å resolution. This was accomplished using X-ray crystallography and scattering experiments (2). Shortly thereafter, the structure of human rhino virus 14 was solved (3) by Rossmann *et al* to an atomic resolution. These initial studies brought to light the complexities and intricacies of virus capsid organization and established structural virology as a prominent research field. The complexity and

elegance of these capsids continued to progress with advances in X-ray crystallography methodology and instrumentation (4). However, alongside the advances in structural determination of virus capsids that painted a static picture of these biological entities, there was an accumulation of solution-phase biochemical evidence that suggested these were very dynamic nucleo-protein assemblies. It is now clear from an ever growing collection of experimental evidence that capsid protein dynamics plays an essential role in all the functions exhibited by a virus.

Key Themes in Protein Dynamics

Proteins are in constant motion in solution, shifting between conformational micro-states with slightly differing energies. This conformational space can be best explained by an energy landscape where the different micro-states are populated based on the energy barriers between states and depths of local minima(5, 6). If the barrier is too high, the micro-state may never be populated. Determining the energy of these micro-states is very appealing although it is practically an impossible task. The native folded state of a protein is one or a small ensemble of such micro-state(s) and has the global minimum free energy of all kinetically accessible structures. The ability to sample different micro-states is critical to protein function including protein-protein interactions, ligand binding, signal transduction and enzyme catalysis. The study of protein dynamics serves as a unifying theme to elucidate a range of protein functions. The mechanisms of action, all have their roots in two fundamental biophysical themes 1. Flexibility and 2. Stability of a protein.

Flexibility

Flexibility, in its most basic essence, is defined as the capacity to be bent or pliable. From a protein's perspective, flexibility is adaptability. A quick survey of the literature gives us various definitions, each one defining a different subset of molecular transitions as "flexibility". For example, one definition by Kamerzell and Middaugh describes it in terms of thermodynamics, fluctuations and equilibrium events (5) while another definition by Zaccai refers to flexibility as molecular motions ranging from picosecond scale thermal fluctuations to millisecond-scale (or slower) conformational changes (7). While both these statements are true depending on the solution and experimental conditions of measurement, our understanding of what exactly encompasses flexibility is complex, yet undeniably necessary for protein design and applied protein science. Hence, as an attempt to unify these explanations, we define flexibility as a set of well-defined local and global fluctuations and transitions in protein structure; for example, bond vibrations, backbone/sidechain motions, unfolding/refolding/disorder of specific domains, and molecular switching (Figure 1). Flexibility is primarily a function of the timescale and magnitude of these motions, their equilibrium behavior, and their contribution to the conformational free energy and they together populate the micro-states of a protein (Table 1) (5, 6, 8). The degree of flexibility varies in every protein facilitating adaptation and recognition in diverse molecular events. The complexity of these fluctuations increases by several orders of magnitude when applied to multi-subunit protein-genome complexes like viruses. Specific examples of these motions are documented later in this chapter.

Table 1: Time scales and ranges of internal motion in proteins that describe flexibility (8)

Protein Motion	Range (in nm)	Timescale (in seconds)
Bond vibrations	0.2-0.5	10^{-14} to 10^{-13}
Side chain rotations	1-2	10^{-12} to 10^{-11}
Disorder/Molecular switching	1-2	10^{-11} to 10^{-7}
Binding induced transitions	0.5-4	10^{-5} to 10^{0}
Local unfolding/refolding	0.5-1	10^{-5} to 10^{+1}

Rigidity, in physical terms, is the resistance of a substance to deformation (external strain). In terms of protein structure, rigidity is a reduction in the degrees of freedom or conformational entropy of a protein. It is an opposing and complementary force to flexibility and is equally vital for biological function. In simpler terms, a loss of flexibility is rigidity. With this definition in mind, we can see that rigidity is an inherent property of any atom. If we were able to hold an atom rigidly fixed in one place, we could observe its distribution of electrons in an ideal situation. The image would be dense towards the center with the density falling off further from the nucleus (Gaussian profile). When you look at experimental electron density distributions, however, the electrons usually have a wider distribution than this ideal. This may be due to vibration of the atoms, or differences between the many different molecules in the crystal lattice. The observed electron density will include an average of all these small motions, yielding a slightly smeared image of the molecule. These motions, and the resultant smearing of the electron density, are incorporated into the atomic model by a B-value or temperature factor. Rigidity at amino acid level, described in the Ramachandran plot, is controlled by steric factors and rotation

angles of the Cα chain. Two classic examples of this are the amino acids Glycine and Proline. Glycine does not have a side chain and its rotation is not hindered by steric factors. Proline on the other hand is known to introduce kinks in the protein structure. Due to the ring formation on the β-carbon, the number of allowed rotation angles is heavily restricted and locking the aminoacid in a rigid structure. Interestingly, both these amino acids are known to introduce disorder in the protein structure.

The complementarity of flexibility and rigidity comes from the protein's degrees of freedom (dihedral angles, sidechain rotamers) (9). Such adaptability of a protein is essential for its function. The rules of flexibility/rigidity apply to virus capsids just as much. Viruses possess and combine all the above characteristics to invent new features for their own adaptability. For example, quasi-equivalence is conceptually defined as the interchangeable formation of hexamers and pentamers by the same protein molecule. This flexibility to create an efficient genome scaffold just by switching subunits is termed conformational polymorphism and is the basis for the formation of icosahedral virus capsids. Along with such subunit level flexibility, several examples of viruses that show domain flexibility, that result in critical molecular functions, are described in this chapter.

Stability

Protein stability has been broadly classified into two sub-themes depending on the type of work a researcher is involved with. A protein biochemist may define it as thermodynamic stability where the relative free energy difference between the native and unfolded forms determines the stability of the protein to denaturation. These two states are assumed to be in equilibrium, unfolding and refolding rapidly and reversibly, following a

two-state mechanism. The equilibrium between the two states can be related to the free energy difference by

$$-RT\ln(K_u) = \Delta G = \Delta H - T\Delta S$$

where K_u is the equilibrium constant for unfolding, ΔG is the Gibbs free energy, ΔH is theenthalpic contribution or the binding energy involved in the system ($\Delta H_{protein}$ and ΔH_{water}), and ΔS ($\Delta S_{protein}$ and ΔS_{water}) is the entropy of the system where $\Delta S_{protein}$ is defined as the conformational entropy of the protein (10). The major enthalpic contributors of protein stability are the hydrophobic effect/hydrophobic free energy and hydrogen bonds/free energy of hydrogen bonds. The segregation of hydrophobic and hydrophilic domains of the protein is the basic principle underlying the folding of a protein and in turn its stability. Other non-covalent and covalent contributions from Van der Waals, electrostatic interactions and disulfide linkages also play critical stabilizing roles (11). Conformational entropy is defined as the measure of degrees of freedom of the protein and plays a vital role as a stabilizing factor by populating the micro-states. Nonpolar groups of a hydrophobic domain cannot form hydrogen bonds when exposed to an aqueous environment (unfolded state). This forces the water to order itself enclosing the hydrophobic domain so as to recover the lost hydrogen bonding energy. Water also induces a strong dipole in the nonpolar residues of the hydrophobic domains. Therefore, the $\Delta S_{protein}$ is a negative value that favors an unfolded state but these factors are easily compensated by a ΔS_{water}. Folding of the protein allows many water molecules to interact favorably with each other forming an extensive hydrogen bonding network. Hydrogen bonds are also formed with polar residues of a protein. This indicates that protein folding is clearly an

entropically driven process. Hence, ΔS_{water} for an unfolded protein is a large and positively compensating force strongly favoring protein folding. The binding energy ($\Delta H_{protein}$) is a positive value for an unfolded protein due to dipole induction while it is compensated by a large negative $\Delta H_{solvent}$ which favors the folded state. It is enthalpically more or equally favorable for nonpolar molecules molecules to dissolve in water than in a nonpolar media. Hence, it can be seen that a a large entropy ($\Delta S_{water} + \Delta S_{protein}$) and binding energy of the system, to an extent, are the major contributors of thermodynamic stability in a folded protein (12).

A biotechnologist may define stability as the persistence of a protein's molecular integrity or biological function when subject to adverse environmental conditions like temperature, pH and denaturing salt concentrations. The protein's ability to retain function, at least during a certain physiologically relevant time-scale, depends on its reversibility, or for an irreversible protein, on its kinetic stability (rate of unfolding) (13, 14). The rate of irreversible protein unfolding depends on the energy barrier between the native and the non-functional state(s). Irreversible transitions are well defined using the Lumry-Eyring model which is represented by the following scheme:

$$N \leftrightarrow I \rightarrow U$$

where N, I and U are the native, the intermediate and the unfolded, irreversibly denatured states respectively. The native and the intermediate states are assumed to be in equilibrium governed by rate constants k_1 (unfolding) and k_{-1} (folding) while the rate of conversion of I to U is given by k_2. While eventually, the protein will end up in a non-functional state, this model suggests that if the energy barrier between the I and U forms is high enough,

the reaction may progress towards populating the native and more importantly the functional state of the protein. Therefore, kinetic stabilization can play a significant role in biological function.

The interdependence and independence of the thermodynamic and kinetic stabilities comes forth when we consider two particular scenarios. 1. When k_2 is rate-limiting: Under this scenario, it is evident that the rate constant for the irreversible denaturation is a product of k_1 and k_2 k_1 is influenced by the overall thermodynamic stability of the protein and therefore will have a direct impact on the kinetic stability. 2. When k_1 is rate-limiting and is approximately equal to k_2: Here, the rate of irreversible denaturation is determined almost completely by the energy barrier between the native and the unfolded state and therefore thermodynamic parameters may or may not influence kinetic stability (14).

The spatial arrangement of protein subunits into an ordered structure is known as its quaternary structure. Quaternary association is driven by weak forces. Therefore, the favorable interactions that contribute to protein stability include all the above mentioned, hydrophobic interactions and hydrogen bonds playing the most important roles again. The contact regions between subunits closely resemble the interior of a single subunit protein. Subunit associations have several advantages that include 1. Surface-volume ratio of the subunit is reduced which stabilizes the protein energetically 2. Hydrophobic residues tend to be shielded from water 3. Defects can be repaired by simply replacing the flawed subunit 4. Especially in case of viruses, less genetic material is required to code for all the proteins required for its successful proliferation. 5. Multiple subunits generally possess multiple

binding sites for a given ligand increasing the efficiency of binding. All these factors influence the stability of a protein complex and are imperative to nucleo-protein complexes like viruses.

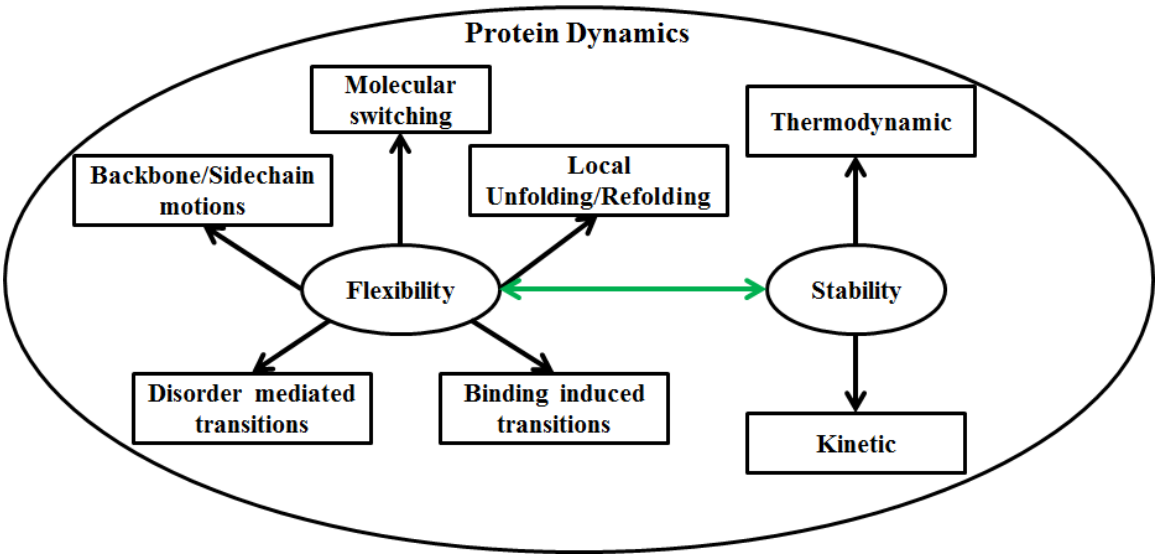


Figure 1. Schematic illustration of dynamics in proteins. Protein dynamics involves both local/globalflexibility and conformational stability.

Virus Capsids are Active Nucleo-Protein Complexes

Icosahedral viruses are specialized protein assemblages composed of multiple copies of monomeric proteins. 60 or more copies of these proteins, arranged into an icosahedral symmetry, show extensive protein-protein interactions leading to an enhanced overall stability of the virus (15, 16). This assembled unit has one daunting yet critical task to perform: evading host defenses while protecting, transporting and aiding the release of viral genome (17). The viral “life” cycle begins with cell receptor binding and entry. Several examples have been noted where receptor binding induces localized changes in the capsid structure (18, 19). This intricate process may involve membrane fusion (enveloped

viruses) and genome release in the cytoplasm or endocytosis (non-enveloped) and release of genome directly in the nucleus (20, 21). In the latter case, the capsids have evolved to resist pH and ionic strength changes while traversing the endocytic pathway (22). Finally, the virus has to perform a thermodynamic balancing act to disassemble and release the genome in conditions where it will later have to reassemble. The above events describe the first half of the viral life cycle. A second set of equally important transitions take place after capsid formation and before virus release from the cell. These involve large scale quaternary transitions (23) and the more subtle solution-phase equilibrium processes (24). Both are equally important for assembly, maturation and infection phases of the viral life cycle. Global large-scale dynamics, which exist due to changes in environmental signals such as pH, ionic strength and receptor binding have been successfully captured in a sequential manner by structure based techniques. The more subtle, local fluctuations, which involve the existence of multiple conformations of the same protein in equilibrium, have been observed with solution-phase biochemical and biophysical techniques. All these characteristics are one of the most obvious indication that capsid proteins and hence viruses as a whole are active and dynamic entities.

By relating the knowledge of the complex inter-relationships between protein flexibility and stability to viruses we are now able to understand 1. Global and local flexibility of a virus capsid 2. Biochemical and conformational stability of the interactions involved. A few examples of model icosahedral virus particles that exhibit such global and local conformational transitions are described along with a discussion of the biochemical

and biophysical knowledge we have gained and techniques used to study such virus particles in solution.

Large-Scale Irreversible Quaternary Transitions in a T7 Icosahedral Virus Maturation

Quaternary transitions involve programmed changes in capsid size, geometry, an overall reorganization of particle structure involving symmetrical subunit rotation though may or may not involve large secondary or tertiary structure transitions. Typically, an autocatalytic viral protease, packaging of nucleic acids or receptor binding individually or collectively are the triggers involved in virus maturation. A classic case of such events have been well studied and documented in the case of the HK97. HK97 is a λ-like coliphage with a 40kbp ds-DNA genome. The capsid is initially assembled into a T=7 spherical capsid (prohead-I state) with 415 identical subunits arranged into 60 hexamers and 11 pentamers. The 12th pentamer is replaced by 12 portal proteins and 50 copies of a putative protease. Maturation begins with digestion of N-terminal 103 amino acids by the protease. This cleaved particle is composed of a 31-kDa head protein and competent to package DNA (prohead-II state). A remarkable reorganization of the capsid quaternary structure is initiated when the 40kbp DNA is inserted into the head through the portal while also increasing the particle diameter from 450Å to 650Å. After this transition, the spherical shape of the capsid changes to an icosahedron and thinning of the capsid cross-section takes place (head-II state). An autocatalytic chemical joining of subunits occurs where Lys-169 and Asn-356 are cross-linked which physically concatenates hexamers and pentamers forming a "chain-mail". A substantial, irreversible stabilization of the capsid is thus

achieved, despite the thinning of the capsid walls which helps withstand the 60 atmospheres of pressure the packaged DNA. Each of these intermediate stages have been well documented by X-ray crystallography and static and time-resolved cryo-EM (25–27).

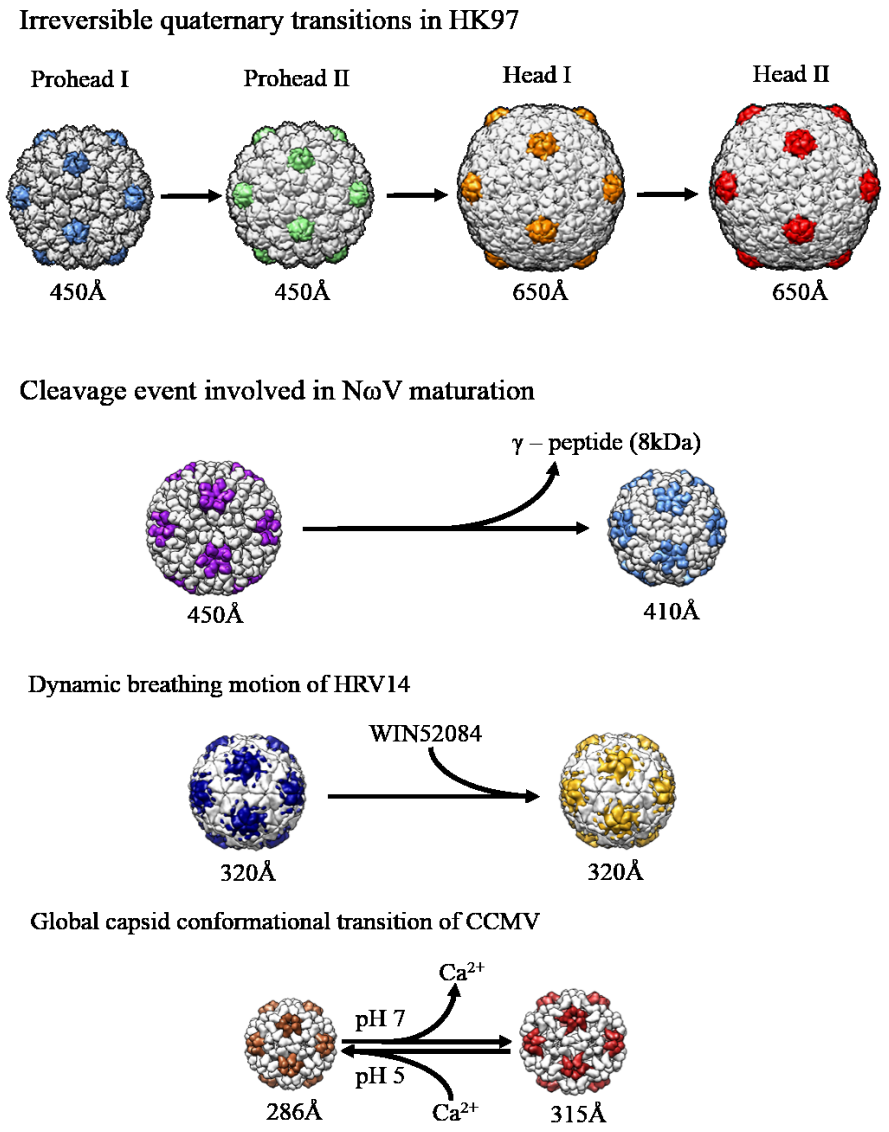


Figure 2. Global and local quaternary conformational and structural transitions seen in four icosahedral viruses

In other tailed phages (such as P22, Φ29 and T7) capsid maturation is similar to HK97,though the mature capsids are stabilized either by additional domains of capsid protein(P22, Φ29 (28, 29); or rearrangement of the capsid protein subunits (T7; (30)).

Tetravirus Capsid Maturation Involves a Cleavage Event

Nudaurelia ω capensis virus (NωV), an insect virus, belongs to the tetravirus family with a T=4 quasi-equivalence and the only known non-enveloped virus to have this quasi-symmetry. At pH 7.6, the newly formed capsid is 450Å in diameter containing 240 identical 70-kDa subunits associated as dimers(31, 32). A cleavage event occurs when the pH is reduced to 5 with a decrease in particle size (410Å) while the subunit arrangement changes to trimers(33). This event is reversible so long as the autohydrolytic cleavage has not proceeded beyond 15% of the subunits (33). The cleavage event works as an irreversible and critical molecular switch for the capsid maturation while covalently liberating an 8-kDa polypeptide (γ). A number of biophysical techniques including mass spectrometry based limited proteolysis, chemical labeling and FT-IR studies, have been used to characterize the two capsid forms (34). Flockhouse virus (FHV) shows a similar cleavage event during its maturation forming a γ-peptide which has been attributed to a membrane lysis function (35). A mutant form of NωV in which the autocatalytic function has been abrogated is known to transition repeatedly between forms (36). NωV is the first animal RNA-virus that has been subject to such intense characterization of the mature capsid and its precursor making it an excellent model system.

Dynamic Breathing Motion
of the Human Rhinovirus (HRV14)

HRV14, the common cold virus, belongs to the Picornavirus family with a T=1 icosahedral symmetry. The capsid is made up of 60 copies of each of the four structural proteins VP1-VP4. From the crystal structure it is known that the VP4 is completely internal to the capsid while the N-terminus of VP1 is partially internalized. The time-course experiments performed combining proteolysis and mass spectrometry revealed results indicative of the transient exposure of internalized capsid proteins. The initial peptides generated were localized to the internalized VP4 subunit. On comparing the proteolysis data and the crystal structure, it became evident that the capsid proteins fluctuated between specific but short-lived conformations. The model proposed that HRV14 existed in at least two thermodynamically different states: one, a static, low-energy state trapped in the crystal structure where VP4 lies at the capsid RNA interface, and the other, a more stochastic, slightly higher energy molecule where the internal VP4 is accessible to proteases (37). Such overall "breathing" motions in the capsid were first observed in FHV by Bothner et al (38). These experiments were then extended to study drug binding effects (WIN 52084) on HRV14. This anti-viral drug binds to hydrophobic pockets of VP1, which lie beneath the 5-fold axis. After drug exposure, a significant decrease in proteolysis was seen along with stabilization of the viral capsid to acid and thermal inactivation and inhibition of the uncoating process (37, 39–41). Such work involving the characterization of global and local dynamics with NωV, HRV14 and FHV demonstrate the power of complementary solution-based approaches in cases where structural data is not sufficient for interpretation or may lead to incorrect conclusions.

Local Rigid Body Movements Govern Capsid Conformational Changes of a Plant Virus

The Cowpea chlorotic mottle virus (CCMV) is a small icosahedral virus of the Bromoviridae family (alphavirus-like superfamily) infecting the cowpea plant resulting in splotchy discoloration of the leaves. CCMV is characterized by its symmetrical construction, its ability to spontaneously assemble *in vitro* and its two distinct conformations; a *closed* conformation promoted by low pH and the presence of divalent cations, and a *swollen* conformation which exists at high pH and low ionic strength (the absence of Ca^{2+}) (42). The CCMV capsid is composed of 180 identical subunits, each 190 amino acids in length. The swelling transitions around the 3-fold axes involve the formation of a 20Å pore primarily due to rigid body movements between the cation binding residues. NMR studies to look at the dynamics of CCMV showed that the disordered N-terminus of the capsid protein interacts with the RNA even during swelling. A recent study compared the dynamics and stability of the wildtype CCMV conformers (43). The study concluded that the closed form has a higher proteolytic resistance compared to the swollen. The study also showed that in addition to the closed and swollen conformations, protein domains localized to the inside of the capsid in structural models can be reversibly exposed to the surface in solution (43). Brome mosaic virus, a virus from the same family as CCMV, shows the similar swelling property. Hydrogen-Deuterium Mass Spectrometry on BMV indicated that the largest deuterium increases induced by structural alteration occurred in the regions around the quasi-threefold axes, which are located at the center of the asymmetric unit (44).

Solution Based Approaches to Studying Virus Capsid Dynamics

In solution, many proteins exist in an ensemble of conformations. Capsid proteins display the same property and the conformations that are sampled are based on solution conditions and the energy barriers between minima on the energy landscape. A wide range of biophysical approaches are available for the determination of these energy barriers and hence an overall energy landscape for a protein.

Viral capsids are highly flexible and undergo conformational transitions based on solution and environmental conditions. Though most of the standard biophysical approaches have proven challenging, a wide variety of creative new approaches have also proven successful for studying protein dynamics in viral capsids. The thermodynamically low-energy form of the capsid is the one most often captured in crystal structures whereas the higher-energy form is generally the functional species. Among the techniques most commonly employed, researchers have seen tremendous success with NMR(45), Mass Spectrometry based methods (Limited Proteolysis (24) and Hydrogen-Deuterium Exchange (44)) while a new array of techniques, including Calorimetry based methods (Differential Scanning Calorimetry(46, 47), Isothermal Titration Calorimetry (48)), Light scattering approaches (49) and Fluorescence experiments (50, 51) have shown promising progress in this field Additionally, In-silico work using Molecular Dynamics simulations (52) have been used to hypothesize and predict virus capsid behavior in solution and finally the structures of these virus capsids have been captured at near-physiological conditions using cryo-electron microscopy (26, 42, 53). Contributions of a few of the above

techniques will be briefly described here along with details of techniques used in this dissertation.

NMR had been one of the few techniques that could be applied to probe capsid dynamics in solution (45, 54) and since then has been instrumental in characterizing these motions. However, limits in the current instrumentation to probe large complexes resulting in crowded spectra and the slow tumbling of capsids in solution resulting in enhanced relaxation speed make NMR not feasible to use for intact capsids. It does hold the advantage of being able to selectively detect any large localized motion in the capsid due to the lack of signal from ordered regions. Recently, NMR has also been used in conjunction with cryo-EM to probe inter-subunit interactions of the HIV-1 capsid (55). With the advances in technology and data analysis, we have been able to collect and analyze data on the picosecond time scale at a sub-angstrom level resolution. NMR falls into this category. NMR in conjunction with hydrogen-deuterium exchange (HDX) has been vital for deducing protein structures. Another such technique that can supply us with sub-angstrom level resolution is HDX Mass Spectrometry. Briefly, amide and side-chain hydrogen atoms in the protein are exchangeable with Deuterium in the solvent and act as reporters for local protein structure. The exchange rates of these hydrogens range from nearly instantaneous to effectively zero over the course of months, depending on the stability and solvent exposure at a specific site (56). The exchange introduces a mass shift of one dalton per hydrogen exchanged and is detected on the mass spectrometer. After exchange, the protein is cleaved in the presence of pepsin and the change in mass of the peptides are mapped onto the structure. Dynamic regions tend to show more exchange rates

and higher changes in mass. The main advantages of this method include 1. Very small sample quantities and therefore less subject to scaling issues 2. Residue level exchange information 3. Straightforward data analysis 4. Potentially high throughput. Though HDX is a reversible process, controlling the pH, temperature and minimizing time of analysis reduce the phenomenon of back-exchange. While the use of a non-specific protease like pepsin increases the number of peptides formed and therefore the complexity of analysis, the homo-oligomeric nature of viruses limits this complexity and presents a unique opportunity to study high-resolution dynamics in supramolecular protein complexes.

Summary

Biochemical and biophysical investigations of virus particles in solution are critical to understanding their functional properties. Together with structural models, information on the location and extent of capsid dynamics provides a basis for linking structure to function with greater detail. Dynamic regions are noveltargets for antiviral therapy and viruses are excellent model systems for studying allostery and dynamics in supramolecular complexes. Viruses are currently being used and developed as bioinspired nanomaterials, with applications from gene delivery, MRI contrast agents and nano-reactors. Scientists are now seeking next generation nanomaterials that can actively respond to various stimuli and a thorough understanding of the dynamic properties of capsids will be critical for an efficacious development of these new age tools.

Literature Cited

1. Bamford DH, Grimes JM, Stuart DI. 2005. What does structure tell us about virus evolution? Current opinion in structural biology 15:655–63.

2. Harrison SC. 1969. Structure of tomato bushy stunt virus. Journal of Molecular Biology 42:457–483.

3. Rossmann MG, Arnold E, Erickson JW, Frankenberger EA, Griffith JP, Hecht H-J, Johnson JE, Kamer G, Luo M, Mosser AG, Rueckert RR, Sherry B, Vriend G. 1985. Structure of a human common cold virus and functional relationship to other picornaviruses. Nature 317:145–153.

4. Veesler D, Quispe J, Grigorieff N, Potter CS, Carragher B, Johnson JE. 2012. Maturation in action: CryoEM study of a viral capsid caught during expansion. Structure (London, England : 1993) 20:1384–90.

5. Kamerzell TJ, Middaugh CR. 2008. The complex inter-relationships between protein flexibility and stability. Journal of Pharmaceutical Sciences 97:3494–3517.

6. M Karplus and J. A. McCammon. 1983. Dynamics of Proteins: Elements and Function. Annual review of biochemistry 53:263–300.

7. Zaccai G. 2000. How Soft Is a Protein? A Protein Dynamics Force Constant Measured by Neutron Scattering. Science 288:1604–1607.

8. McCammon JA. 1984. Protein dynamics. Reports on Progress in Physics 47:1–46.

9. Ramachandran G. 1968. Ramachandran plot for multiple structures. Advances in protein chemistryrotein chemistry 23:283–437.

10. Pace CN, Laurents D V. 1989. A new method for determining the heat capacity change for protein folding. Biochemistry 28:2520–5.

11. Ponnuswamy PK, Gromiha MM. 1994. On the Conformational Stability of Folded Proteins. Journal of Theoretical Biology 166:63–74.

12. Murphy KP. 2001. Stabilization of protein structure. Methods in molecular biology (Clifton, N.J.) 168:1–16.

13. Sanchez-Ruiz JM. 1992. Theoretical analysis of Lumry-Eyring models in differential scanning calorimetry. Biophysical Journal 61:921–935.

14. Sanchez-Ruiz JM. 2010. Protein kinetic stability. Biophysical chemistry 148:1–15.

15. Zlotnick A. 2005. Theoretical aspects of virus capsid assembly. Journal of molecular recognition : JMR 18:479–90.

16. Caspar DLD, Klug A. 1962. Physical principles in the construction of regular viruses. Cold Spring Harbor Symposia on Quantitative Biology 27th:1–24.

17. Bothner B, Hilmer JK. 2010. Probing virus capsids in solution. Royal Society of Chemistry, Cambridge.

18. Rizzuto CD. 1998. A Conserved HIV gp120 Glycoprotein Structure Involved in Chemokine Receptor Binding. Science 280:1949–1953.

19. Levy HC, Bowman VD, Govindasamy L, McKenna R, Nash K, Warrington K, Chen W, Muzyczka N, Yan X, Baker TS, Agbandje-McKenna M. 2009. Heparin binding induces conformational changes in Adeno-associated virus serotype 2. Journal of Structural Biology 165:146.

20. Weiss RA. 2008. HIV receptors and cellular tropism. IUBMB life 53:201–5.

21. Agbandje-McKenna M, Kleinschmidt J. 2011. AAV Capsid Structure and Cell Interactions, p. 47–92. *In* Snyder, RO, Moullier, P (eds.), Methods in Molecular Biology. Humana Press.

22. Cotmore SF, Tattersall P. 2007. Parvoviral host range and cell entry mechanisms. Advances in virus research 70:183–232.

23. Duda RL, Hempel J, Michel H, Shabanowitz J, Hunt D, Hendrix RW. 1995. Structural transitions during bacteriophage HK97 head assembly. Journal of Molecular Biology 247:618–635.

24. Hilmer JK, Zlotnick A, Bothner B. 2008. Conformational Equilibria and Rates of Localized Motion within Hepatitis B Virus Capsids. Journal of Molecular Biology 375:581–94.

25. Gertsman I, Gan L, Guttman M, Lee K, Speir JA, Duda RL, Hendrix RW, Komives EA, Johnson JE. 2009. An unexpected twist in viral capsid maturation. Nature 458:646–50.

26. Gan L, Speir JA, Conway JF, Lander G, Cheng N, Firek BA, Hendrix RW, Duda RL, Liljas L, Johnson JE. 2006. Capsid Conformational Sampling in HK97 Maturation Visualized by X-Ray Crystallography and Cryo-EM. Structure 14:1655–65.

27. Gertsman I, Fu C-Y, Huang R, Komives EA, Johnson JE. 2010. Critical salt bridges guide capsid assembly, stability, and maturation behavior in bacteriophage HK97. Molecular & cellular proteomics : MCP 9:1752–63.

28. Parent KN, Khayat R, Tu LH, Suhanovsky MM, Cortines JR, Teschke CM, Johnson JE, Baker TS. 2010. P22 coat protein structures reveal a novel mechanism for capsid maturation: stability without auxiliary proteins or chemical crosslinks. Structure (London, England : 1993) 18:390–401.

29. Morais MC, Koti JS, Bowman VD, Reyes-Aldrete E, Anderson DL, Rossmann MG. 2008. Defining molecular and domain boundaries in the bacteriophage phi29 DNA packaging motor. Structure (London, England : 1993) 16:1267–74.

30. Ionel A, Velázquez-Muriel JA, Luque D, Cuervo A, Castón JR, Valpuesta JM, Martín-Benito J, Carrascosa JL. 2011. Molecular rearrangements involved in the capsid shell maturation of bacteriophage T7. The Journal of biological chemistry 286:234–42.

31. Helgstrand C, Munshi S, Johnson JE, Liljas L. 2004. The refined structure of Nudaurelia capensis omega virus reveals control elements for a T = 4 capsid maturation. Virology 318:192–203.

32. Munshi S, Liljas L, Cavarelli J, Bomu W, McKinney B, Reddy V, Johnson JE. 1996. The 2.8 A structure of a T = 4 animal virus and its implications for membrane translocation of RNA. Journal of molecular biology 261:1–10.

33. Canady MA, Tihova M, Hanzlik TN, Johnson JE, Yeager M. 2000. Large conformational changes in the maturation of a simple RNA virus, nudaurelia capensis omega virus (NomegaV). Journal of molecular biology 299:573–84.

34. Bothner B, Taylor D, Jun B, Lee KK, Siuzdak G, Schlutz CP, Johnson JE. 2005. Maturation of a tetravirus capsid alters the dynamic properties and creates a metastable complex. Virology 334:17–27.

35. Janshoff A, Bong DT, Steinem C, Johnson JE, Ghadiri MR. 1999. An animal virus-derived peptide switches membrane morphology: possible relevance to nodaviral transfection processes. Biochemistry 38:5328–36.

36. Taylor DJ, Krishna NK, Canady MA, Schneemann A, Johnson JE. 2002. Large-scale, pH-dependent, quaternary structure changes in an RNA virus capsid are reversible in the absence of subunit autoproteolysis. Journal of virology 76:9972–80.

37. Lewis JK, Bothner B, Smith TJ, Siuzdak G. 1998. Antiviral agent blocks breathing of the common cold virus. Proceedings of the National Academy of Sciences 95:6774–6778.

38. Bothner B, Dong XF, Bibbs L, Johnson JE, Siuzdak G. 1998. Evidence of Viral Capsid Dynamics Using Limited Proteolysis and Mass Spectrometry. Journal of Biological Chemistry 273:673–76.

39. Fox MP, Otto MJ, McKinlay MA. 1986. Prevention of rhinovirus and poliovirus uncoating by WIN 51711, a new antiviral drug. Antimicrobial agents and chemotherapy 30:110–6.

40. Rombaut B, Andries K, Boeyé A. 1991. A comparison of WIN 51711 and R 78206 as stabilizers of poliovirus virions and procapsids. The Journal of general virology 72 (Pt 9):2153–7.

41. Gruenberger M, Pevear D, Diana GD, Kuechler E, Blaas D. 1991. Stabilization of human rhinovirus serotype 2 against pH-induced conformational change by antiviral compounds. The Journal of general virology 72 (Pt 2):431–3.

42. Speir JA, Munshi S, Wang G, Baker TS, Johnson JE. 1995. Structures of the native and swollen forms of cowpea chlorotic mottle virus determined by X-ray crystallography and cryo-electron microscopy. Structure (London, England : 1993) 3:63–78.

43. Speir JA, Bothner B, Qu C, Willits DA, Young MJ, Johnson JE. 2006. Enhanced Local Symmetry Interactions Globally Stabilize a Mutant Virus Capsid That Maintains Infectivity and Capsid Dynamics 80:3582–3591.

44. Wang L, Lane LC, Smith DL. 2001. Detecting structural changes in viral capsids by hydrogen exchange and mass spectrometry. Protein science : a publication of the Protein Society 10:1234–43.

45. G Vriend,M.A. Hemminga,B.J.M. Verduin TJS. 1982. Swelling of Cowpea chlorotic mottle virus studied by proton NMR. FEBS Lett. 146:319–321.

46. Krell T, Manin C, Nicolaï M-C, Pierre-Justin C, Bérard Y, Brass O, Gérentes L, Leung-Tack P, Chevalier M. 2005. Characterization of different strains of poliovirus and influenza virus by differential scanning calorimetry. Biotechnology and applied biochemistry 41:241–6.

47. Shnyrov VL, Zhadan GG, Cobaleda C, Sagrera A, Muñoz-Barroso I, Villar E. 1997. A differential scanning calorimetric study of Newcastle disease virus:

identification of proteins involved in thermal transitions. Archives of biochemistry and biophysics 341:89–97.

48. Jeembaeva M, Jönsson B, Castelnovo M, Evilevitch A. 2010. DNA heats up: energetics of genome ejection from phage revealed by isothermal titration calorimetry. Journal of molecular biology 395:1079–87.

49. Zlotnick A, Aldrich R, Johnson JM, Ceres P, Young MJ. 2000. Mechanism of capsid assembly for an icosahedral plant virus. Virology 277:450–6.

50. Yi G, Vaughan RC, Yarbrough I, Dharmaiah S, Kao CC. 2009. RNA binding by the brome mosaic virus capsid protein and the regulation of viral RNA accumulation. Journal of Molecular Biology 391:314–26.

51. Ni P, Wang Z, Ma X, Das NC, Sokol P, Chiu W, Dragnea B, Hagan M, Kao CC. 2012. An examination of the electrostatic interactions between the N-terminal tail of the Brome Mosaic Virus coat protein and encapsidated RNAs. Journal of molecular biology 419:284–300.

52. Ode H, Nakashima M, Kitamura S, Sugiura W, Sato H. 2012. Molecular dynamics simulation in virus research. Frontiers in microbiology 3:258.

53. Kronenberg S, Kleinschmidt J a, Böttcher B, Kronenberg J. A. Kleinschmidt, and B. Bottcher S. 2001. Electron cryo-microscopy and image reconstruction of adeno-associated virus type 2 empty capsids. EMBO reports 2:997–1002.

54. Vriend G, Verduin BJ, Hemminga M a. 1986. Role of the N-terminal part of the coat protein in the assembly of cowpea chlorotic mottle virus. A 500 MHz proton nuclear magnetic resonance study and structural calculations. Journal of molecular biology 191:453–60.

55. Byeon I-JL, Meng X, Jung J, Zhao G, Yang R, Ahn J, Shi J, Concel J, Aiken C, Zhang P, Gronenborn AM. 2009. Structural convergence between Cryo-EM and NMR reveals intersubunit interactions critical for HIV-1 capsid function. Cell 139:780–90.

56. Tsutsui Y, Wintrode PL. 2007. Hydrogen/deuterium exchange-mass spectrometry: a powerful tool for probing protein structure, dynamics and interactions. Current medicinal chemistry 14:2344–58.

CHAPTER 2

VIRUS PARTICLES AS ACTIVE NANOMATERIALS THAT CAN RAPIDLY CHANGE THEIR VISCOELASTIC PROPERTIES IN RESPONSE TO DILUTE SOLUTIONS

Contribution of Authors and Co-Authors

Manuscript in Chapter 2

Author: Vamseedhar Rayaprolu

Contributions: Optimized and established the method, collected and analyzed data, prepared the manuscript

Co-Author: Benjamin M. Manning

Contributions: Optimized the method, aided in initial data collection.

Co-Author: Trevor Douglas

Contributions: Provided samples and sample purification procedures, aided in critical discussion of data and editing of the manuscript

Co-Author: Brian Bothner

Contributions: Obtained funding, discussed the results and implications and edited the manuscript.

Manuscript Information Page

Vamseedhar Rayaprolu, Benjamin M. Manning, Trevor Douglas, Brian Bothner

Journal: RSC Softmatter

Status of Manuscript:
____ Prepared for submission to a peer-reviewed journal
____ Officially submitted to a peer-review journal
____ Accepted by a peer-reviewed journal
_x__ Published in a peer-reviewed journal

Publisher: Royal Society of Chemistry

Issue in which Manuscript Appears: Volume 6, 5286–5288 (2010)

CHAPTER 2

VIRUS PARTICLES AS ACTIVE NANOMATERIALS THAT CAN RAPIDLY CHANGE THEIR VISCOELASTIC PROPERTIES IN RESPONSE TO DILUTE SOLUTIONS

Abstract

Swelling of the plant virus CCMV has been monitored in real time, revealing that the transition occurs rapidly, is readily reversible, and is accompanied by a change in particle rigidity.

Introduction

Modified protein cages and icosahedral virus capsids are increasingly being used as bio-inspired nanomaterials. Synthesis and assembly of nanomaterials have seen new direction due to the application of biomimetic approaches. By utilizing the high symmetry of protein cage architectures, especially virus capsids, a variety of functional nanomaterials have been created (1–7). Structural models based on X-ray and Cryo-Electron Microscopy (EM) data have been critical to the design and modification of cages for these applications (8,9). From the models, near atomic level details are provided. However, properties such as rigidity, conformational dynamics and viscoelasticity are generally not well understood and must be obtained by other means. Knowledge and use of these properties are critical for the development of active nanomaterials. Cowpea chlorotic mottle virus (CCMV) is a small icosahedral RNA virus of the Bromoviridae family. The CCMV capsid is composed

of 180 identical protein subunits, 190 amino acids in length, arranged with T = 3 icosahedral symmetry. The symmetrical capsid can be assembled in vitro and has two distinct forms: a closed conformation promoted by the presence of divalent cations (Ca^{2+} or Mg^{2+}) and a swollen conformation in the absence of divalent cations, (9–11) Figure 1. Swelling causes the particle diameter to increase by 10%, leading to a more fenestrated structure. The driving force for expansion is charge repulsion between side chains of three acidic residues located at the three fold axes of symmetry (9). CCMV is a model system for understanding the biophysical properties of capsids and is a popular scaffold for nanomaterials. The ability to reassemble the particle in vitro or to induce reversible swelling has been used to encapsulate drugs and replace the nucleic acid core with a variety of synthetic cargo (1,6,12). We have used the quartz crystal microbalance with dissipation (QCM-D) technology to investigate the viscoelasticity of CCMV during structural transition and after mineralization. QCM-D is based on the piezoelectric properties of quartz. The crystal is driven by applying pulses of alternating electric current to metal electrodes on either side which causes it to oscillate at a precise frequency. Odd multiples (harmonics) of the fundamental frequency are also monitored. When materials are deposited onto the electrode surface, the frequency decreases relative to the mass deposited (14,15). In addition to determining the mass added to the crystal by tracking the changes in frequency, information on the viscoelasticity of the material can be obtained by monitoring the frequency decay when the current is interrupted. The rate of frequency decay, known as dissipation or damping, is the sum of all energy losses in the system per oscillation. The dissipation is defined as:

$$D = \frac{E_{dissipated}}{2\pi E_{stored}} = \frac{1}{\pi f \tau}$$

where D is the dissipation, E dissipated is the energy lost from the crystal when damped, E stored is the energy retained in the crystal when damped, f is the frequency and s is the decay time constant. Dissipation is unitless. A soft material is deformed during oscillation which leads to high dissipation, while a rigid material exhibits low dissipation as it strongly couples to the crystal (16) CCMV is a good test system for the application of QCM-D for the study of viscoelastic properties of protein cages because a substantial amount of complimentary data already is available. Structural studies show that the closed form of the viral capsid is more compact and less fenestrated than the swollen form (9–11) Solution phase analysis for protease sensitivity (11) and nanoindentation studies by atomic force microscopy (AFM) in liquid medium indicate that the closed form is less dynamic and more rigid (17–19) Capsid swelling is believed to play a role in nucleic acid release, suggesting a biological role for destabilization. It has also been shown that in addition to the closed and swollen conformations, protein domains localized to the inside of the capsid in structural models can be reversibly exposed to the surface in solution (11).

Results and Discussion

The QCM-D experiments were conducted by adsorbing CCMV to a gold-coated quartz crystal. Conformational change between the closed and swollen forms was induced by buffer exchange. Frequency and dissipation values from the fundamental (5 MHz) and its three harmonics (15 MHz, 25 MHz and 35 MHz) were collected (16) Data acquisition

began by establishing a baseline in closing buffer (10 mM Sodium Acetate, 100 mM NaCl, 5 mM CaCl 2 , and pH 7.15) (Figure. 2a). A CCMV layer was formed by adding one 0.3 mL aliquot followed by three 0.1 mL aliquots of 0.05 mg/mL virus solution (deposition). The surface was then washed with closing buffer (wash) to remove

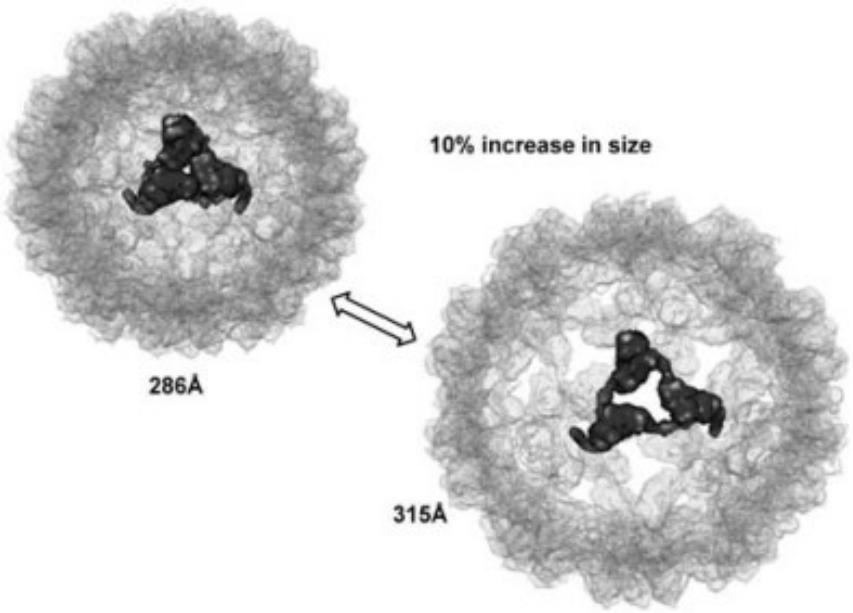


Figure 1. Closed and swollen forms of CCMV. Images made using UCSF Chimera (13) and PDB ID—1CWP (9)

loosely bound viral particles. CCMV readily adhered to the gold surface on the crystal. Previously it has been shown that CCMV packs as a dense monolayer when applied to a surface (20) The structural transition to the swollen form was initiated by flowing 600 mL of swelling buffer (10 mM Sodium Acetate, 100 mM NaCl, 1 mM EDTA, and pH 7.15) over the layer (swollen). This resulted in a large change in dissipation and a very small change in frequency. The observed slight change in frequency after numerous buffer exchanges indicated that a small amount of material was washed off the sensor surface

each time (<1%). The conformational change was reversible as shown by the rapid alternation between closed and swollen forms with buffer changes. Buffer exchange before loading with virus confirmed that the signal variation was not caused by the buffer (Figure. S3†). The transition occurred faster than the time resolution of the instrument (2–3 seconds). A small but consistent change in dissipation continued for ~15 minutes before the baseline stabilized. The nature of the slower change remains to be determined. The swollen form had higher dissipation values than the closed form. Higher dissipation values are associated with flexible materials. A comparison of particle rigidity was made by taking the ratio of frequency to the dissipation for each transition. The $\Delta f/\Delta D$ ratio of a material is directly proportional to rigidity (16). The closed form showed a $\Delta f/\Delta D$ ratio of 15.4 ± 0.1 MHz whereas the swollen form showed 12.9 ± 0.2 MHz (Table 1 and ESI†). Experiments were conducted with different loadings on the crystal and while the measured values changed, the $\Delta f/\Delta D$ ratio did not. This suggests that the conformational change alters the rigidity of the virus. Each overtone has a slightly different ratio because the frequency and dissipation scale as $n^{1/2}$ and $n^{-1/2}$, respectively for Newtonian fluids, where n is the overtone number (21). To put the magnitude of the ratios in perspective, a similar analysis of Mefp-1 mussel adhesive protein at 25 mg/mL had a ratio of 5.5 MHz, 22 and a 500 mg/mL agarose gel had a ratio of 3.65 MHz (16). These ratios are 3 to 4 times lower than our measurements, indicating that the virus layer is much more rigid and that the ~20% change in the $\Delta f/\Delta D$ ratio between closed and swollen represents a substantial change in protein rigidity. Electron micrographs of particles under the buffer conditions used confirm the presence of particles (Figure. 2b and c). The increased fenestration and expansion of

the swollen form decrease the buried surface area between the subunits by ~5% (8) suggesting that this decreased subunit–subunit interactions decrease rigidity.

Table 1. Frequencies and Dissipations of CCMV

At 15 MHz	Closed $\|\Delta f/\Delta D\|$ (in MHz)	Swollen $\|\Delta f/\Delta D\|$ (in MHz)
CCMV	15.4 ± 0.1	12.9 ± 0.2
Cross-linked CCMV	49.6 ±2.5	33.3 ± 2.7
Mineralized CCMV	62.3 ±1.7	55.9 ±0.3

Virus particles and protein cages are held together by forces which can be relatively weak between subunit pairs (23). Materials applications of protein cages and noncovalent virus particles require modification of the exterior, interior, or subunit interfaces. Modifications such as a mineralized core and intrasubunit cross-linking likely alter the local and/or global stability and viscoelastic properties. To investigate the effects of protein modification and cargo packaging, CCMV particles were chemically cross-linked and loaded with a mineralized core. The capsid subunits were covalently cross-linked with glutaraldehyde, then an ammonium molybdate $(NH_4)_2MoO_4$ core was added via a biomimetic mineralization process (1,7). Covalent cross-linking was confirmed by raising the pH to 10, which leads to disassembly of unmodified CCMV capsids. Furthermore, the cross-linking also seemed to help the capsid to resist high temperature since we could not see any traces of the subunits on SDS-PAGE gels.

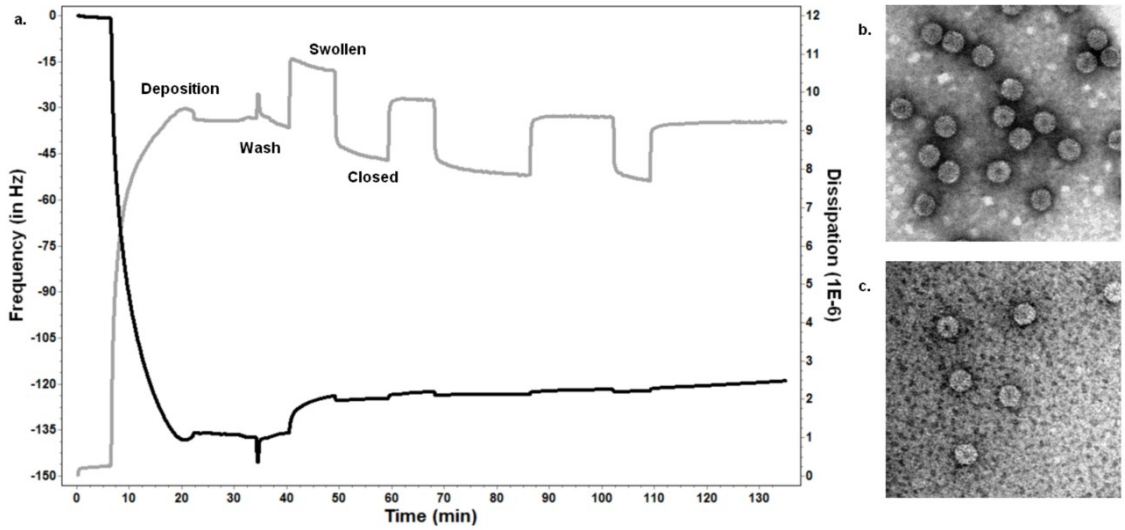


Figure 2. QCM-D analysis of CCMV. (a) Trace shows the frequency (in black, on Y1 axis) and dissipation values (in gray, on Y2 axis) of the 3rd overtone beginning with surface loading of a gold-coated crystal through multiple cycles between swollen and closed conformations. The ratio of frequency to dissipation provides information about the solution phase modulus of the material. (b and c) Negative stain electron micrographs of closed and swollen CCMV, respectively.

QCM-D analysis of the modified capsids revealed large changes in overall particle rigidity. The $\Delta f/\Delta D$ ratio for the glutaraldehyde cross-linked form was more than threefold higher than unmodified CCMV (Table 1 and ESI†). This was not due to a change in the binding of capsids to the gold surface, because the observed frequency before and after rinsing was similar to unmodified capsids. The change in $\Delta f/\Delta D$ was due to a decrease in dissipation, indicating that cross-linking increased capsid rigidity. Analysis of the cross-linked and mineralized capsids showed a further increase in the $\Delta f/\Delta D$ ratio. The additional rigidity could be a direct effect of the mineral nanoparticle inside CCMV or indirect via electrostatic interactions between the negatively charged mineral core and the inner surface of the protein subunits which are rich in positively charged amino acids (1,9). The ability to directly investigate the physical properties of protein cages is important to the process

of materialization as well as in understanding their biology. AFM is the major technique that has been used to date. Resistance to indentation and load at failure can be accurately assessed with AFM (17,19,24) Viscoelastic properties such as Young's modulus can be calculated, allowing protein cages to be compared with other materials. For example, RNA filled CCMV capsids were more resistant to indentation than empty capsids (17) while both forms were highly elastic showing reversible deformation up to 20–30% of their radius. AFM has also been used to measure strength at different symmetry axes in icosahedrons and materialized samples (17).

The QCM-D results presented here follow the same trends as AFM with respect to protein cage stiffness. However, there are several noteworthy differences in what the techniques are measuring and implications for biology and materials applications. AFM measurements are based on relatively large scale deformations of a few to tens of nanometres, whereas protein layers are believed to conserve their shape during quartz crystal oscillations (14). Our data are consistent with this, showing that sparsely loaded and densely packed surfaces have similar $\Delta f/\Delta D$ ratios, ruling out large scale deformations. QCM-D is therefore measuring viscoelasticity associated with small scale protein perturbations which are much closer to the range of motions associated with biological function and active materials (9–11). A further difference between the AFM and QCM-D measurements is that the former is directional by nature, and as discussed above, can be dependent on particle orientation, whereas QCM-D measures global properties.

Conclusions

CCMV swelling has intrigued structural biologists for decades and the associated opening of pores (gating) was used to create one of the first bioinspired nanomaterials (1). The data presented here show that swelling is rapid, reproducible and is accompanied by a change in particle rigidity. Interestingly, covalent cross-linking increased the overall rigidity of both closed and swollen forms, while maintaining sensitivity to calcium and a difference between forms. The difference in rigidity between the forms of the mineralized CCMV was subtle though they were comparatively higher than the cross-linked conformations. This indicates a strong coupling between protein and the mineralized core. The application of QCM-D technology for the biophysical analysis of large protein structures has been largely unexplored. We have demonstrated the ability to follow the changes in such virus-based materials in real-time. The observed differences in behaviour of the CCMV samples correlate with expected changes to the stiffness and dynamics of the capsid and modified capsids. The ability to characterize materials that respond to environmental signals, in liquid, with high precision, and a minimum of effort will be of great benefit.

Supporting Information: Additional QCM-D traces and expanded tables for this study are available free of charge via the Internet at http://www.rsc.org/suppdata/sm/c0/c0sm00459f/c0sm00459f.pdf.

The relevant data is located in Appendix A

Literature Cited

1. T. Douglas and M. Young, Nature, 1998, 393, 152.

2. W. Qian, L. Tianwei, T. Liang, E. J. John and M. G. Finn, Angew.Chem., Int. Ed., 2002, 41, 459–462.

3. P. Singh, G. Destito, A. Schneemann and M. Manchester, J. Nanobiotechnol., 2006, 4, 2.

4. L. Liepold, S. Anderson, D. Willits, L. Oltrogge, J. A. Frank, T. Douglas and M. Young, Magn. Reson. Med., 2007, 58, 871–879.

5. R. A. Miller, A. D. Presley and M. B. Francis, J. Am. Chem. Soc., 2007, 129, 3104.

6. J. Sun, C. DuFort, M.-C. Daniel, A. Murali, C. Chen, K. Gopinath, B. Stein, M. De, V. M. Rotello, A. Holzenburg, C. C. Kao and B. Dragnea, Proc. Natl. Acad. Sci. U. S. A., 2007, 104, 1354–1359.

7. M. T. Klem, M. Young and T. Douglas, J. Mater. Chem., 2008, 18, 3821–3823.

8. H. Liu, C. Qu, J. E. Johnson and D. A. Case, J. Struct. Biol., 2003, 142, 356.

9. J. A. Speir, S. Munshi, G. Wang, T. S. Baker and J. E. Johnson, Structure, 1995, 3, 63.

10. L. O. Liepold, J. Revis, M. Allen, L. Oltrogge, M. Young and T. Douglas, Phys. Biol., 2005, 2, S166.

11. J. A. Speir, B. Bothner, C. Qu, D. A. Willits, M. J. Young and J. E. Johnson, J. Virol., 2006, 80, 3582–3591.

12. M. Uchida, M. T. Klem, M. Allen, P. Suci, M. Flenniken, E. Gillitzer, Z. Varpness, L. O. Liepold, M. Young and T. Douglas, Adv. Mater., 2007, 19, 1025–1042.

13. E. F. Pettersen, T. D. Goddard, C. C. Huang, G. S. Couch, D. M. Greenblatt, E. C. Meng and T. E. Ferrin, J. Comput. Chem., 2004, 25, 1605–1612.

14. G. V. Lubarsky, M. R. Davidson and R. H. Bradley, Biosens. Bioelectron., 2007, 22, 1275.

15. V. M. Mecea, Anal. Lett., 2005, 38, 753–767.

16. A. K. Dutta and G. Belfort, Langmuir, 2007, 23, 3088–3094.

17. J. P. Michel, I. L. Ivanovska, M. M. Gibbons, W. S. Klug, C. M. Knobler, G. J. L. Wuite and C. F. Schmidt, Proc. Natl. Acad. Sci. U. S. A., 2006, 103, 6184–6189.

18. A. Evilevitch, L. T. Fang, A. M. Yoffe, M. Castelnovo, D. C. Rau, V. A. Parsegian, W. M. Gelbart and C. M. Knobler, Biophys. J., 2008, 94, 1110.

19. W. S. Klug, R. F. Bruinsma, J.-P. Michel, C. M. Knobler, I. L. Ivanovska, C. F. Schmidt and G. J. L. Wuite, Phys. Rev. Lett., 2006, 97, 228101.

20. P. A. Suci, M. T. Klem, T. Douglas and M. Young, Langmuir, 2005, 21, 8686.

21. A. R. Patel and C. W. Frank, Langmuir, 2006, 22, 7587–7599.

22. F. Hook, B. Kasemo, T. Nylander, C. Fant, K. Sott and H. Elwing, Anal. Chem., 2001, 73, 5796.

23. P. Ceres and A. Zlotnick, Biochemistry, 2002, 41, 11525.

24. I. L. Ivanovska, P. J. de Pablo, B. Ibarra, G. Sgalari, F. C. MacKintosh, J. L. Carrascosa, C. F. Schmidt and G. J. L. Wuite, Proc. Natl. Acad. Sci. U. S. A., 2004, 101, 7600–7605.

CHAPTER 3

COMPARATIVE ANALYSIS OF ADENO ASSOCIATED VIRUS CAPSID STABILITY AND DYNAMICS

Contribution of Authors and Co-Authors

Manuscript in Chapter 3

Author: Vamseedhar Rayaprolu

Contributions: Optimized and established the method, collected and analyzed data, prepared the manuscript

Co-Author: Shannon Kruse

Contributions: Collected and analyzed data

Co-Author: Navid Movahed

Contributions: Analyzed and developed data analysis strategies, aided in critical discussions of the manuscript

Co-Author: Tim Potter

Contributions: Established protocols and collected preliminary data

Co-Author: Balasubramaniam Venkatakrishnan

Contributions: Prepared samples, collected and analyzed data, participated in critical discussion of the manuscript

Co-Author: Bridget Lins

Contributions: Prepared samples and participated in discussions of the data

Co-Author: Antonette Bennett

Contributions: Prepared samples and participated in discussions of data

Contribution of Authors and Co-Authors - Continued

Co-Author: Robert McKenna

Contributions: Participated in critical discussion of the data and manuscript

Co-Author: Mavis Agbandje-McKenna

Contributions: Obtained funding, discussed the results and implications and edited the manuscript.

Co-Author: Brian Bothner

Contributions: Obtained funding, discussed the results and implications and edited the manuscript.

Manuscript Information Page

Vamseedhar Rayaprolu, Shannon Kruse, Navid Movahed, Tim Potter, Balasubramanian Venkatakrishnan, Bridget Lins, Antonette Bennett, Robert McKenna, Mavis Agbandje-McKenna, and Brian Bothner

Journal: Journal of Virology

Status of Manuscript: (Put an x in one of the options below)
____ Prepared for submission to a peer-reviewed journal
_x__ Officially submitted to a peer-review journal
____ Accepted by a peer-reviewed journal
____ Published in a peer-reviewed journal

Publisher: American Society of Microbiology

Date of Submission: 12/27/2012

CHAPTER 3

COMPARATIVE ANALYSIS OF ADENO ASSOCIATED VIRUS CAPSID STABILITY AND DYNAMICS

Abstract

Icosahedral viral capsids are obligated to perform a thermodynamic balancing act. Capsids must be stable enough to protect the genome until a suitable host cell is encountered, yet be poised to bind receptor and initiate cell entry, navigate the cellular milieu, and release their genome in the appropriate replication compartment. In this study, closely related serotypes of Adeno Associated Virus (AAV) have been used to compare physical properties of the capsids that influence the thermodynamic balance of virions. A series of experiments that address the stability and dynamics of AAV1, AAV2, AAV5, and AAV8 capsids are reported. Thermal stability measurements using differential scanning fluorometry, differential scanning calorimetry, and electron microscopy showed that capsid melting temperatures differed by more than 20 °C from the most stable, AAV5, to the least stable, AAV2. Limited proteolysis and peptide mass mapping of intact particles were used to investigate capsid protein dynamics. Dynamic hot spots mapped to the region surrounding the 3-fold axis of symmetry for all serotypes. Surprisingly, cleavages also mapped to the unique region of VP1 which contains the phospholipase domain and is believed to be internalized before receptor binding. These results are a starting point for the characterization of particle integrity, thermal and thermodynamic stability, as well as functional implications of conformational dynamics. Knowledge of the biophysical

properties of different AAV serotypes is an important factor in understanding cellular trafficking and is critical to the production, storage, and use for gene therapy.

Introduction

The capsids of icosahedral viruses are complex supramolecular structures that display multifunctional attributes in the viral life cycle. Depending on the virus type, capsid viral protein (VP) functions include receptor binding, cell entry, intracellular trafficking, genome release, capsid assembly, and genome packaging. Additional selective pressure on VPs can also arise from the host immune response. Several small non-enveloped icosahedral viruses, including the ssDNA packaging *Parvoviridae*, have a capsid that is composed of essentially a single multifunctional VP (35). Adeno-associated virus (AAV) serotypes belong to the *Dependovirus* genus of the *Parvoviridae*. They successfully replicate only in the presence of a helper virus, such as *Adenovirus* or *Herpesvirus* (2, 63) and have distinct capsid-associated tissue specificities and strict host ranges (1, 29). Twelve distinct human and non-human primate AAV serotypes (AAV1-12) have been isolated to date and more than 100 AAV genomes have been identified using PCR (28, 29, 61, 80, 81). These viruses have been classified into eight clades and clonal isolates (AAV1/AAV6, AAV2, AAV2/AAV3, AAV4, AAV5, AAV7, AAV8, and AAV9) based on VP sequence and antigenicity (1, 29) .

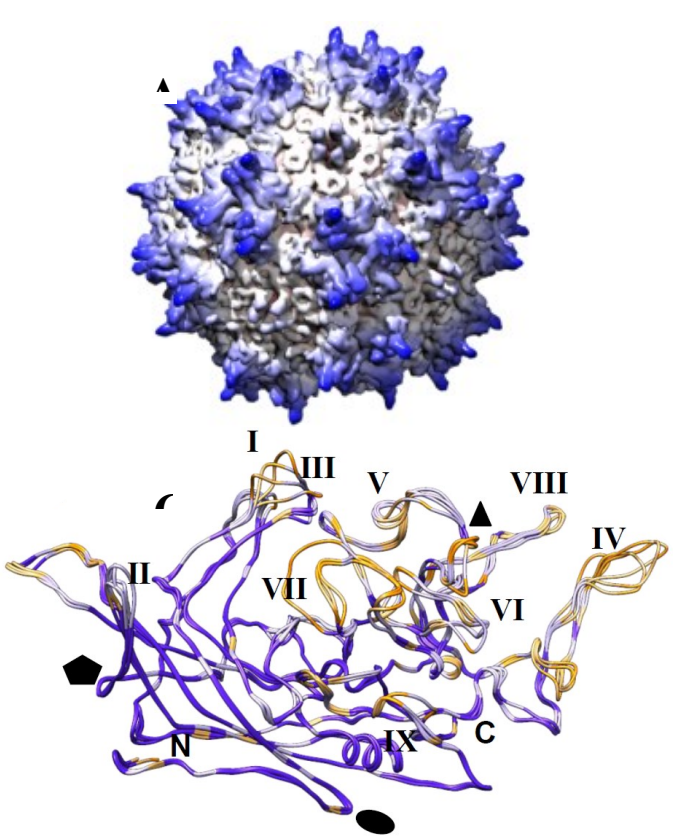
The AAVs have shown significant promise as vectors for gene delivery for the correction of monogenetic defects. They possess the following positive attributes; do not cause disease, have a stable virus particle that can be purified by industry-accepted methods

used for recombinant protein products, can be produced void of viral coding genes, can transduce dividing and non-dividing cells, and they can induce long-term transgene expression in certain cell types (59, 93). The majority of gene therapy applications to date have used AAV2, including the treatment of blindness in patients with Leber's Congenital Amaurosis (55, 59). Interest in the use of other serotypes (AAV1, AAV5, AAV6, and AAV8 for example) is growing because of their different tissue specificities, cell transduction efficiencies, and antigenicity (19, 21, 28, 29, 59). AAV2 has also received the most attention with respect to dissecting the mechanisms of cellular entry and trafficking. For this serotype attachment to the host cell surface is mediated by heparan sulfate proteoglycans (HSPG) (46, 52, 69, 90) and several secondary or co-receptors have been reported to mediate entry via dynamin dependent clathrin mediated endocytosis (3, 5, 45, 74, 82, 88, 89). AAV2 may also enter cells via a dynamin and clathrin-independent route (68). HSPG have been found to bind AAV3 strains B (51) and H while receptor binding of strain H extends to Heparin and Fibroblast growth factor receptor -1 (9) in addition to HSPG. Linkage specific sialic acid binding is utilized by AAV1, AAV4, AAV5 and AAV6 (44, 96, 100). For AAV5, platelet derived growth factor receptor has been identified as the glycoprotein receptor (72). A terminal glycan receptor has yet to be identified for AAV8, while it has been reported to utilize the 37/67-kilodalton laminin receptor for cellular transduction (3). AAV9 shares ~85% sequence similarity with AAV8 and also utilizes the laminin receptor (3, 83) as well as N-linked glycans with terminal galactosyl residues. Lastly, AAV7 which shares ~88% sequence similarity with AAV2 and AAV8, has yet to be associated with a specific receptor.

AAV capsids have T=1 icosahedral symmetry and are approximately 250Å in diameter (Figure 1A**)**. Their relatively small capsid size limits their genome to ~4.7 kb with two open reading frames, *rep* and *cap*. The *rep* orf encodes four replication proteins required for genome replication and packaging. The *cap* orf encodes for three structural VPs, VP1, VP2, and VP3, made from alternately spliced mRNAs (93). The proteins overlap with common C-termini. VP3 is ~61 kDa and constitutes 85% of the capsid's protein content. The less abundant capsid proteins, VP1 (~87 kDa) and VP2 (~73 kDa), contain unique N-terminal extensions containing a phospholipase A2 (PLA2) domain (VP1 N-terminal region, VP1u) and nuclear localization signals (VP1/2 common region), respectively (85). A total of 60 copies of the three VPs, in a ratio of 1:1:8/10 (for VP1:VP2:VP3) based on gel densitometry (15, 77), form the T=1 icosahedral viral particle (20). During AAV entry, it is believed that exposure to acidic conditions in endosomes leads to a conformational change and exposure of the VP1u and VP1/2 common regions (85). Interaction with cellular proteases and pH activated autohydrolysis have also been implicated in the entry process (79). In vitro studies typically use a heat pulse as a surrogate for cellular triggers of VP1u and VP1/2 externalization although characterization of capsids after heating has primarily been limited to antibody detection and electron microscopy (EM) studies (10, 73, 85, 92).

The capsid structures of nine clade and clonal isolate representative AAV serotypes have been determined by cryo-electron microscopy and/or X-ray crystallography (33, 51, 65, 67, 95, 101) and Govindasamy and Agbandje-McKenna, unpublished data). In all cases, the subunits have a conserved eight-stranded β-barrel (βB-βI) and a-helix (αA) core

which forms the contiguous capsid with loop regions inserted between the strands of the core β regions (Figure. 1C). Structural studies and mutational analyses of AAVs have identified differences on the surface of capsids that localize to common variable regions (VRs) (Figure 1C and 1D involved in receptor binding, host tropism, and antigenic determinants (reviewed in 1, 2, 17, 30). Sequence differences can be minor, as in the case of AAV1 and AAV6, which differ by only 6 out of 736 amino acids (0.8%), yet lead to functional changes in receptor binding affinities and transduction rates (98). Larger differences also exist, such as between AAV5 and AAV1 which share only 58% amino acid sequence (Figure 1D). This study focused on the biophysical characterization of virus like particles (VLP) for four AAV serotypes, AAV1, AAV2, AAV5, and AAV8. These viruses were selected because they are from four different clades and represent a range of sequence and structural diversity (Table 1) across the eight antigenic clades and clonal isolate groups. Complimentary thermal stability assays using differential scanning fluorescent dye binding (DSF), differential scanning calorimetry (DSC), and negative stain electron microscopy revealed that the temperature at which capsid degradation occurred differed among the serotypes, with AAV5 being the most stable with a melting temperature (T_m) that was ~5, ~20, and ~17°C higher than AAV1, AAV2, and AAV8, respectively. Protein dynamics, assessed by limited proteolysis, showed that each serotype has a specific proteolytic profile, yet the most dynamic region of the capsid in all cases clustered around the icosahedral 3-fold axes of symmetry reported to play a role in receptor attachment for AAV2 and AAV8 (3, 46, 52, 57, 65, 69). Proteolysis was also observed in the VP1u region,



Sequence identity of AAVs	
AAV1 : AAV2	83%
AAV1 : AAV5	58%
AAV1 : AAV8	84%
AAV2 : AAV5	58%
AAV2 : AAV8	83%
AAV5 : AAV8	58%

Figure 1. Structure and conservation of Adeno-associated viruses. A) Surface topology of AAV2 T=1 particle (left). Blue indicates peaks, white shows the valleys. B) Shows an icosahedral grid overlayed on depth-cued structural model of AAV2 with 2- (oval), 3- (triangle), and 5-fold (pentagon) axes indicated in black. Four subunits are shown in different colors. C) Superimposition of Cα positions of the VP3 monomers of AAV1, AAV2, AAV5, and AAV8. Amino acid sequence conservation is shown in the color scheme, purple highest, gold lowest. The core of the subunit is highly conserved with the sequence variability being localized primarily to loops I-IX. The N and C termini are also indicated. The triangle, pentagon and oval indicate the position of the 3-, 5- and 2-fold axes. D) The table shows the sequence identity between serotypes. Data obtained from multiple sequence alignment of AAV1, AAV2, AAV5 and AAV8 using ClustalW.

including the PLA2 domain. The detection of protein dynamics in VP1u and the receptor binding region is consistent with models that have been developed for other icosahedral viruses in which functional VP domains are dynamic and that internal domains can be transiently exposed on the capsid surface.

Materials and Methods

Virus-like Particle Production and Purification

Recombinant baculovirus encoding VP1, VP2, and VP3 of AAV1, AAV2, AAV5, and AAV8 were generated using the Bac-to-Bac expression system (Invitrogen, cat#10359-016). The virus-like particles (VLPs) of each virus was expressed in sf9 cells and purified according to previously established protocols (22, 47, 50, 58). AAV2 was purified using a step iodixanol gradient followed by anion exchange chromatography (56, 106), and AAV1, AAV5, and AAV8, were purified on a sucrose cushion followed by a step sucrose gradient (22, 47, 50, 58). The pellets were resuspended in lysis buffer (50mM Tris-HCl, pH8.0, 100mM NaCl, 1mM EDTA, and 0.2% Triton X-100) and freeze/thawed three times in a dry ice-ethanol slurry and 37°C water bath with the addition of 1 µL of Benzonase (Sigma, cat#E1014; 50 U/ml final concentration) and incubated at 37°C for 30min after the second freeze/thaw cycle. The crude cell lysate was clarified by centrifugation at 12,100 x g at 4°C for 15 min. For AAV2, the clarified supernatant was loaded onto a discontinuous 15-60% iodixanol (Optiprep) step gradient (Nycomed, cat#1114542), and centrifuged at 350,000 x g at 18°C for 1 hr and the gradient fractionated. The 25% iodixanol gradient fraction, enriched with AAV2 VLPs, was further purified on a 5ml HiTrap Q anion exchange column (GE Healthcare, cat#17-5159-01). The sample was diluted with Buffer A (20Mm Tris-HCl, 15mM NaCl, pH8.5), loaded onto the column, washed with 50 ml of Buffer A, eluted with a gradient of 30 ml of Buffer A and Buffer B (20 Mm Tris, 15 mM NaCl, pH 8.5), and the peak fractions collected. The cell lysates of AAV1, AAV5, and AAV8 were pelleted by ultracentrifugation at 149,000 x g at 4°C for 3

hr through a 20% sucrose [wt/v] cushion in TNET buffer (25 mM Tris-HCl pH 8.0, 100Mm NaCl, imM EDTA, 0.06% Triton X-100). The pellets was resuspended in TNTM buffer (25 mM Tris-HCl pH 8.0, 150 mM NaCl, 2 mM $MgCl_2$, 0.06% Triton X-100) at 4°C O/N. The samples were loaded onto a 5-40% sucrose [wt/v] gradient and ultracentrifuged at 151,000 x g at 4°C for 3 hr. The visible blue band (under a white light) at the 20-25% sucrose layer were extracted and dialyzed into 20 mM Tris-HCl, pH 7.5, 150 mM NaCl. The purity and integrity of the VLPs were monitored using Coomassie stained SDS-PAGE and negative-stain electron microscopy (EM) on a JEOL JEM-100CX III microscope. An AAV2/8 vector packaging the gene for green fluorescent protein driven by a CMV promoter (AAV2/8.CMV.EGFP) obtained as a gift from the PennVector Core (Dr. James Wilson,U. Pennsylvania) was also used for studies below.

Differential Scanning
Fluorescence (DSF) Stability Assay

AAV VLP samples were diluted into PBS (20mM Na_2HPO_4, 20mM NaH_2PO_4, 150mM NaCl, 2mM $MgCl_2$) pH 7.0 at 25°C. PBS was selected because the pH of the buffered solution has low temperature dependence. Experiments were also conducted with Citrate-Phosphate buffer, pH 7.0 and there was no change in the reported T_m. T_m was defined as the maximum value of the first derivative (dF/dT) from the raw signal. Assays were run with protein concentration of 0.1- 0.24 mg/mL. To each sample, 2.5 µL of 1% Sypro-Orange dye (Invitrogen Inc. S6651) was added to bring the final volume of each reaction to 25 µL. The assays were conducted in a qPCR instrument (Corbett Research, RG-3000) temperature ramping from 30-99 °C, increasing 0.1 degrees every 6 seconds. To

verify that the data obtained for the VLPs are consistent with virus particles with packaged DNA, an AAV2/8.CMV.EGFP vector was also used in the Sypro-Orange dye binding assays. A control sample of lysozyme, at a concentration of 0.24 mg/ml, was included in each run as a positive control. The lysozyme T_m was calculated to be 67 °C, with a maximum fluorescence at 74°C.

Differential Scanning Calorimetry (DSC)

AAV VLP samples were dialyzed into PBS (as above) at pH 7.3 as the final buffer which also served as the reference. The AAV samples were run at 0.24-0.7 mg/mL. Triplicate assays were conducted in a VP-DSC instrument (MicroCal), with buffer and sample loaded in two different chambers, with temperature ramping from 10 to 100°C at a scan rate of 60°C/hr. The thermal scans were plotted and analyzed using the Origin software suite (Origin Lab). The triplicate scans were averaged to improve the signal to noise ratio. Averaged data was used to calculate standard deviations, which provided error values.

Electron Microscopy

Samples were diluted to a working concentration of 0.1mg/mL into PBS, pH 7. Ten microlitres of each sample was heated to 37, 45, 55, 65, 75, 85, 95 °C for 3 minutes each using a thermal cycler. Five microlitres of each sample, after cooling down to RT, was applied to a carbon coated copper grid, stained with 2% uranyl Acetate and viewed using a Transmission Electron Microscope (a LEO 912 with a 2K X 2K CCD camera) at 31,000

X magnification. Experiments were repeated three times using VLPs from different preparations.

Proteolysis and Peptide Mapping

Proteinase K reactions to compare rates of proteolysis of the AAV VLPs were carried out in 100 mM Tris-HCl pH 7.4, 100 mM NaCl, at a final concentration of 0.2 mg/mL and 0.07 mg/mL of VLP and enzyme, respectively. This equates to 43.5nM of VLP and 2.45μM of enzyme, ~ approximately a1:1 molar ratio of VP to protease. Protein and enzyme were incubated at 37°C and aliquots were removed for analysis by SDS-PAGE, using gradient gels (4-20%) with a Tris buffer system (192mM Tris-base, 25mM Glycine, 3.4mM SDS, pH 8.0). Protease was inactivated by rapid heating in 2X standard gel loading buffer. Cleavage site mapping experiments were conducted using trypsin and thermolysin which have high specificity. VLP and enzyme concentrations were 0.2 mg/mL and 0.01 mg/mL, respectively. Reactions were conducted at 25°C and were stopped by spotting onto a MALDI plate with alpha cyano or sinapinic acid matrixes at time points 5, 10, and 20 min.

Results

Stability of AAV Capsids

To obtain information on AAV capsid stability two thermal denaturation assays, DSF and DSC, were run. DSF uses a hydrophobic dye that increases fluorescence intensity upon binding to hydrophobic pockets in proteins that become accessible during heating (102). Thermal denaturation curves for each of the AAV serotypes were recorded using

DSF (Figure 2). Differences between the serotypes were evident both in their T_m and the shapes of the curves. AAV2 was the least thermally stable, having a T_m of 69.6 $\pm$ 0.5 °C followed by AAV8, AAV1, and AAV5 at 72.5 ± 0.5, 84.5 ± 0.8 and 89.7 ± 0.7°C , respectively. Transitions over a narrow temperature range such as with AAV2, AAV5,

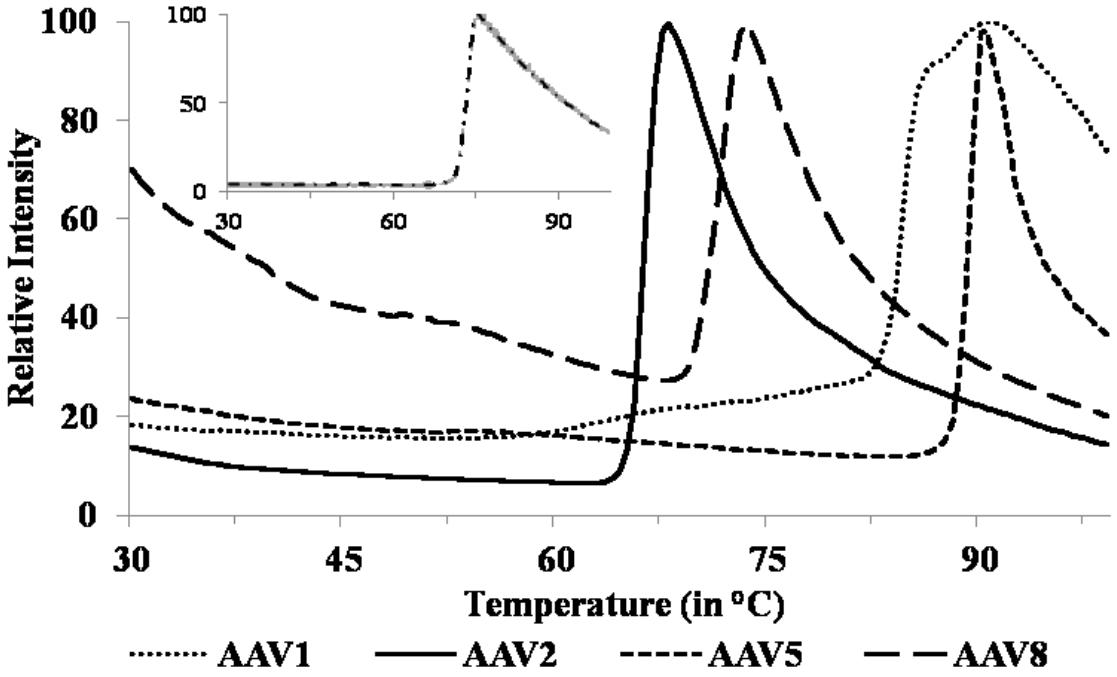


Figure 2. Temperature dependence of fluorescent dye binding. Measurements of fluorescence intensity during heating show that AAV serotypes denature at different temperatures. Increases in intensity are associated with binding of Sypro orange into hydrophobic pockets that become accessible as the protein unfolds. Data shown are the normalized average of three temperature scan experiments. Data was collected at pH 7. Inset: Representative image showing AAV2/8 with error bars.

and AAV8 are indicative of cooperative protein unfolding, whereas the double peak observed for AAV1 shows a biphasic response. T_m was also determined using DSC and were 67.8 ± 0.2 AAV2, 74.7 ± 0.4 and 79.1 ± 0.3 (double-peak) AAV8, 84.4±0.2 AAV1, 89.6±0.1 °C AAV5. The values were within 2°C for the different techniques, expect for

AAV8 which had a double peak in the DSC profile (not shown), again suggesting biphasic behavior in response to thermal denaturation. A last measurement was taken to determine the effect of genome packaging on capsid stability. AAV8 particles harboring a therapeutic gene were analyzed in the DSF assay. The T_m of these genome filled AAV2/8 particles were 74.5 ± 0.5 °C, an increase of 2°C over the AAV8 VLP. This change in stability is consistent with data on *Cowpea chlorotic mottle virus* (CCMV) and *Flockhouse Virus* where nucleic acid and other negatively charged cargo have been shown to stabilize authentic icosahedral virions (13, 76). The DSF and DSC results both showed a relatively large range in thermal stabilities for AAV serotypes. Since temperature is often used to induce exposure of VP1u and initiate lipase activity, we were interested in correlating Tm with particle integrity.

Visualization by negative-stain EM is a suitable method for studying protein complexes and can be used to detect structural differences in virus particles due to changes in protein conformation (8, 27) and particle integrity. A heat pulse of 3 min at different temperatures was used for the AAV investigation because this is the standard treatment used to externalize the VP1u and VP1/VP2 common region of AAV particles in lipase assays and antibody screens (85, 97). At 37°C, there was no evidence of particle clumping or degradation for any of the AAV serotypes (Figure 3). AAV2 was the most sensitive to heating. Particles remained intact, but showed signs of aggregation at 65°C and no particles were observed at 75°C. The AAV8 particles were intact and non-aggregated up to 65°C, but were also absent at 75°C. Particles of AAV1 and AAV5 remained intact and non-aggregated up to 75°C and 85°C, respectively. This experiment revealed a clear differential

thermal stability of the AAVs analyzed. The loss of capsid integrity observed in the post heating electron micrographs correlated with the DSF and DSC data (Figure 3).

Two factors that contribute to capsid stability, and in general to the stability of protein complexes, are subunit contact energies (23, 105) and free energy of subunit folding (6). To investigate the contribution of these factors to AAV capsid stability, subunit association energies and buried surface area for each of the AAVs were compared. Values for each unique icosahedral interface were obtained from the VIPER database (17) from which values for whole capsids were computed (Table 2).

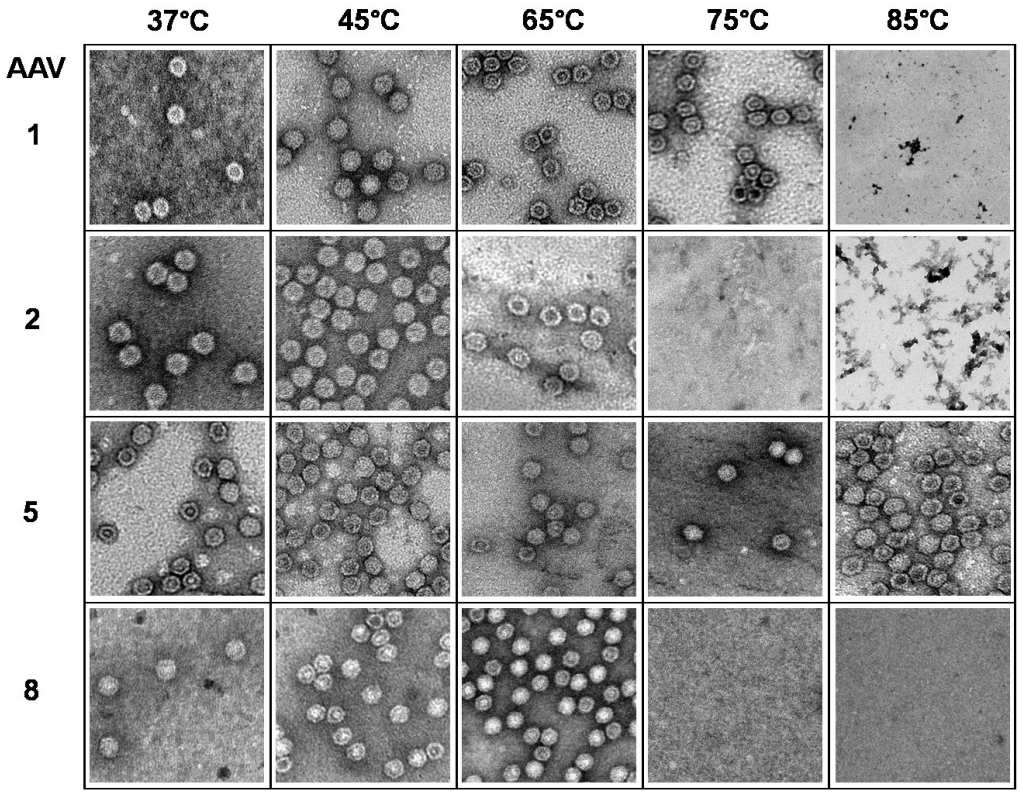


Figure 3. Thermal stability of AAV particles after heating. AAV capsids were heated at 37, 45, 65, 75 and 85°C for three minutes and then analyzed by negative stain electron microscopy. Representative images at 31K magnification show a serotype dependence to the temperature at which morphological changes, including complete disruption, occur. Heating experiments were repeated 3 times using particles from different virus preparations.

No correlation between T_m and buried surface area, association energy, or a combination of the two was evident. For example, AAV5 which had the highest T_m has lower values for both buried surface area and association energy than either AAV2 or AAV8. The lack of a correlation between solution phase properties and crystal structure contact data is consistent with studies looking at particle assembly (65) and uncoating in solution. A factor missing in this analysis is conformational plasticity. If AAV serotypes had different levels of protein dynamics, this could influence the observed T_m and the information would not be reflected in the contact tables.

Table 1. Subunit contact energies as calculated by VIPER (virus particle explorer). Viruses are listed from top to bottom with increasing association energy. Figure 1 shows subunit interfaces which were used to calculate the data in the table. Also shown in the table is the total association energy for each of the capsids calculated from the subunit interface values.

	AAV1	**AAV2**	**AAV5**	**AAV8**
	Association energies (in kcal/mol)			
2-fold	-56.5	-63.4	-50.1	-72.9
3-fold	-214	-213.2	-211.6	-213.3
5-fold	-95	-100.1	-99.4	-103.6
Total Capsid	-21930	-22602	-21666	-23388
	Buried surface area (in nm^2)			
2-fold	27.5	30.5	26.3	34.4
3-fold	103.4	103.5	99.3	103.4
5-fold	48.2	49.4	49.1	51.3
Total Capsid	10758.5	11016.72	10492.2	11356.14

Capsid Protein Dynamics

Inspired by the differences in the response of AAVs to temperature, limited proteolysis experiments (12, 39, 71) to characterize solution-phase dynamics of less folded or exposed regions of the capsids were initiated. For this reason Proteinase K, which has low sequence specificity, was used in the initial comparison of the AAV serotypes. Our interest was in the initial cleavage events, when the majority of capsid protein was intact. Time course reactions of each AAV serotype with protease were analyzed by SDS-PAGE after 10, and 60 minute incubations with Proteinase K (Figure 4). AAV1 and AAV2 produced a stable band at ~55kDa that was absent in AAV5 and AAV8, while AAV2 and AAV5 had a stable band at ~33kDa and a slightly larger product (~37kDa) was seen with AAV8. These bands are composed of well-folded domains that have had flexible regions trimmed away. The significant point is that the different band patterns show that each serotype has a unique landscape of relative dynamics, which is consistent with a report that trypsin and chymotrypsin could distinguish AAV2 from AAV1 and AAV5(92). The Van Vliet study also demonstrated that proteolytic digestion of AAV2 virions with trypsin was highly specific and did not cause immediate degradation of the particles. Densitometry of the intact VP3 in each lane of the gel confirmed the visual differences in the amount of protein remaining (Figure 4). VP3 of AAV1 and 2 were hydrolyzed most rapidly, with only ~60% remaining after 60 minutes. AAV5 and 8 were hydrolyzed more slowly with > 80% remaining after exposure to the protease for 60 minutes. Therefore, there was no straight-forward relationship between thermal stability and overall capsid dynamics.

To identify the dynamic regions of the VPs, the limited proteolysis experiment was repeated using trypsin and chymotrypsin. These proteases have higher specificity than

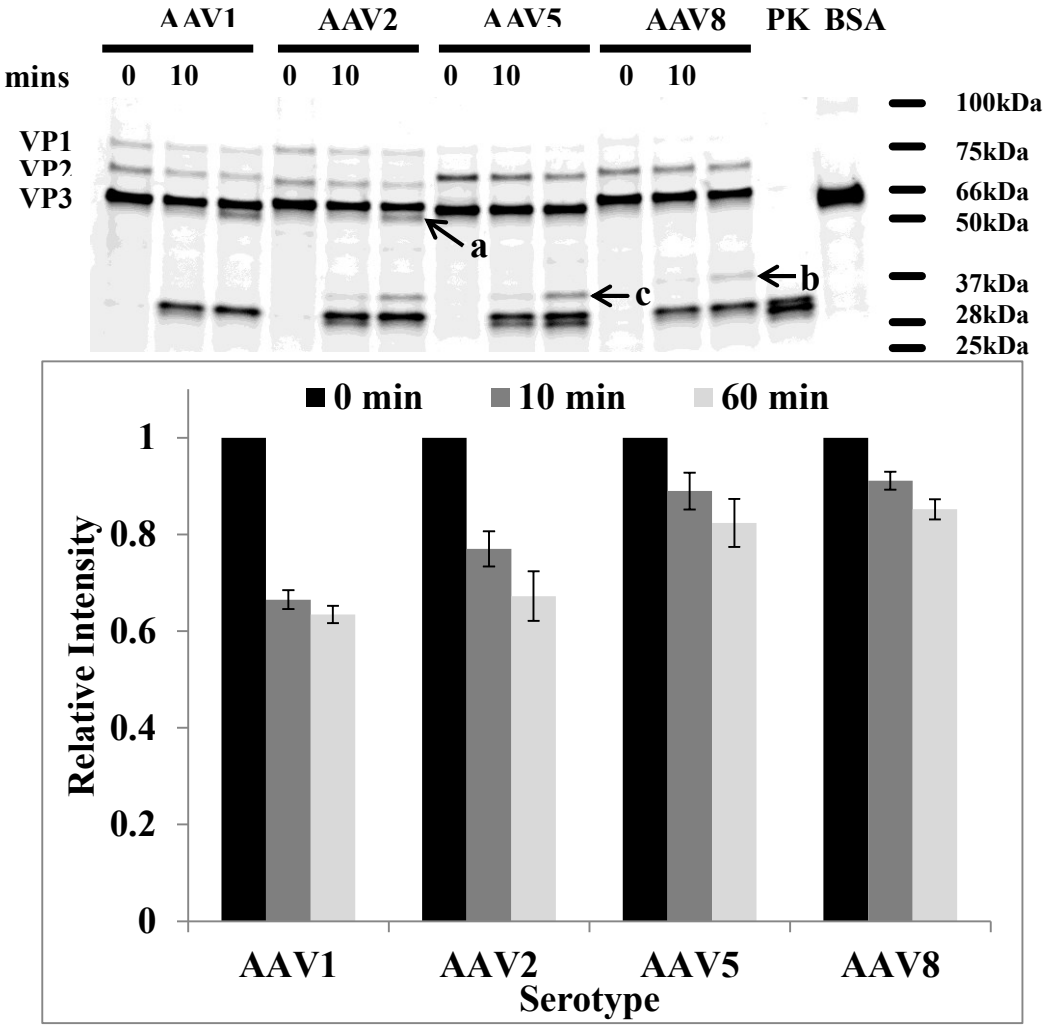


Figure 4. Proteolysis of AAV serotypes monitored using SDS-PAGE. The top panel shows the SDS-PAGE gel for the 4 serotypes, Proteinase K (PK), and BSA going from left to right. Each serotype was subjected to Proteinase K treatment at three time points (0, 10, and 60 mins) as marked on the wells. Bands marked a, b, and c have molecular weights of 55 kDa, 37 kDa, and 33 kDa respectively. The bottom panel shows a graphical representation of the proteolytic trends of the 4 serotypes observed on the gels with the X-axis being the time and Y-axis, the relative intensity.

proteinase K which greatly simplifies unequivocal identification of cleavage sites using mass spectrometry. Using the data from the trypsin experiment, the cleavage sites mapped primarily to the VP1u and common VP3 domains (Table 1). As presented, residues in the same row in Table 1 are analogous across serotypes. The cleavage sites shown represent less than 25% of the possible positions for proteolysis, with lysine and arginine residues being distributed throughout the VP in each serotype (Figure S2). The first significant point revealed in Table 1 is that the majority of the sites were common with at least one other serotype (also see Table S1). The second point is that the VP1u region of AAV2 has fewer cleavage events than the other serotypes; whereas the C-terminal end of AAV5 (residues 484-724) had no cleavage. This data is consistent with the one other study to map exogenous protease sites on AAV2, with residues 566, 585, and 588 being among the very first sites to be cleaved (92).

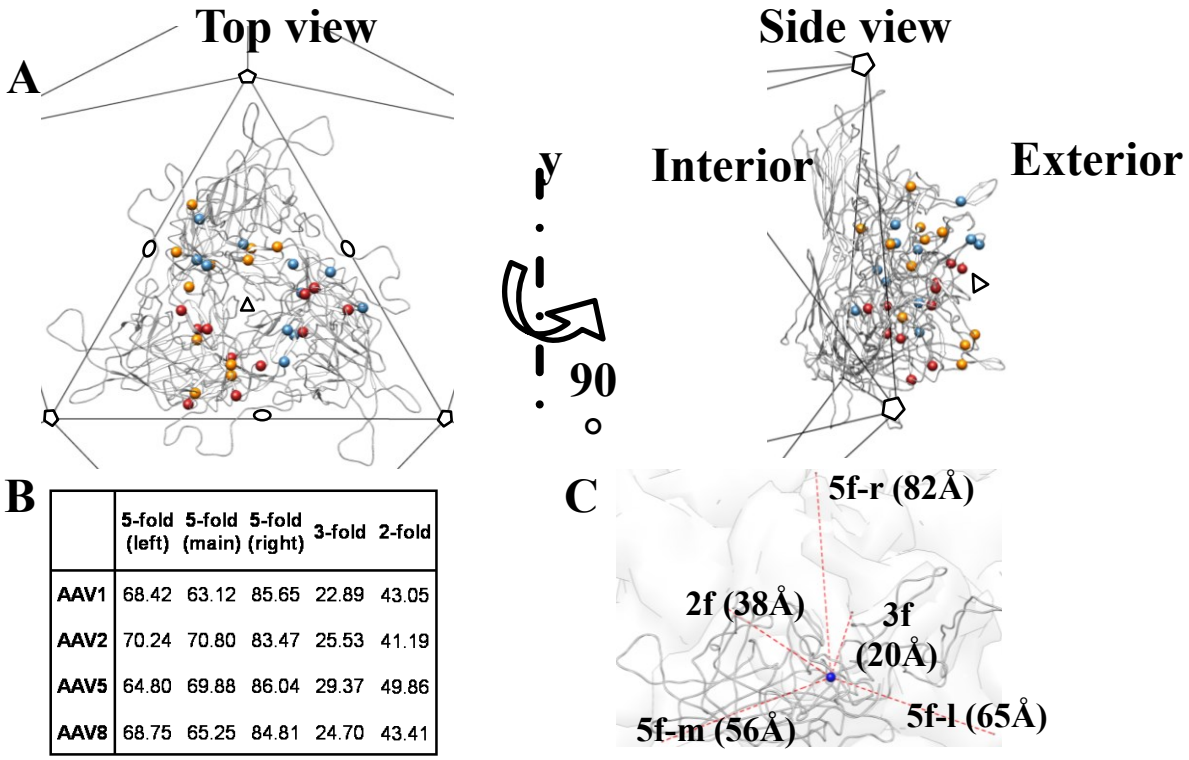
To initiate a structure/function analysis of the dynamic regions of the VP identified with proteolysis, the location of the cleavage sites were mapped on to the structural models of the particles. A close up of AAV2 highlights the cleavage sites as shown in Figure 5A, and had the same general pattern on VP3 in all serotypes (Figure S2) Across the 4 serotypes, a number of these residues were located in the structurally variable regions (see Figure 1C) and this information is listed in Table 1. A second category of residues were located below the surface loops. This included AAV1 476, 567; AAV2 475, 566, 609, 620; AAV5 235; and AAV8 435. Visual inspection suggested that the sites clustered on the protrusions that surround the icosahedral 3-fold axes and known receptor binding sites (Figure 5C and Movie S1). For example, residues 585 and 588 in AAV2 are critical for

N-term

AAV1	AAV2	AAV5	AAV8	VRs and motifs	
-	*39.K*	-			
-	-	*42.R*	-	1	
51.K	51.K	-	-	2	
61.K	-	60.R	61.K		
-	-	-	*77.K*		VP1
84.K	-	-	-		
92.R	-	91.K	92.R	3	
103.R	-	102.K	103.R		
116.R	-	115.K	116.R		
122.K	-	121.K	-		
123.K	-	-	-		
142.K	-	143.R	142.K		VP2
-	-	153.K	152.R		
161.K	-	-	-	4	
-	-	***235.R, 248.R***	-		
-	-	425.K	435.R		
-	-	***437.R***	-		
-	-	-	***450.R***		VP
-	-	***451.K, 456.R***	-	IV	
-	***459.R***	-	-	IV	
476.K	475.R	462.K	478.K	IV	
485.R	-	471.R	-		
-	-	***483.R***	-		
-	-	-	***490.R***	V	
491.K	-	-	-	V	
-	507.K	-	510.K		
-	513.R	-	516.R		
-	532.K	-	535.R	VI	
545.K	544.K	-	547.K	VII	
567.K	566.R	-	-		
576.R	-	-	-		
-	***585.R, 588.R***	-	-	VIII	
-	609.R	-	612.R		
621.K	620.K	-	623.K		

C-term

Table 2. Numbers in bold type are present in the structural models and are highlighted in Figure 5, others are in the VP1/VP2 N-terminal domains. Residues unique to one serotype are italicized. The residue name is indicated after each residue number where R = Arginine K = Lysine. Motifs predicted by Popa-Wagner et al, 2012 to be functionally important are labeled 1. Sorting signal (dileucine motif); 2. Sorting signal (YXXΦ); 3. SH2-binding domain; and 4. FHA-binding domain. Residues in VRs are indicated with roman numerals.



	5-fold (left)	5-fold (main)	5-fold (right)	3-fold	2-fold
AAV1	68.42	63.12	85.65	22.89	43.05
AAV2	70.24	70.80	83.47	25.53	41.19
AAV5	64.80	69.88	86.04	29.37	49.86
AAV8	68.75	65.25	84.81	24.70	43.41

Figure 5**.** A) The top and side views of 3 subunits of AAV2 VP3 with proteolytic residues of each subunit marked with a different color. The hollow black symbols indicate the approximate symmetry fold axis. B) A table with the average distance of each of the residues shown in (A) from each icosahedral symmetry axes. C) A representative image of the icosahedral symmetry axes, 2f, 3f and 5f (l-left, r-right, m-main) and the approximate distances of a representative residue 609 of AAV2 from each of these axes.

heparan sulfate recognition (46, 52, 69), transduction efficiency, and tissue tropism (98). Distance measurements from the sites of cleavage to the 2,3, and 5-fold axes confirmed that the residues clustered near the 3-fold axes at an average distance of ~25Å (Figure 5B). These observations establish the protrusions surrounding the 3-fold as a dynamic region and indicate that the protein motion within this capsid region is sufficient to translocate buried residues to the surface. The third category of cleavage sites mapped to the VP1u and VP1/VP2 common regions which are not ordered in any of the crystal structures. These

domains are believed to be internalized at least until the entry process begins (49, 85). It is important to note that the cleavage locations shown in Figure 5 represent the initial ~10-20% of the cleavage reaction (80-90% of VP3 remained intact), which corresponds to less than 10 minutes for the reactions shown in Figure 4. The particles also remain intact, which is consistent with the report by Van Vliet(4, 92), and similar experiments conducted on canine parvovirus (66).

Discussion

Structural virology has been a cornerstone for understanding virus particle assembly, receptor binding, and cell entry ever since the model for quasi-equivalence was put forth (18). Slowly, it became evident that in addition to structure, dynamics is an integral part of VP function (12, 25, 26, 32, 39, 43, 48, 49, 52, 92). This study has focused on characterizing the solution phase properties of four AAV serotypes for which high-resolution structures are available. A premise behind this work is that structural differences and sequence variations between the serotypes could be related to differences in the solution phase properties that were targeted by the described experiments. What they revealed was that broad similarities were punctuated by specific differences between serotypes. For example, the region surrounding the 3-fold axes of symmetry was dynamic in all of the serotypes, while the VP1u domain of AAV2 appeared to have less surface exposure than in the other serotypes. Capsid melting temperatures varied by greater than 20^{o}C as well. We believe that the observed differences in capsid VP stability and dynamics evolved to take advantage of different entry pathways and expand tissue tropism. In

addition to highlighting biological differences, biophysical studies can direct the use and development of serotypes with high stability to improve production AAV for therapeutic uses, extend the shelf life of vectors, and enhance transduction efficiency.

Thermal denaturation of assembled capsids monitored by DSF, DSC, and EM showed that the melting temperatures between the least and most stable serotype differ by more than 20°C. We are unaware of similar data for other viruses that are naturally occurring variants in a population. The differences cannot be accounted for simply by changes in amino acid sequence, as AAV 5 is equally different from AAV1, AAV2, and AAV8. Thermal disassembly of a virus particle or any protein complex can be separated into at least two distinct events, disruption of subunit contacts and protein unfolding. Formation of a multimeric complex can add thermodynamic and thermal stability to proteins (40) and the stabilization provided by subunit-subunit contacts can raise the T_m of the complex significantly above the point where a monomeric subunit is stable. Hence, thermal denaturation curves for complexes may show only a single sharp transition, because once disassembly begins, unfolding of the monomers is rapid since they are well above their T_m. The DSF curves for AAV2, 5, and 8 have a sharp transition suggesting cooperative, two-state behavior. AAV1, on the other hand has a more complex DSF melting curve that is broader than the others, whereas AAV8 had a doublet by DSC. This could be a sign that under the conditions of assay, particle disassembly and subunit unfolding can be separated or that thermodynamically distinct particles were present. As reported here, DSF are a powerful method for relative and quantitative comparison of

capsid thermal stability, which is surprising, given that it has only been reported a few times (94, 103).

The DNA filled form of AAV2/8 begins the melting transition at a slightly higher temperature than the empty particles (~ 2ºC), followed by a more pronounced shift (~10ºC) after the point of maximum fluorescence. One explanation is that packaged nucleic acid has a relatively large effect on global capsid stability (downward slope, see inset Figure 2) while allowing for conformational transitions such as those associated with the externalization of VP1 and VP2 N-terminal domains (rising side of the curve). This interpretation is consistent with the structural models which show extensive interaction between the nucleic acid residues on the inner surface of the capsid and that specific conformational changes related to pH and endocytosis occur (64). The EM images served as a complementary approach to particle denaturation. The transition temperatures observed by DSF and DSC were consistent with visual loss of particle integrity from negative stain EM imaging.

Conformational changes are also occurring in each of the AAVs investigated before heating. This was shown in the limited-proteolysis experiments conducted at 25°C. Serotype dependent patterns of cleavage and susceptibility were evident upon proteinase K treatment (Figure 4). This extends previous work that showed it was possible to distinguish AAV1, 2, and 5 based on banding patterns using Trypsin and chymotrypsin (92). When used in limited proteolysis experiments, the relatively low sequence specificity of proteinase K minimizes sequence bias, emphasizing differences in the dynamic landscape of proteins. AAV1 and AAV2 are more rapidly digested based on the rate of

VP3 hydrolysis, indicating that they are more dynamic than AAV5 and AAV8 (39, 71). The different banding patterns across the serotypes show that subtle differences in the energy landscapes also exist.

Shifting to a highly sequence specific protease allowed the kinetically favored cleavage sites to be precisely mapped onto the protein sequence. The first sites of cleavage in VP3 by trypsin cluster around the 3-fold axes of symmetry with AAV5 having a different pattern (see Figure 5 and Table 1). Cleavages also map to the VP1u region and here AAV2 is the most different. Data from mutagenesis and structural studies localize the primary receptor binding site in AAVs to the region surrounding the 3-fold axis (3, 11, 52, 54, 69). Protein flexibility plays an important role in receptor binding for a wide range of viruses (25, 66, 84) and this experiment shows that the receptor binding regions of AAVs fit this model. Structural studies of AAV2 show that the binding of heparin induces a conformation change at the 3-fold and also distally at the 5-fold axes (52, 67). The proteolytic map also overlays with a recent cryo-EM reconstruction of AAV8 in complex with neutralizing antibodies, highlight the 3-fold region as an important antigenic determinant as well (34). Residues on the 3-fold protrusions of AAV8 also determine receptor binding and transduction efficiency (3, 34, 75). Cleavage sites near the 5-fold axis did not show up in our maps, indicating that this region is not highly dynamic under the conditions used. The 5-fold axis has been implicated in externalization of the VP1 PLA2 domain and genome release, both of which would require substantial remodeling of the 5 fold (24, 49). This suggests that the heparin induced conformational changes at the AAV2 5-fold must be triggered. Such a model is consistent with the idea that mature icosahedral

capsids are metastable complexes poised to initiate the entry process in response to an external trigger (8, 14).

The identification of cleavages on the VP1 and VP2 unique domains even though these particles have not undergone heat treatment has three possible explanations; i) VP1 is transiently exposed on the capsid surface, ii) a small population of broken particles are present, iii) proteolysis leads to externalization of VP1 N-terminus. Transient externalization of capsid protein domains that are buried in structural models is well documented in icosahedral viruses and is consistently linked with protein domains involved with cell entry (12, 26, 39, 104). This could explain the presence of cleavages in the VP1u region, but is contrary to immunoblotting data with monoclonal antibody A1 which indicates that the AAV2 VP1u cannot be detected unless particles have been heated or disrupted (49, 92). It is possible that the "native" orientation of externalized VP1u conceals the A1 epitope until heat treatment. With respect to option 2, aggregated or broken particles were not detected by size exclusion analysis of purified AAVs and because VP1 makes up less than 10% of the total protein, a significant percentage of capsids would need to be damaged for VP1 cleavages to be detectable in comparison to VP3. The third option is supported by data showing that cathepsins are important uncoating factors for AAV2 and 8. AAV2 VP3 cleavage by the endosomal proteases Cathepsin B and L can occur *in vivo* and *in vitro* (4). Consistent with our data, particles remain intact after cathepsin proteolysis and the products are serotype specific. The bands generated by in vitro exposure of AAV2 and 8 to Cathepsin L, closely match the major products of Proteinase K treatment at 33 and 37 kDa for AAV2 and 8, respectively after 10 and 60 minutes (Figure 4). The study by

Akache *et al*. went on to show that AAV5 did not interact with Cathepsin B or L, but likely relies on a different cellular protease. A band very similar in size to the Proteinase K product of AAV2 was present in AAV5 as well. In the experiments by van Vliet (92) trypsin and chymotrypsin fail to generate a stable band near that generated by Cathepsin or Proteinase K (92). It is tempting to speculate that Proteinase K cleavage is mimicking host mediated processing during endocytosis, however, there is another part to the story. Autohydrolysis of AAV VPs has recently been demonstrated (79). The appearance of degradation bands on SDS-PAGE gels as particles age is known to those that work with these viruses and has also been shown to occur with canine parvovirus as well (66). It now appears that the VPs have an active role in the generation of cleavage products. Together these results suggest a set of experiments to test the hypothesis that proteolysis is a trigger for externalization of VP1u as was also recently suggested based on the identification of a protease function in AAV2 (79).

We discovered through a series of complementary approaches that the thermal stability and capsid protein dynamics of AAVs are serotype specific. Previous studies have shown that these viruses have different tissue preferences and entry pathways (19, 28, 37, 99). The data presented here suggests that capsid stability and dynamics are likely to be important factors in navigation of entry pathways and tissue tropism. These results are also a starting point for the characterization of particle integrity, thermal, and thermodynamic stability, as well as conformational dynamics which together are the basis for establishing protocols that can be used to compare AAV serotypes, assess factors that affect particle integrity, and determine suitability of use in gene therapy (6). These findings raise

important questions about the relationship of structure to function well beyond AAVs and virus capsids while having specific implications for the efficacious development of AAVs as vectors and emphatically point out the functional complexity of virus capsids.

Acknowledgements

BB, MAM, and RM receive support from the National Institutes of Health (R01 AI081961-01A1 and the Center for Bio-Inspired Nanomaterials (Office of Naval Research grant #N00014-06-01-1016). The AAV1 and AAV5 structure determinations were supported by NIH R01 NIH R01 GM082946 to MAM and RM. We would like to thank the Murdock Charitable Trust and NIH Grant Numbers P20 RR-020185 and 1P20RR024237 from the COBRE Program of the National Center for Research Resources for support of the MSU mass spectrometry facility. SK received support from Montana NIH InBRE program for undergraduate scholars. The content is solely the responsibility of the authors and does not necessarily represent the official views of the National Institutes of Health.

Supporting Information: The relevant data is located in Appendix B

Literature Cited

1. Halder S, Ng R, Agbandje-McKenna M. 2012. Parvoviruses: structure and infection. Future Virology 7:253–78.

2. Muzyczka N, Berns KI. 2001. Parvoviridae: The viruses and their replication, p. 2327–60. *In* Howley, DMK and PM (ed.), Fields Virology, 4th ed. Lippincott Williams and Wilkins, New York.

3. Agbandje-McKenna M, Kleinschmidt J. 2011. AAV Capsid Structure and Cell Interactions Adeno-Associated Virus, p. 47–92. *In* Snyder, RO, Moullier, P (eds.), Methods in Molecular Biology. Humana Press.

4. Agbandje-McKenna M, Chapman MS. 2006. Correlating structure with function in the viral capsid, p. 125–39. *In* Kerr, JR, Cotmore, SF, Bloom, ME, Linden, R., Parrish, CR (eds.), Parvoviruses. Hodder Arnold Publication.

5. Gao G, Vandenberghe LH, Alvira MR, Lu Y, Calcedo R, Zhou X, Wilson JM. 2004. Clades of Adeno-Associated Viruses Are Widely Disseminated in Human Tissues. Journal of Virology 78:6381–88.

6. Gao G-P, Alvira MR, Wang L, Calcedo R, Johnston J, Wilson JM. 2002. Novel adeno-associated viruses from rhesus monkeys as vectors for human gene therapy. Proceedings of the National Academy of Sciences 99:11854–59.

7. Mori S, Wang L, Takeuchi T, Kanda T. 2004. Two novel adeno-associated viruses from cynomolgus monkey: pseudotyping characterization of capsid protein. Virology 330:375–83.

8. Sanlioglu S, Benson PK, Yang J, Atkinson EM, Reynolds T, Engelhardt JF. 2000. Endocytosis and Nuclear Trafficking of Adeno-Associated Virus Type 2 Are Controlled by Rac1 and Phosphatidylinositol-3 Kinase Activation. Journal of Virology 74:9184–96.

9. Schmidt M, Voutetakis A, Afione S, Zheng C, Mandikian D, Chiorini JA. 2008. Adeno-Associated Virus Type 12 (AAV12): a Novel AAV Serotype with Sialic Acid- and Heparan Sulfate Proteoglycan-Independent Transduction Activity. Journal of Virology 82:1399–1406.

10. Van Vliet KM, Blouin V, Brument N, Agbandje-McKenna M, Snyder RO. 2008. The role of the adeno-associated virus capsid in gene transfer., p. 51–91. *In* Jain, KK (ed.), Methods in Molecular Biology. Humana Press.

11. Mingozzi F, High KA. 2011. Therapeutic in vivo gene transfer for genetic disease using AAV: progress and challenges. Nature Review, Genetics 12:341–55.

12. Maguire AM, Simonelli F, Pierce EA, Pugh EN, Mingozzi F, Bennicelli J, Banfi S, Marshall KA, Testa F, Surace EM, Rossi S, Lyubarsky A, Arruda VR, Konkle B, Stone E, Sun J, Jacobs J, Dell'Osso L, Hertle R, Ma J, Redmond TM, Zhu X, Hauck B, Zelenaia O, Shindler KS, Maguire MG, Wright JF, Volpe NJ, McDonnell JW, Auricchio A, High KA, Bennett J. 2008. Safety and Efficacy of Gene Transfer for Leber's Congenital Amaurosis. New England Journal of Medicine 358:2240–48.

13. Chao H, Liu Y, Rabinowitz J, Li C, Samulski RJ, Walsh CE. 2000. Several Log Increase in Therapeutic Transgene Delivery by Distinct Adeno-Associated Viral Serotype Vectors. Molecular Therapy 2:619–23.

14. Davidson BL, Stein CS, Heth JA, Martins I, Kotin RM, Derksen TA, Zabner J, Ghodsi A, Chiorini JA. 2000. Recombinant adeno-associated virus type 2, 4, and 5 vectors: Transduction of variant cell types and regions in the mammalian central nervous system. Proceedings of the National Academy of Sciences 97:3428–32.

15. Kern A, Schmidt K, Leder C, Muller OJ, Wobus CE, Bettinger K, Von der Lieth CW, King JA, Kleinschmidt JA. 2003. Identification of a Heparin-Binding Motif on Adeno-Associated Virus Type 2 Capsids. Journal of Virology 77:11072–81.

16. Levy HC, Bowman VD, Govindasamy L, McKenna R, Nash K, Warrington K, Chen W, Muzyczka N, Yan X, Baker TS, Agbandje-McKenna M. 2009. Heparin binding induces conformational changes in Adeno-associated virus serotype 2. Journal of Structural Biology 165:146–56.

17. Opie SR, Warrington JKH, Agbandje-McKenna M, Zolotukhin S, Muzyczka N. 2003. Identification of Amino Acid Residues in the Capsid Proteins of Adeno-Associated Virus Type 2 That Contribute to Heparan Sulfate Proteoglycan Binding. Journal of Virology 77:6995–7006.

18. Summerford C, Samulski RJ. 1998. Membrane-Associated Heparan Sulfate Proteoglycan Is a Receptor for Adeno-Associated Virus Type 2 Virions. Journal of Virology 72:1438–45.

19. Akache B, Grimm D, Pandey K, Yant SR, Xu H, Kay MA. 2006. The 37/67-Kilodalton Laminin Receptor Is a Receptor for Adeno-Associated Virus Serotypes 8, 2, 3, and 9. Journal of Virology 80:9831–36.

20. Asokan A, Hamra JB, Govindasamy L, Agbandje-McKenna M, Samulski RJ. 2006. Adeno-Associated Virus Type 2 Contains an Integrin α5β1 Binding Domain Essential for Viral Cell Entry. Journal of Virology 80:8961–69.

21. Kashiwakura Y, Tamayose K, Iwabuchi K, Hirai Y, Shimada T, Matsumoto K, Nakamura T, Watanabe M, Oshimi K, Daida H. 2005. Hepatocyte Growth Factor Receptor Is a Coreceptor for Adeno-Associated Virus Type 2 Infection. Journal of Virology 79:609–14.

22. Qing K, Mah C, Hansen J, Zhou S, Dwarki V, Srivastava A. 1999. Human fibroblast growth factor receptor 1 is a co-receptor for infection by adeno-associated virus 2. Nature Medicine 5:71–7.

23. Seisenberger G, Ried MU, Endreβ T, Büning H, Hallek M, Bräuchle C. 2001. Real-Time Single-Molecule Imaging of the Infection Pathway of an Adeno-Associated Virus. Science 294:1929–32.

24. Suikkanen S, Aaltonen T, Nevalainen M, Vālilehto O, Lindholm L, Vuento M, Vihinen-Ranta M. 2003. Exploitation of Microtubule Cytoskeleton and Dynein during Parvoviral Traffic toward the Nucleus. Journal of Virology 77:10270–79.

25. Summerford C, Bartlett JS, Samulski RJ. 1999. αVβ5 integrin: a co-receptor for adeno-associated virus type 2 infection. Nature Medicine 5:78–82.

26. Nonnenmacher M, Weber T. 2011. Adeno-Associated Virus 2 Infection Requires Endocytosis through the CLIC/GEEC Pathway. Cell Host & Microbe 10:563–76.

27. Lerch TF, Xie Q, Chapman MS. 2010. The structure of adeno-associated virus serotype 3B (AAV-3B): Insights into receptor binding and immune evasion. Virology 403:26–36.

28. Blackburn SD, Steadman RA, Johnson FB. 2006. Attachment of adeno-associated virus type 3H to fibroblast growth factor receptor 1. Archives of Virology 151:617–23.

29. Kaludov N, Brown KE, Walters RW, Zabner J, Chiorini JA. 2001. Adeno-Associated Virus Serotype 4 (AAV4) and AAV5 Both Require Sialic Acid Binding for Hemagglutination and Efficient Transduction but Differ in Sialic Acid Linkage Specificity. Journal of Virology 75:6884–93.

30. Wu Z, Miller E, Agbandje-McKenna M, Samulski RJ. 2006. Alpha2,3 and alpha2,6 N-linked sialic acids facilitate efficient binding and transduction by adeno-associated virus types 1 and 6. Journal of Virology 80:9093–103.

31. Walters RW, Yi SMP, Keshavjee S, Brown KE, Welsh MJ, Chiorini JA, Zabner J. 2001. Binding of Adeno-associated Virus Type 5 to 2,3-Linked Sialic Acid Is Required for Gene Transfer. Journal of Biological Chemistry 276:20610–16.

32. Pasquale G Di, Davidson BL, Stein CS, Martins I, Scudiero D, Monks A, Chiorini JA. 2003. Identification of PDGFR as a receptor for AAV-5 transduction. Nature Medicine 9:1306–12.

33. Shen S, Bryant KD, Brown SM, Randell SH, Asokan A. 2011. Terminal N-linked galactose is the primary receptor for adeno-associated virus 9. The Journal of Biological Chemistry 286:13532–40.

34. Sonntag F, Bleker S, Leuchs B, Fischer R, Kleinschmidt AJ. 2006. Adeno-associated virus type 2 capsids with externalized VP1/VP2 trafficking domains are generated prior to passage through the cytoplasm and are maintained until uncoating occurs in the nucleus. Journal of Virology 80:11040–54.

35. Buller RM, Rose JA. 1978. Characterization of adenovirus-associated virus-induced polypeptides in KB cells. Journal of Virology 25:331–8.

36. Rose JA, Maizel J V, Inman JK, Shatkin AJ. 1971. Structural Proteins of Adenovirus-Associated Viruses. Journal of Virology 8:766–70.

37. Chapman MS, Agbandje-McKenna M. 2006. Atomic structure of viral particles, p. 107–23. *In* Kerr, JR, Cotmore, SF, Bloom, ME, Linden, R., Parrish, CR (eds.), Parvoviruses. Edward Arnold Ltd., New York.

38. Salganik M, Venkatakrishnan B, Bennett A, Lins B, Yarbrough J, Muzyczka N, Agbandje-McKenna M, McKenna R. 2012. Evidence for pH-dependent protease activity in the adeno-associated virus capsid. Journal of Virology 86:11877–85.

39. Van Vliet K, Blouin V, Agbandje-McKenna M, Snyder RO. 2006. Proteolytic mapping of the adeno-associated virus capsid. Molecular Therapy 14:809–21.

40. Popa-Wagner R, Porwal M, Kann M, Reuss M, Weimer M, Florin L, Kleinschmidt JA. 2012. Impact of VP1-specific protein sequence motifs on adeno-associated virus type 2 intracellular trafficking and nuclear entry. Journal of Virology 86:9163–74.

41. Bleker S, Pawlita M, Kleinschmidt JA, Kleinschmidt A. 2006. Impact of Capsid Conformation and Rep-Capsid Interactions on Adeno-Associated Virus Type 2 Genome Packaging. Journal of Virology 80:810–20.

42. Govindasamy L, Padron E, McKenna R, Muzyczka N, Kaludov N, Chiorini JA, Agbandje-McKenna M. 2006. Structurally Mapping the Diverse Phenotype of Adeno-Associated Virus Serotype 4. Journal of Virology 80:11556–70.

43. Ng R, Govindasamy L, Gurda BL, McKenna R, Kozyreva OG, Samulski RJ, Parent KN, Baker TS, Agbandje-McKenna M. 2011. Structural Characterization of the

Dual Glycan Binding Adeno-Associated Virus Serotype 6. Journal of Virology 84:12945–57.

44. Walters RW, Agbandje-McKenna M, Bowman VD, Moninger TO, Olson NH, Seiler M, Chiorini JA, Baker TS, Zabner J. 2004. Structure of Adeno-Associated Virus Serotype 5. Journal of Virology 78:3361–71.

45. Xie Q, Bu W, Bhatia S, Hare J, Somasundaram T, Azzi A, Chapman MS. 2002. The atomic structure of adeno-associated virus (AAV-2), a vector for human gene therapy. Proceedings of the National Academy of Sciences 99:10405–10.

46. Nam H-J, Lane MD, Padron E, Gurda B, McKenna R, Kohlbrenner E, Aslanidi G, Byrne B, Muzyczka N, Zolotukhin S, Agbandje-McKenna M. 2007. Structure of Adeno-Associated Virus Serotype 8, a Gene Therapy Vector. Journal of Virology 81:12260–71.

47. Wu Z, Asokan A, Grieger JC, Govindasamy L, Agbandje-McKenna M, Samulski RJ. 2006. Single Amino Acid Changes Can Influence Titer, Heparin Binding, and Tissue Tropism in Different Adeno-Associated Virus Serotypes. Journal of Virology 80:11393–97.

48. McCraw DM, O'Donnell JK, Taylor KA, Stagg SM, Chapman MS. Structure of adeno-associated virus-2 in complex with neutralizing monoclonal antibody A20. Virology 431:40–9.

49. DiMattia M, Govindasamy L, Levy HC, Gurda-Whitaker B, Kalina A, Kohlbrenner E, Chiorini JA, McKenna R, Muzyczka N, Zolotukhin S, Agbandje-McKenna M. 2005. Production, purification, crystallization and preliminary X-ray structural studies of adeno-associated virus serotype 5. Acta Crystallographica Section F 61:917–21.

50. Kohlbrenner E, Aslanidi G, Nash K, Shklyaev S, Campbell-Thompson M, Byrne BJ, Snyder RO, Muzyczka N, Warrington KH, Zolotukhin S. 2005. Successful Production of Pseudotyped rAAV Vectors Using a Modified Baculovirus Expression System. Molecular Therapy 12:1217–25.

51. Lane MD, Nam H-J, Padron E, Gurda-Whitaker B, Kohlbrenner E, Aslanidi G, Byrne B, McKenna R, Muzyczka N, Zolotukhin S, Agbandje-McKenna M. 2005. Production, purification, crystallization and preliminary X-ray analysis of adeno-associated virus serotype 8. Acta Crystallographica Section F 61:558–61.

52. Miller EB, Gurda-Whitaker B, Govindasamy L, McKenna R, Zolotukhin S, Muzyczka N, Agbandje-McKenna M. 2006. Production, purification and

preliminary X-ray crystallographic studies of adeno-associated virus serotype 1. Acta Crystallographica Section F 62:1271–74.

53. Mah C, Fraites JTJ, Zolotukhin I, Song S, Flotte TR, Dobson J, Batich C, Byrne BJ. 2002. Improved Method of Recombinant AAV2 Delivery for Systemic Targeted Gene Therapy. Molecular Therapy 6:106–12.

54. Zolotukhin S, Potter M, Zolotukhin I, Sakai Y, Loiler S, Fraites TJ, Chiodo VA, Phillipsberg T, Muzyczka N, Hauswirth WW, Flotte TR, Byrne BJ, Snyder RO. 2002. Production and purification of serotype 1, 2, and 5 recombinant adeno-associated viral vectors. Methods 28:158–67.

55. Yeh AP, McMillan A, Stowell MHB. 2006. Rapid and simple protein-stability screens: application to membrane proteins. Acta crystallographica. Section D, Biological crystallography 62:451–7.

56. Bothner B, Schneemann A, Marshall D, Reddy V, Johnson JE, Siuzdak G. 1999. Crystallographically identical virus capsids display different properties in solution. Nature Structural & Molecular Biology 6:114–6.

57. Rayaprolu V, Manning BM, Douglas T, Bothner B. 2010. Virus particles as active nanomaterials that can rapidly change their viscoelastic properties in response to dilute solutions. Soft Matter 6:5286–88.

58. Belnap DM, Filman DJ, Trus BL, Cheng N, Booy FP, Conway JF, Curry S, Hiremath CN, Tsang SK, Steven AC, Hogle JM. 2000. Molecular Tectonic Model of Virus Structural Transitions: the Putative Cell Entry States of Poliovirus. Journal of Virology 74:1342–54.

59. Gan L, Speir JA, Conway JF, Lander G, Cheng N, Firek BA, Hendrix RW, Duda RL, Liljas L, Johnson JE. 2006. Capsid Conformational Sampling in HK97 Maturation Visualized by X-Ray Crystallography and Cryo-EM. Structure 14:1655–65.

60. Wu P, Xiao WW, Conlon T, Hughes J, Agbandje-McKenna M, Ferkol T, Flotte T, Muzyczka N. 2000. Mutational analysis of the adeno-associated virus type 2 (AAV2) capsid gene and construction of AAV2 vectors with altered tropism. Journal of Virology 74:8635–47.

61. Endres D, Zlotnick A. 2002. Model-Based Analysis of Assembly Kinetics for Virus Capsids or Other Spherical Polymers. Biophysical Journal 83:1217–30.

62. Zlotnick A. 2003. Are weak protein–protein interactions the general rule in capsid assembly? Virology 315:269–74.

63. Ausar SF, Foubert TR, Hudson MH, Vedvick TS, Middaugh CR. 2006. Conformational Stability and Disassembly of Norwalk Virus-like Particles. Journal of Biological Chemistry 281:19478–88.

64. Carrillo-Tripp M, Shepherd CM, Borelli IA, Venkataraman S, Lander G, Natarajan P, Johnson JE, Brooks CL, Reddy VS. 2009. VIPERdb2: an enhanced and web API enabled relational database for structural virology. Nucleic Acids Research 37:D436–42.

65. Bothner B, Dong XF, Bibbs L, Johnson JE, Siuzdak G. 1998. Evidence of Viral Capsid Dynamics Using Limited Proteolysis and Mass Spectrometry. Journal of Biological Chemistry 273:673–76.

66. Hilmer JK, Zlotnick A, Bothner B. 2008. Conformational Equilibria and Rates of Localized Motion within Hepatitis B Virus Capsids. Journal of Molecular Biology 375:581–94.

67. Park C, Marqusee S. 2004. Probing the High Energy States in Proteins by Proteolysis. Journal of Molecular Biology 343:1467–76.

68. Kronenberg S, Bottcher B, Von der Lieth CW, Bleker S, Kleinschmidt JA. 2005. A Conformational Change in the Adeno-Associated Virus Type 2 Capsid Leads to the Exposure of Hidden VP1 N Termini. Journal of Virology 79:5296–303.

69. Akache B, Grimm D, Shen X, Fuess S, Yant SR, Glazer DS, Park J, Kay MA. A Two-hybrid Screen Identifies Cathepsins B and L as Uncoating Factors for Adeno-associated Virus 2 and 8. Molecular Therapy 15:330–9.

70. Nelson CDS, Minkkinen E, Bergkvist M, Hoelzer K, Fisher M, Bothner B, Parrish CR. 2008. Detecting small changes and additional peptides in the canine parvovirus capsid structure. Journal of Virology 82:10397–407.

71. Caspar DLD, Klug A. 1962. Physical principles in the construction of regular viruses. Cold Spring Harbor Symposia on Quantitative Biology 27th:1–24.

72. Fricks CE, Hogle JM. 1990. Cell-induced conformational change in poliovirus: externalization of the amino terminus of VP1 is responsible for liposome binding. Journal of Virology 64:1934–45.

73. Fricks CE, Icenogle JP, Hogle JM. 1985. Trypsin sensitivity of the Sabin strain of type 1 poliovirus: cleavage sites in virions and related particles. Journal of Virology 54:856–59.

74. Golden JS, Harrison SC. 1982. Proteolytic dissection of turnip crinkle virus subunit in solution. Biochemistry 21:3862–6.

75. Johnson JE. 2003. Virus Particle Dynamics. Advances in Protein Chemistry 64:197–218.

76. Kowalski H, Maurer-Fogy I, Vriend G, Casari G, Beyer A, Blaas D. 1989. Trypsin sensitivity of several human rhinovirus serotypes in their low pH-induced conformation. Virology 171:611–4.

77. Horton N, Lewis M. 1992. Calculation of the free energy of association for protein complexes. Protein Science 1:169–81.

78. Vedadi M, Niesen FH, Allali-Hassani A, Fedorov OY, Finerty PJ, Wasney GA, Yeung R, Arrowsmith C, Ball LJ, Berglund H, Hui R, Marsden BD, Nordlund P, Sundstrom M, Weigelt J, Edwards AM. 2006. Chemical screening methods to identify ligands that promote protein stability, protein crystallization, and structure determination. Proceedings of the National Academy of Sciences 103:15835–40.

79. Yi G, Vaughan RC, Yarbrough I, Dharmaiah S, Kao CC. 2009. RNA binding by the brome mosaic virus capsid protein and the regulation of viral RNA accumulation. Journal of Molecular Biology 391:314–26.

80. Nam H-J, Gurda BL, McKenna R, Potter M, Byrne B, Salganik M, Muzyczka N, Agbandje-McKenna M. 2011. Structural studies of adeno-associated virus serotype 8 capsid transitions associated with endosomal trafficking. Journal of Virology 85:11791–9.

81. Bleker S, Sonntag F, Kleinschmidt JA, Kleinschmidt A. 2005. Mutational Analysis of Narrow Pores at the Fivefold Symmetry Axes of Adeno-Associated Virus Type 2 Capsids Reveals a Dual Role in Genome Packaging and Activation of Phospholipase A2 Activity. Journal of Virology 79:2528–40.

82. Lochrie MA, Tatsuno GP, Christie B, McDonnell JW, Zhou S, Surosky R, Pierce GF, Colosi P. 2006. Mutations on the External Surfaces of Adeno-Associated Virus Type 2 Capsids That Affect Transduction and Neutralization. Journal of Virology 80:821–34.

83. Skehel JJ, Bayley PM, Brown EB, Martin SR, Waterfield MD, White JM, Wilson IA, Wiley DC. 1982. Changes in the conformation of influenza virus hemagglutinin at the pH optimum of virus-mediated membrane fusion. Proceedings of the National Academy of Sciences 79:968–72.

84. Gurda BL, Raupp C, Popa-Wagner R, Naumer M, Olson NH, Ng R, McKenna R, Baker TS, Kleinschmidt JA, Agbandje-McKenna M. 2012. Mapping a Neutralizing Epitope onto the Capsid of Adeno-Associated Virus Serotype 8. Journal of Virology 86:7739–51.

85. Raupp C, Naumer M, Muller OJ, Gurda BL, Agbandje-McKenna M, Kleinschmidt JA. The threefold protrusions of AAV8 are involved in cell surface targeting as well as post attachment processing. Journal of Virology doi: 10.1128/JVI.00209–12.

86. Farr GA, Tattersall P. 2004. A conserved leucine that constricts the pore through the capsid fivefold cylinder plays a central role in parvoviral infection. Virology 323:243–56.

87. Bothner B, Taylor D, Jun B, Lee KK, Siuzdak G, Schlutz CP, Johnson JE. 2005. Maturation of a tetravirus capsid alters the dynamic properties and creates a metastable complex. Virology 334:17–27.

88. Zádori Z, Szelei J, Lacoste M-CC, Li Y, Gariépy S, Raymond P, Allaire M, Nabi IR, Tijssen P. 2001. A Viral Phospholipase A2 Is Required for Parvovirus Infectivity. Developmental Cell 1:291–302.

89. Wu Z, Asokan A, Samulski RJ. 2006. Adeno-associated virus serotypes: vector toolkit for human gene therapy. Molecular Therapy 14:316–27.

90. Hauck B, Xiao W. 2003. Characterization of Tissue Tropism Determinants of Adeno-Associated Virus Type 1. Journal of Virology 77:2768–74.

CHAPTER 4

LEARNING NEW TRICKS FROM AN OLD DOG;

STUDIES OF CCMV CAPSID SWELLING

Contribution of Authors and Co-Authors

Manuscript in Chapter 4

Author: Vamseedhar Rayaprolu

Contributions: Optimized and established purification and data collection, collected and analyzed data, prepared the manuscript

Co-Author: Navid Movahed

Contributions: Assisted in establishing protocols, analyzed data, participated in critical discussion of the data and the manuscript

Co-Author: Ravikant Chaudhary
Contributions: Collected and analyzed data, participated in critical discussion of the data and manuscript

Co-Author: Geoff Blatter

Contributions: Collected and analyzed data

Co-Author: Alec Skuntz

Contributions: Assisted in sample preparation

Co-Author: Sue Brumfield

Contributions: Assisted in sample preparation and data collection

Co-Author: Jonathan K Hilmer

Contributions: Assisted in data optimization and collection

Co-Author: Mark J Young

Contribution of Authors and Co-Authors - Continued

Contributions: Provided sample preparation protocols and critically discussed the data.

Co-Author: Trevor Douglas

Contributions: Provided critical insights into the project, preparation protocols, critically discussed the data and was instrumental in providing funding.

Co-Author: Brian Bothner

Contributions: Obtained funding, provided critical intellectual input and mentoring, discussed data and the manuscript

Manuscript Information Page

Vamseedhar Rayaprolu, Navid Movahed, Ravikant Chaudhary, Geoff Blatter, Alec Skuntz, Sue Brumfield, Jonathan K. Hilmer, Mark J. Young, Trevor Douglas, Brian Bothner

Journal of Virology

Status of Manuscript:
__x_ Prepared for submission to a peer-reviewed journal
____ Officially submitted to a peer-review journal
____ Accepted by a peer-reviewed journal
____ Published in a peer-reviewed journal

Publisher: American Society of Microbiology

Issue in which Manuscript Appears: In Preparation

CHAPTER 4

LEARNING NEW TRICKS FROM AN OLD DOG; STUDIES OF CCMV CAPSID SWELLING

Abstract

Icosahedral virus particles are known to be dynamic and due to their high symmetry are accessible model systems for detailed studies of protein dynamics in megadalton sturctures. One such system is the Cowpea chlorotic mottle virus (CCMV). CCMV is a small plant virus that has been well studied for its reversible structural transitions. The virus is known to exist in two distinct conformations; a closed conformation, promoted by the presence of divalent cation binding, and a swollen conformation existing when the cations are stripped from the capsid. The swelling of CCMV has been the subject of structural and biophysical studies. This conformational change is proposed to destabilize the particle and alter the subunit interactions though the specific effects of conformation on capsid stability and dynamics are still unclear. To investigate CCMV swelling, capsid stability and dynamics, two viral strains, wild-type and the salt-stable mutant were used. The mutant has a single mutation (K42R) in each subunit which introduces 660 extra hydrogen bonds making it, in theory, more stable to for example, salt concentrations and temperature. To investigate and compare the stability and dynamics of the different particles, a multi-dimensional approach involving Differential Scanning Fluorimetry (DSF), Size-exclusion chromatography, Intact protein Hydrogen-Deuterium exchange Mass Spectrometry (HDX-MS) and Limited Proteolysis has been applied. DSF and Size-

exclusion report on the global conformational changes whereas HDX-MS and Limited Proteolysis provides information at the subunit level of the particle. Analysis by these methods shows that the stability (rigidity) of the closed forms was consistently higher than those of the swollen forms along with higher melting temperatures. When the wildtype (WT) and the K42R mutant forms (SS) are compared, the SS strain shows enhanced melting temperatures, lower hydrodynamic radii using size-exclusion, lower subunit dynamics when probed with HDX-MS and higher resistance to Trypsin along with a biphasic proteolysis profile corresponding to the presence of two products with distinct digestion patterns. Each of these approaches shed light on the biophysical properties of the virus from a different point of view while complementing each other. The research presented here probes particle stability and conformational dynamics of wild-type and a K42R mutant (SS-CCMV).

Introduction

Icosahedral virus particles that infect plants and animals are known to be highly dynamic. Because of the precise symmetry of the capsid, they have become favorite model systems for detailed studies of protein dynamics in megadalton complexes. X-ray crystallography and cryo-electron microscopy have provided structural details of these supramolecular model systems. Biophysical studies of the solution phase properties have been able to bring into light the dynamics that are a critical part of capsid function. One such model system is Cowpea chlorotic mottle virus (CCMV) which has been extensively studied with respect to structure, conformational dynamics and assembly (5, 9, 10). CCMV

was also one of first viruses to be developed as a bioinspired nanomaterial, with applications ranging from MRI imaging to enzyme based nanoreactors (4, 6, 8, 13). CCMV is a small RNA plant virus belonging to the *Bromovirus* genus in the *Bromoviridae* family. The structure of the virion, showing the quasi-three fold asymmetric unit (subunits A, B and C) (Figure 1A) has been solved to a 3.2Å resolution (9) . The CCMV capsid has a truncated icosahedral (T=3) morphology composed of 180 chemically identical subunits arranged as pentamers and hexamers. The 189 amino acid subunit comprises of the canonical eight-stranded, antiparallel, β-barrel core with the residues in the N- and C-termini involved in a comprehensive network of intercapsomere and intracapsomere interactions. Namely, the N-terminus participates in three different interactions. 1) The first 26 residues of the protein sequence comprise mostly of basic residues enabling the N-terminus to dynamically interact with the genetic material. 2) The six amino-terminal arms of the hexamer (residues 27-35) converge at the quasi six-fold axes and form a hexameric tubular structure (Figure 1B) 3) The amino acids 44-51 act as the clamp for the invading C-terminal (9).

The capsid exhibits two major conformations of interest. In the presence of divalent cations (Ca^{2+} or Mg^{2+}), low pH (~5.0) and low ionic strength (< 0.2), the capsid exists in a smaller *closed* conformation (~28.6nm in size). Five residues involved (Glu81, Glu85, Glu148, Gln149, Asp153) A larger *swollen* conformation (~31.5nm) exists at a higher pH (~7.0) and in the absence of divalent cations while keeping the ionic strength low (< 0.2) (Figure 1). The swollen form when subjected to a higher ionic strength (> 0.4) falls apart into subunit dimers. The expansion of the capsid occurs primarily due to

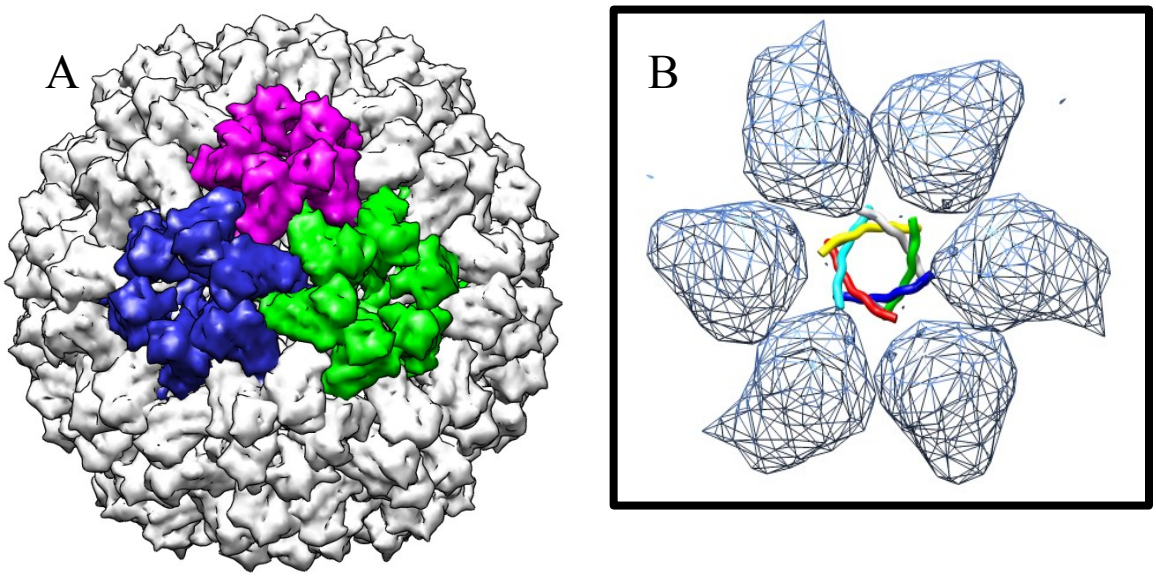


Figure 1 A) Closed form of the CCMV capsid. The overall radial increase when the capsid swells is ~10%. The hexamers are shown in blue and green and pentamers in magenta. B) N-termini of the B and C subunits intertwine to form a ring inside the quasi 6-fold axes rendering stability to the capsid.

repulsions between acidic residues of opposing subunits in the quasi 3-fold axes. A clear separation, involving mostly rigid body movements between these cation binding residues, leads to the opening of 2nm pores at these axes producing a more fenestrated structure while virtually leaving the five-fold and the quasi six-fold axes untouched (9) . The biological role of swelling is not known, however, it is believed to be involved in nucleic acid release, suggesting that this form is less stable. It has also been shown that in addition to the closed and swollen conformations, protein domains localized to the inside of the capsid in structural models can be reversibly exposed to the surface in solution (10) . Molecular aggregation of minerals based on the electrostatic interactions of the N-terminus of the protein and the metal species has been shown to work efficiently leading to mineralization inside the capsid (4).

Several mutations were introduced into CCMV with nitrous acid treatment by Bancroft et al following methods first developed by Siegel et al. Among these, the K42R mutation has particularly interesting properties. The lysine to arginine mutation at position 42 of the subunit helps the virion tolerate 1M salt and yet retain 70% of wildtype infectivity. The structure of the SS-CCMV was solved to a 2.7Å resolution and analyzed to understand its enhanced stability (10). When compared to the structure of the asymmetric unit of WT-CCMV, the SS-CCMV crystal structure shows few key differences, namely 1. Two additional ordered residues on the N-terminus of the A subunit (Gln40, Gly41) 2. One additional ordered residue on the N-terminus of the B and C subunits (Arg26) 3. New RNA interactions of the Arg42 of the A subunit 4. New salt bridges and hydrogen bonds around the β-hexamer made by the R42 in the B and C subunits. This leads to the formation of, in total, 660 new weak interactions across the entire capsid. Similar to the WT-CCMV, the SS-CCMV particle also undergoes the swelling transition under appropriate conditions. The acidic residues that cause the swelling in the WT-CCMV capsid are present in the same relative positions of the SS-CCMV quasi three fold axes. Therefore, as seen with the WT-CCMV, electrostatic repulsions of these residues could be expected to cause the swelling in the SS-CCMV capsid.

CCMV has been historically known to exist only in its closed and swollen forms. There is very little documented data that suggests the existence of intermediary conformations though intriguing assembly products have been demonstrated to exist with change in salt concentrations (1, 2). In this work, with simple variations in pH and divalent cation concentration, we show that there exist two more distinct conformations that have

not been studied before. With the stripping of Ca^{2+} ions, the classical closed form shifts into a pseudo-swollen (PS) form. Similarly, introducing Ca^{2+} into the swelling buffer (no Ca^{2+}, pH 7.15) produces a pseudo-closing (PC) form. These distinct new conformations show diverse biophysical properties and provide experimental insights into the capsid swelling mechanism. The SS-CCMV mutant also shows similar though restricted transitions indicating the effect of the extra interactions and hence it's enhanced stability.

Materials and Methods

Virus Purification

CCMV was propagated in cowpea plants (*Vigna unguiculata).* Secondary leaves picked from the plant were blended in a Waring blender with cold homogenization buffer (200mM Sodium Acetate, 10mM Ascorbic Acid, 10mM EDTA, pH 4.8) for three minutes and then filtered through cheesecloth. The strained lysate was centrifuged at 8K RPM for 20 minutes at 4°C. PEG 8000 was added to the supernatant (10% w/v) and it was left to stir overnight at 4°C. The suspension was centrifuged again at 8K RPM for 20 minutes at 4°C and the pellet was resuspended in virus buffer (50mM Sodium Acetate, 1mM EDTA, pH 4.8) using a volume that is 10% of the volume used above for the homogenization buffer. The suspension was then centrifuged again at 8K RPM for 20 minutes at 4°C. PEG 8000 was added to the supernatant (15% w/v) and left to stir overnight at 4°C. The suspension was pelleted at 8K RPM for 20 minutes at 4°C, the pellet resuspended (virus buffer) in 5%, instead of 10%, of the first measured supernatant volume. The supernatant was then centrifuged on a 39% (w/v) CsCl gradient in virus buffer at 37,000 rpm for 18

hours at 4°C. The isolated virus bands were then dialyzed/diluted into four different buffers namely, Closing (10mM Sodium Acetate, 100mM NaCl, 5mM $CaCl_2$, pH 4.8), Pseudo-swelling (10mM Sodium Acetate, 100mM NaCl, 1mM EDTA, pH 4.8), Pseudo-closing (10mM Sodium Acetate, 100mM NaCl, 5mM $CaCl_2$, pH 7.15) and Swelling (10mM Sodium Acetate, 100mM NaCl, 1mM EDTA, pH 7.15) buffers, for 4-6 hours each with 4 buffer changes. These samples were further diluted appropriately for the experiments.

Differential Scanning
Fluorimetry (DSF) Stability Assay

22.5µL of ~130µg/mL (~6.4nM) virus samples diluted into the appropriate buffers were mixed with 2.5µL of 150X diluted Sypro Orange in 200µL domeless PCR tubes to make up a reaction volume of 25µL with a final dye concentration of 3X. The tubes were then subjected to a temperature range from 30°C to 99°C in a qPCR machine (Corbett Research Rotorgene - 3000) with a temperature ramping of 0.5°C/min. The experiments were run in triplicates and the fluorescence intensities collected at 550nm and normalized to a 100% were plotted against the temperature. T_m was defined as the maximum value of the first derivative (dF/dT) from the raw signal. The data is shown in Figure 2a and 2b.

Size-exclusion Chromatography

Size-exclusion chromatography was performed using a tandem setup of Agilent SEC-5 (1000Å pore size). The column was incubated with the appropriate buffer (Closing, Pseudo-closing, Pseudo-swelling or Swelling) till a constant baseline is reached. The WT and SS samples were diluted into the appropriate buffer to get a final concentration of 0.2mg/mL of virus. The samples were injected in triplicates onto the tandem setup using

the autosampler at 500uL/min. The normalized absorbances plotted against time are shown in Figure 3.

Hydrogen-Deuterium Exchange
Mass Spectrometry (HDX-MS)

Virus samples were diluted into D_2O (1:10) to obtain a concentration of ~0.2mg/mL concentration. The reaction mixture was incubated at 25°C and samples were run at 0.5, 10, 20, 30, 40, 50 and 60 minute intervals on a Hamilton C8 reverse phase column. The column was equilibrated at 37°C and the samples were run at 800uL/minute using an Agilent 1290 HPLC and analyzed using a micrOTOF™ Electrospray Ionization Mass Spectrometer. 2 blank runs were performed between each injection to eliminate carry over. The data is shown in Figure 4.

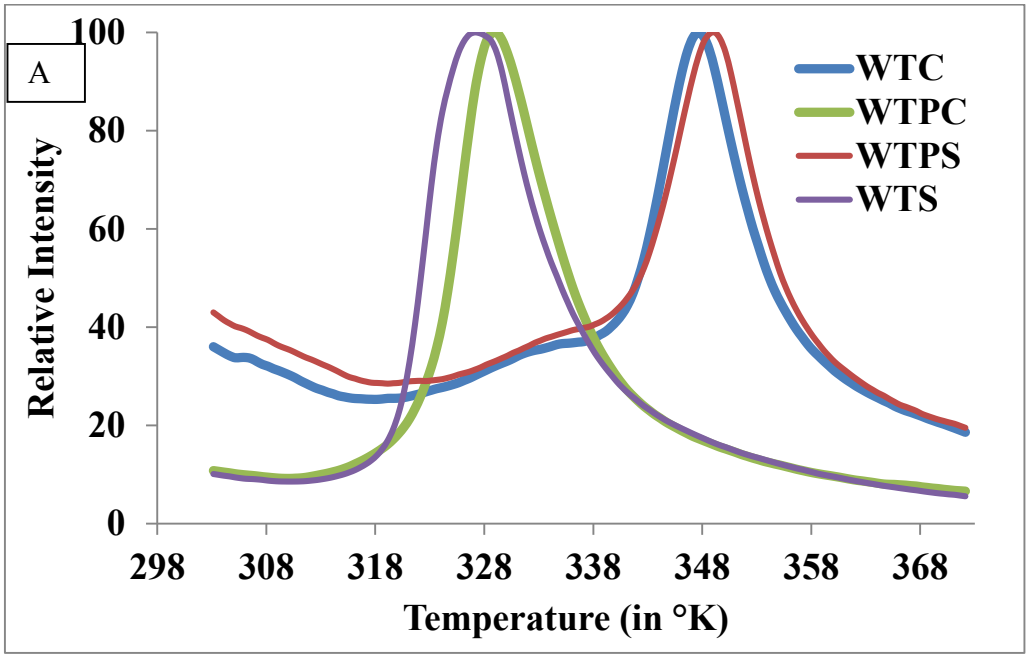
Limited Proteolysis

35.71µg of the CCMV sample was taken and mixed with 1.44uL of 0.025mg/mL of Trypsin getting to a stoichiometry of 1000:1 of virus to enzyme concentration in solution. 12uL of Ammonium Bicarbonate buffer, 500mM, pH 7 was added and the volume made up to 72µL with water. The reactions were incubated at 25°C in the thermocycler. Samples were taken at the following time points 0, 5, 10, 15, 30, 45, 60, 75, 90, 105, 120. Each sample was boiled and stored at -20°C till the reaction was completed. The samples run on SDS-PAGE gels and the bands quantitated using Image J software. The intensity of the intact capsid at time zero was taken as the reference and the data was normalized according to this value. The results are shown in Figure 5.

Results

Thermal Stability Measurements Show Distinct Differences

Thermal denaturation experiments are an important tool for the study of protein stability and provide detailed biophysical information about complexes as well. Capsid thermal stability information was obtained from Differential Scanning Fluorimetry. Briefly, the dye shows an increase in fluorescence intensity when bound to hydrophobic pockets in proteins which are exposed during unfolding. The melting temperatures obtained from DSF curves (Figure 2a and 2b) showed profound differences between the four different forms and between the wildtype and K42R mutant. The closed forms of the WT and SS showed a significant but not a drastic difference between them (~2°C). The melting temperatures do not change when the pH was kept constant and the Ca^{2+} was stripped away using EDTA (WTPS and SSPS forms), while the melting temperatures reduce by ~19°C and ~4°C when the pH is increased in the presence of Ca^{2+} (WTPC and SSPC forms). High pH and the absence of Ca^{2+} induce the swollen form and decreases the melting temperature of the WTS by ~22°C and SSS by ~8°C. The DSF curves are shown in Figure 2. Differences seen in association energies of the WT and K42R from crystal structure (VIPERdb) though mostly localized to the quasi-six fold axis with the K42R being higher by about 24 kcal/mol per hexameric unit while the pentameric units showed values of 20kcal/mol higher. The buried surface area is greater in the K42R compared to the WT.



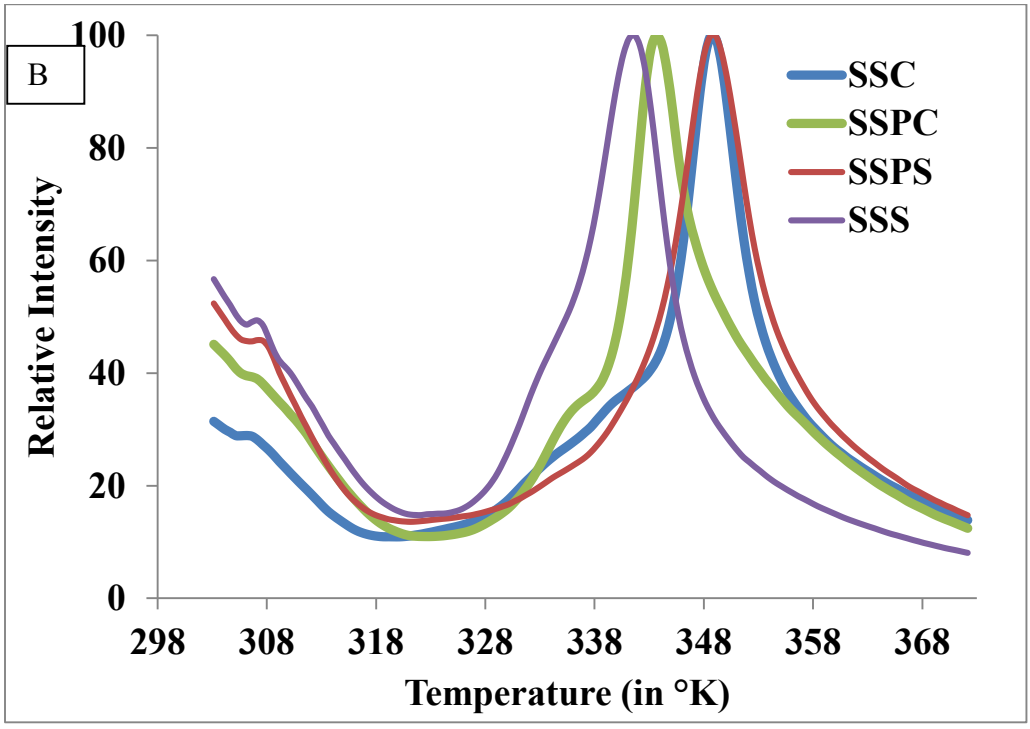


Figure 2A and 2B - DSF profiles of WT and SS conformations

High Resolution Analysis of
Capsid Hydrodynamic Radii

Distinct changes in DSF were seen with change in pH or Ca^{2+} ion concentration. To investigate the progression of the capsid from a closed to a swollen form we probed the change in its hydrodynamic radius with change in solution conditions using size-exclusion chromatography. The closed forms of the WT and SS eluted almost at the same time while

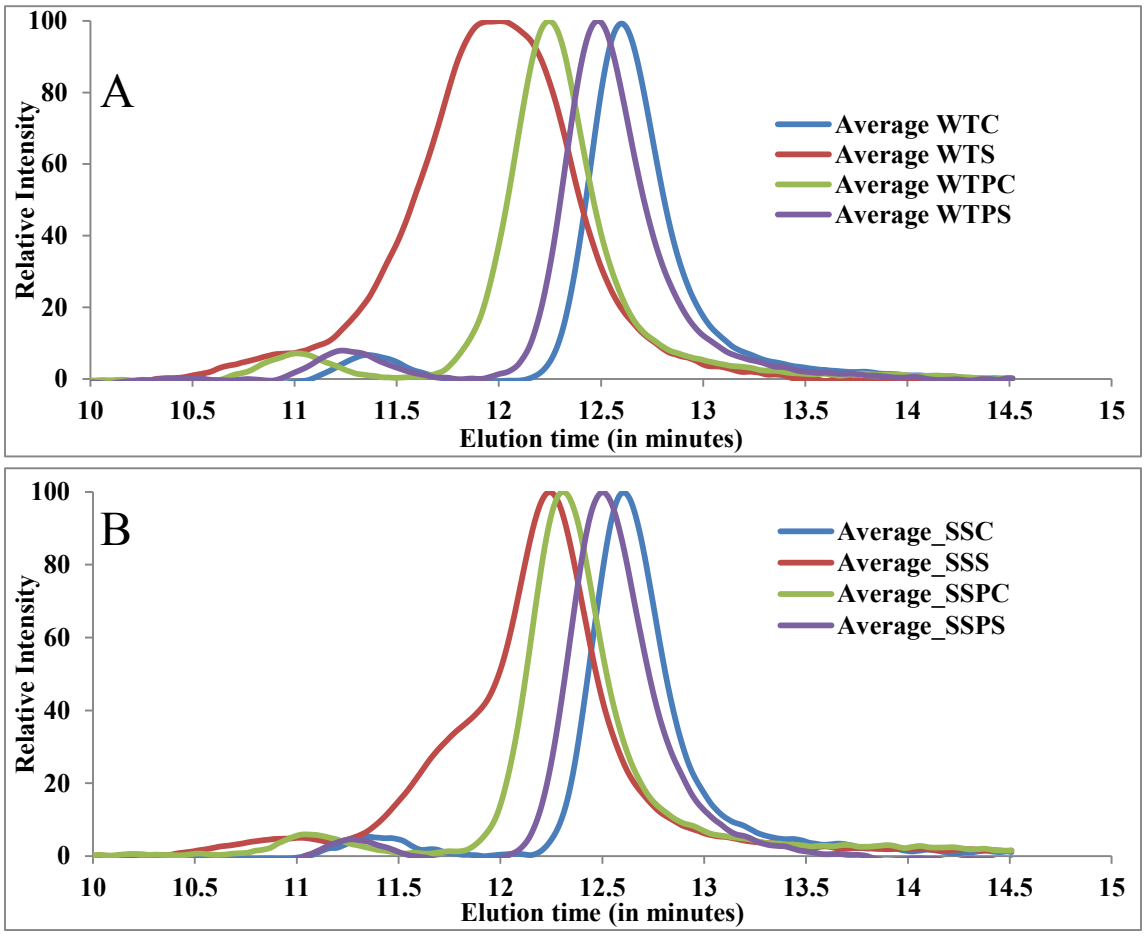


Figure 3A and 3B. Size-exclusion profiles of the conformations of the WT and SS capsids. Samples were run on a tandem setup of Agilent SEC-5 (1000Å) columns at a 500uL/min constant flowrate on an Agilent 1200 HPLC. The error on the elution times was less than ± 0.01 minutes on all the runs.

the pseudo-swollen forms showed a slight but definite difference with the SS eluting first (Figure 3A and 3B). The elution difference increased with the WTPC and SSPC samples. Both the WTS and SSS showed a much broader peak while the SSS capsid peak, which eluted at the same time as the SSPC, was preceded by a smaller, lower intensity shoulder. The SSS form eluted much later compared to its corresponding WTS form.

Intact Protein HDX-MS Differentiates Swollen and Pseudo-closed Forms

The swollen form of the CCMV capsid has been implicated to be involved in genome release and virus replication. To understand the dynamics of the swollen forms and to tease out the differences between the extent and effect of swelling in WT and K42R mutant, intact protein hydrogen-deuterium exchange experiments were performed on the swollen forms. To also investigate the effect of Ca^{2+} on the swollen forms, the HDX experiments were repeated for the respective pseudo-closed forms. The swollen form of the WT showed ~86 daltons of exchange per subunit in comparison with the K42R mutant which showed only 46 daltons of exchange after 1 hour of incubation with D_2O. The protein has 182 amide hydrogens (7 of 190 residues are proline) and the exchange rate indicates that isotope exchange was incomplete on this time scale. These results show that exchange in the virus particle occurs over a time scale of several orders of magnitude. At the intial time point (0.5 minutes), the exchange rate was also much higher for the WTS form (~67% of total exchange) while only ~22% of the exchangeable protons were replaced in the SSS form. A similar trend was seen with the pseudo-closed forms with WTPC showing ~79Da

of total exchange while the SSPC reached only 49Da of exchange. The data is shown in Figure 4.

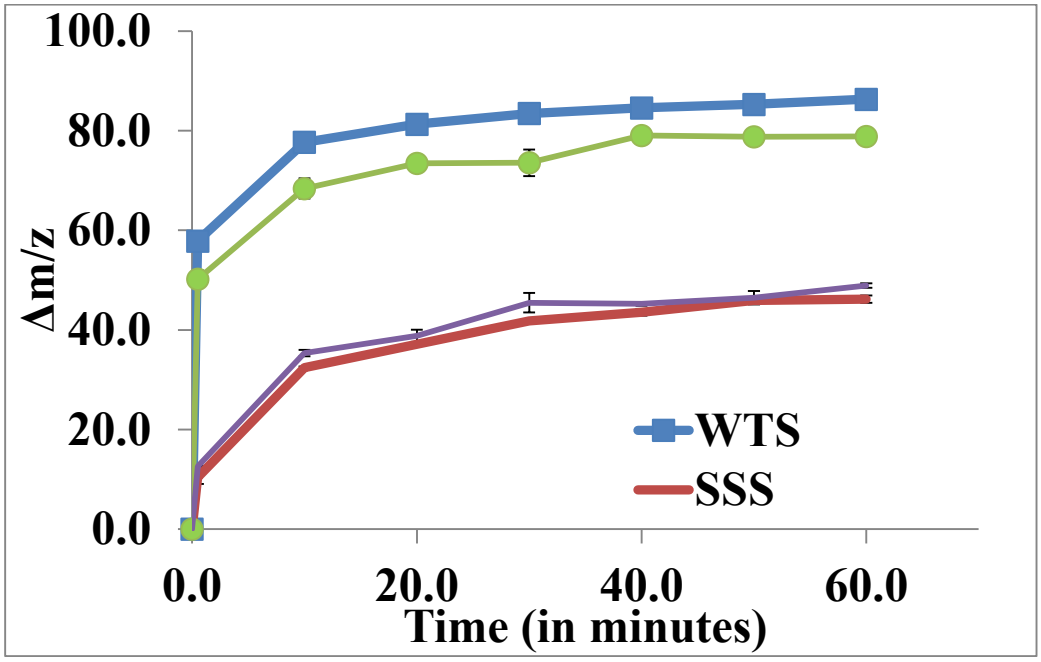


Figure 4. HDX-MS profile of the WT and SS pseudo-closed and swollen forms. The X-axis shows the time points at which the deuteration was measured and Y-axis shows the change in m/z.

Deterministic Trends Seen in
Proteolytic Profiles of SS-CCMV

To further explore the dynamic regions in the swollen forms and the pseudo-closed forms WT and SS particles were incubated with trypsin. All forms of CCMV were readily digested, Figure 5A, Figure 5B and Figure 5C show the proteolysis profiles of the pseudo-closed forms of WT and SS-CCMV capsids over a period of 120 minutes. The WT intact protein disappeared at a slower rate compared to the SS intact protein. There were four prominent peptides (Peptides I, II, III and IV) that appeared with time as the intact subunit disappeared. The intensity of peptide I seemed to be low due to the limited accessibility of

the cleavage site by Trypsin. Peptide II appeared almost instantaneously with the intensity plateauing off and decreasing over time. Peptide III also appeared along with Peptide II while its intensity increased linearly with time till the end of the proteolysis. The intensity of peptide IV increased gradually over the course of the reaction. The time-course proteolysis of the SS-CCMV had different kinetics. All the four prominent peptides showed up during the course of the experiment with much higher relatives abundances compared to the WT-CCMV. Peptide III appeared first immediately followed by Peptide I. After the initial rise, the relative abundances of both, peptide I and III, reduced to half its maximal level. Peptide IV showed an almost linear increase till the end of the reaction where it started to taper off. These cleavage sites were mapped to residues, R15, R23, R26 and K42 on the N-terminus of the CCMV subunit. Peptide I is mapped to residues 16-190.

The WT-CCMV intact capsid protein concentration decreased linearly with time. The intensity of the intact protein of wildtype swollen form almost disappeared while 20% of the WTPC remained by the end of the reaction. The intact protein profile of the SS-CCMV showed an exponential decay which was the most dramatic change of all. The intact peptide of SS-CCMV showed an initial higher rate of decay compared to the WT-CCMV and then tapered off. The intensities of the SSPC and SSS remained almost the same (~35% intact) till the end of the reaction with a very similar reaction profile.

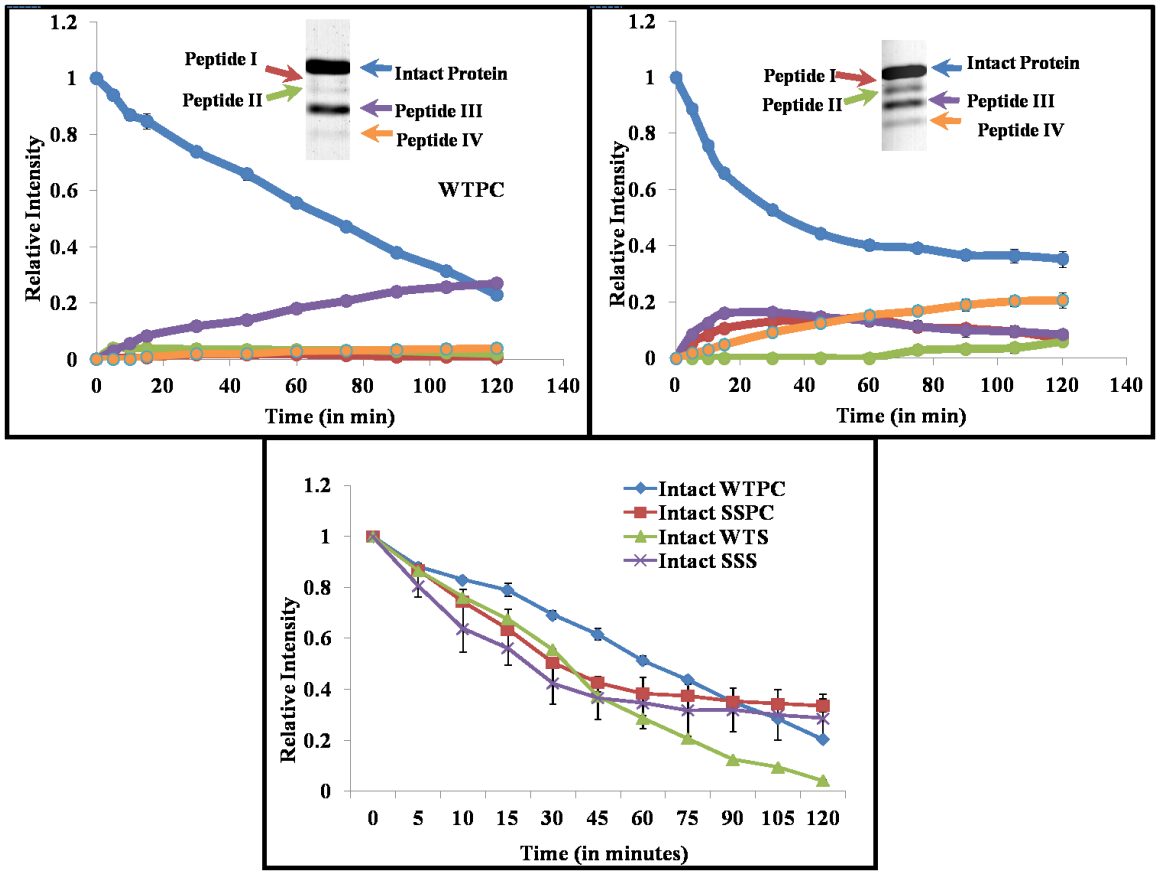


Figure 5 A). Proteolysis profile of WTPC. B). Proteolysis profile of SSPC. C) The plot shows the relative intensity of the disappearance of intact capsid protein (WTPC, WTS, SSPC, and SSS) over a period of 120 minutes. Samples were collected at each time point and run on an SDS-PAGE gels and the intensities of the bands were obtained by densitometric analysis using ImageJ.

Discussion

CCMV has been one of the most studied model systems for the past 40 years and yet we continue to discover something new in the system. Researchers have developed intricate systems using CCMV for a barrage of medical applications and yet our approach has brought forth the existence of two novel conformations of this "well understood" capsid. Our study has focused on characterizing the solution phase properties of WT and SS CCMV and the capsid conformational changes due to change in pH and Ca^{2+}

concentration. CCMV has been well studied and is considered a model system yet the solution phase dynamics have not yet been fully characterized. A premise behind this work is that pH changes and Ca^{2+} concentration affect the capsid dynamics, structure and stability in not just a concerted fashion but also individually extend their effects. These solution conditions were targeted by the described experiments and the results showed profound differences among the capsid conformations while helping us follow up and extend the work done by Bancroft et al (1). For example, the conformational change from the closed to the swollen form involves rigid body movements of the subunits around the quasi 3-fold axes leading to the formation of a 2nm pore. It has been generally agreed the the more fenestrated swollen form is less stable. The intertwining of the N-termini is attributed to the formation of the β-hexamer in the quasi 6-fold axes. The observed differences in capsid stability and dynamics are influenced by the conformational changes and the presence or absence of the extra bonds around the β-hexamer.

Thermal denaturation of intact capsids showed that the melting temperatures of the WT samples varied by more than 20°C though the difference for the SS samples was only by 8°C highlighting 1) the concerted effect of pH and Ca^{2+} in swelling 2) the stabilizing effect of the extra 660 bonds formed in the β-hexamer of the SS 3) the effect of subunit-subunit interactions in enhancing the global stability of the capsid. These results in conjunction with the association energy data (Table 1) obtained from VIPERdb clearly indicate that the enhanced capsid stability of the closed forms and of the SS compared to the WT is primarily due to the quasi 6-fold axes. The general trend of the DSF curves is smooth and states that there is a single melting transition that takes place. DSF curves is

smooth and states that there is a single melting transition that takes place. Thermal melting of multimeric proteins involves the simultaneous disruption of subunit-subunit interactions and the melting of the subunit. The single transitions seen in DSF indicate such behavior. The differences in thermal stability of samples also suggests that these are thermodynamically distinct particles.

The genetic material in CCMV has been found to interact with 13 specific residues in the capsid which imparts stability to the capsid (9). It is known from cryo-EM and pseudo-atomic models that the capsid swelling is maximum along the icosahedral and quasi 2-fold axes disrupting RNA-protein interactions while leaving the β-hexamer virtually intact. These conformational changes lead to a decrease in solution phase stability for the swollen forms. This decrease can be attributed to a concerted effect of the increased pH and absence of Ca^{2+}. The effect of pH or Ca^{2+} alone is seen with WTPS/SSPS and WTPC/SSPC samples. The change in melting temperatures is insignificant in the case of pseudo-swollen samples while the change is quite drastic with the pseudo-closed samples. These observations led us to believe that pH is the major effector in the structural transitions while Ca^{2+} plays a secondary role helping in amino acid charge neutralization.

Information obtained from size-exclusion chromatography clarified, strengthened and extended the results of DSF. The tandem column setup clearly resolved all four forms of the viruses. The lower pH induces deprotonation of the metal binding aminoacids though the pH 4.8, being closer to the pK values of the side chains, induces only partial/transient deprotonation. This deprotonation aids the formation of a salt bridge using Ca^{2+} as the metal ion hence neutralizing the charges and keeping the capsid in a stable, closed

conformation. When the Ca^{2+} is chelated out with EDTA, these partial charges are exposed to each other causing weak repulsions among the metal binding residues. This causes an

Table 1. Subunit contact energies as calculated by VIPER (virus particle explorer).

Symmetry axis	Association Energy(kcal/mol)	Buried Surface Area($Å^2$)
Icosahedral 2-fold	-69.9	3218.5
Quasi 2-fold	-69.9	3216.2
Quasi 6-fold	-48.6	2404.3
Quasi 6-fold	-48.3	2390.7
Icosahedral 5-fold	-23.2	1260.4
Symmetry axis	Association Energy(kcal/mol)	Buried Surface Area($Å^2$)
Icosahedral 2-fold	-70.0	3243.4
Quasi 2-fold	-69.9	3186.2
Quasi 6-fold	-53.3	2606.9
Quasi 6-fold	-50.6	2520.6
Icosahedral 5-fold	-27.4	1425.2

incomplete swelling of the capsid. On the other hand, at pH 7.15, the metal binding residues are completely deprotonated and the presence/absence of Ca2+ has a more profound effect on swelling. This is clearly seen with earlier elution times and greater separation between the swollen and the pseudo-closed forms compared to the closed and the pseudo-swollen forms.

CCMV genome is divided unequally into 3 structurally identical particles and all 3 particles are needed for a successful infection. Except for the study that identified the 3 particles that are needed for infection, there are no studies that have tried to characterize these particles. What we see with the swollen forms may imply differential swelling of these 3 different particles. The swollen form of the SS shows an almost discernible smaller front peak indicating at least two sub-populations. Finally, the overall change in the hydrodynamic size of the SS capsid is approximately 40% lesser than the WT. This could imply that the extra bonds in the β-hexamer of the SS influences the interactions in the icosahedral and quasi 2-fold axes and hence prevent the capsid from swelling as much as the WT.

Global conformational changes in the CCMV capsid are caused by local rigid body movements in the subunits. The dynamics involved in such movements have been briefly documented before using mass-spec limited proteolysis (10). As an extension of this work, conformation dependent change in dynamics were explored by us using Hydrogen Deuterium exchange experiments. We were specifically interested in the pseudo-closed and swollen forms as they were the ones that showed the maximum differences with respect to DSF and size-exclusion. The results obtained were congruent with the other experiments and showed that the exchange rates and therefore the flexibility of the WT forms (pseudo-closed and swollen) were much higher than that of their corresponding SS forms. The results from the initial timepoint (0.5minutes) also indicate that the WT samples are much more accessible to deuterium compared to the SS. Similar studies done with Brome mosaic virus (family: Bromoviridae) showed that the deuterium exchange after capsid swelling

localized to the quasi-three fold axes implying the weakening of interactions around here. We see a similar trend in deuterium-exchange with swelling of the CCMV capsid.

Probing the dynamics using HDX-MS showed us that there are very important differences between the WT and the SS forms. Such differences could be teased out with a targeted approach using Limited Proteolysis. The cleavage sites from the proteolysis reaction were residues, R15, R23, R26 and K42 on the N-terminus of the CCMV subunit(10). One hypothesis would be that secondary cleavage took place at R26 on peptide II resulting in increase of peptide III intensity (residues 27-190). Peptide III appeared almost immediately and its concentration increased linearly with time till the end of the proteolysis. Residues 1-26 are predominantly basic and are expected to interact with the RNA. Dominance of cleavage at R26 tells us that this stretch of the protein is very dynamic and was exposed to Trypsin (a 24 kDa protein) which is present only outside the capsid. This is also proven by the fact that residues 1-26 do not have an electron density in the crystal structure. This stretch is also known to be very basic and interacts with the RNA (12, 14). The intensity of peptide IV increased very slowly over the course of the reaction. Peptide IV is mapped to residues 43-190. This would imply that the R26 is much more accessible than the K42 site. The K42 is an ordered residue in the crystal structure of CCMV whereas the R26 is in the dynamic region (9) .

The time-course proteolysis of the SS-CCMV had different kinetics. The rate of appearance of all the four prominent peptides was much higher compared to the WT-CCMV. Peptide III appeared first immediately followed by Peptide I. After the initial rise, the relative abundances of both, peptide I and III, reduced to half of its maximal level.

Peptide IV showed an almost linear increase till the end of the reaction where it started to taper off.

Compared to WT-CCMV, SS-CCMV has 660 extra bonds per capsid, localized around the β-hexamer. One of the reasons for these extra bonds is that the residue R26 is ordered in the B and C subunits of the SS-CCMV structure and interacts with R42. The B and C subunits also form the β-hexamer at the quasi six-fold axis. Peptide I and III map to residues R15 and R26 respectively. The increase in abundance of peptide III was exponential and not linear as compared to the WT-CCMV. Peptide I also followed a similar rise in abundance. R26 cleavages may primarily occur at the five-fold axes. The R15 cleavage could be occurring at both the five-fold and the quasi six-fold axes because N-termini of the B and C subunits are tethered at R26 exposing R15 for cleavage. The profile could be convoluted because of secondary cleavages occurring simultaneously though this could explain the linear increase of peptide IV with gradual decrease of peptide I and III. The proteolytic susceptibility of the WTS form was clearly evident while the SSS form seemed almost as resistant to protease as the SSPC. This trend agrees with our size-exclusion and DSF studies clearly showing that the SSS swollen capsid dynamics are much more restricted compared to the WTS.

Our investigations in this particular study have shown that remarkable differences are still hidden and yet to be discovered in a well-studied model system like CCMV. Thorough investigation was necessary to tease out these differences that existed not only among the WT and its mutant form but also between the different conformations of the virus. Previous studies have been able to show the existence of these conformations though

further studies to bring out the differences were never conducted. CCMV swelling has intrigued structural biologists and virologists alike for decades. The data presented here adds a new dimension to the thoroughly studied CCMV model system. These results also emphasize the need for a multi-disciplinary approach towards understanding in general capsid integrity, conformational changes due to solution conditions and mechanical and thermal stability which in turn have direct implications for the development of bio-inspired nanomaterials(4), gene therapy(11) and specifically enzyme based nanoreactors in the case of CCMV(3).

Abbreviations used – CCMV, Cowpea chlorotic mottle virus; WTC, wildtype closed; WTPS, wildtype pseudo-swollen; WTPC, wildtype pseudo-closed; WTS, wildtype swollen; SSC, saltstable closed; SSPS, saltstable pseudo-swollen; SSPC, saltstable pseudo-closed; SSS, saltstable swollen; QCM-D, Quartz crystal microbalance with dissipation technology (QCM-D); DSF, Differential scanning fluorimetry;

Literature Cited

1. Bancroft JB, Hills GJ, Markham R. 1967. A study of the self-assembly process in a small spherical virus. Formation of organized structures from protein subunits in vitro. Virology 31:354–79.

2. Burns K, Mukherjee S, Keef T, Johnson JM, Zlotnick A. 2010. Altering the Energy Landscape of Virus Self-Assembly to Generate Kinetically Trapped Nanoparticles 439–442.

3. Comellas-Aragonès M, Engelkamp H, Claessen VI, Sommerdijk NAJM, Rowan AE, Christianen PCM, Maan JC, Verduin BJM, Cornelissen JJLM, Nolte RJM. 2007. A virus-based single-enzyme nanoreactor. Nature nanotechnology 2:635–9.

4. Douglas T, Young M. 1998. Host–guest encapsulation of materials by assembled virus protein cages 393:1996–1999.

5. Endres D, Zlotnick A. 2002. Model-Based Analysis of Assembly Kinetics for Virus Capsids or Other Spherical Polymers. Biophysical Journal 83:1217–30.

6. Liepold L, Anderson S, Willits D, Oltrogge L, Frank J a, Douglas T, Young M. 2007. Viral capsids as MRI contrast agents. Magnetic resonance in medicine : official journal of the Society of Magnetic Resonance in Medicine / Society of Magnetic Resonance in Medicine 58:871–9.

7. Rayaprolu V, Manning BM, Douglas T, Bothner B. 2010. Virus particles as active nanomaterials that can rapidly change their viscoelastic properties in response to dilute solutions. Soft Matter 6:5286–88.

8. Singh P, Destito G, Schneemann A, Manchester M. 2006. Canine parvovirus-like particles, a novel nanomaterial for tumor targeting. Journal of nanobiotechnology 4:2.

9. Speir J a, Munshi S, Wang G, Baker TS, Johnson JE. 1995. Structures of the native and swollen forms of cowpea chlorotic mottle virus determined by X-ray crystallography and cryo-electron microscopy. Structure (London, England : 1993) 3:63–78.

10. Speir JA, Bothner B, Qu C, Willits DA, Young MJ, Johnson JE. 2006. Enhanced Local Symmetry Interactions Globally Stabilize a Mutant Virus Capsid That Maintains Infectivity and Capsid Dynamics 80:3582–3591.

11. Van Vliet KM, Blouin V, Brument N, Agbandje-McKenna M, Snyder RO. 2008. The role of the adeno-associated virus capsid in gene transfer., p. 51–91. *In* Jain, KK (ed.), Methods in Molecular Biology. Humana Press.

12. Vriend G, Verduin BJ, Hemminga M a. 1986. Role of the N-terminal part of the coat protein in the assembly of cowpea chlorotic mottle virus. A 500 MHz proton nuclear magnetic resonance study and structural calculations. Journal of molecular biology 191:453–60.

13. Wang Q, Lin T, Tang L, Johnson JE, Finn MG. 2002. Icosahedral virus particles as addressable nanoscale building blocks. Angewandte Chemie (International ed. in English) 41:459–62.

CHAPTER 5

CONCLUDING REMARKS

Ever since the first structure of the virus was solved, we have known viruses as these static, rigid, robust molecules whose primary function was to protect and transfer the genome from one host to another at the expense of their outer shell. As science and scientific curiosity progressed, we have been able to develop technologies which have been able to show us the stochastic nature of these virus particles. The focus of this thesis has been to study, using various biophysical approaches, the dynamic nature of viruses. The two viruses under study, CCMV and AAV, belong to two different classes of viruses and infects completely different hosts. CCMV, a plant virus, is not expected to be neither very dynamic nor very stable though the results obtained here prove otherwise. AAV, an animal virus, impresses with its high stability and diversity even with very little sequence differences. Large scale quaternary changes and small scale local fluctuations have been attributed to such variability and functionality of capsids. The systems described here have tremendous implications in the development of many biomedical applications.

LITERATURE CITED

1. Bamford DH, Grimes JM, Stuart DI. 2005. What does structure tell us about virus evolution? Current opinion in structural biology 15:655–63.

2. Harrison SC. 1969. Structure of tomato bushy stunt virus. Journal of Molecular Biology 42:457–483.

3. Rossmann MG, Arnold E, Erickson JW, Frankenberger EA, Griffith JP, Hecht H-J, Johnson JE, Kamer G, Luo M, Mosser AG, Rueckert RR, Sherry B, Vriend G. 1985. Structure of a human common cold virus and functional relationship to other picornaviruses. Nature 317:145–153.

4. Veesler D, Quispe J, Grigorieff N, Potter CS, Carragher B, Johnson JE. 2012. Maturation in action: CryoEM study of a viral capsid caught during expansion. Structure (London, England : 1993) 20:1384–90.

5. Kamerzell TJ, Middaugh CR. 2008. The complex inter-relationships between protein flexibility and stability. Journal of Pharmaceutical Sciences 97:3494–3517.

6. M Karplus and J. A. McCammon. 1983. Dynamics of Proteins: Elements and Function. Annual review of biochemistry 53:263–300.

7. Zaccai G. 2000. How Soft Is a Protein? A Protein Dynamics Force Constant Measured by Neutron Scattering. Science 288:1604–1607.

8. McCammon JA. 1984. Protein dynamics. Reports on Progress in Physics 47:1–46.

9. Ramachandran G. 1968. Ramachandran plot for multiple structures. Advances in protein chemistryrotein chemistry 23:283–437.

10. Pace CN, Laurents D V. 1989. A new method for determining the heat capacity change for protein folding. Biochemistry 28:2520–5.

11. Ponnuswamy PK, Gromiha MM. 1994. On the Conformational Stability of Folded Proteins. Journal of Theoretical Biology 166:63–74.

12. Murphy KP. 2001. Stabilization of protein structure. Methods in molecular biology (Clifton, N.J.) 168:1–16.

13. Sanchez-Ruiz JM. 1992. Theoretical analysis of Lumry-Eyring models in differential scanning calorimetry. Biophysical Journal 61:921–935.

14. Sanchez-Ruiz JM. 2010. Protein kinetic stability. Biophysical chemistry 148:1–15.

15. Zlotnick A. 2005. Theoretical aspects of virus capsid assembly. Journal of molecular recognition : JMR 18:479–90.

16. Caspar DLD, Klug A. 1962. Physical principles in the construction of regular viruses. Cold Spring Harbor Symposia on Quantitative Biology 27th:1–24.

17. Bothner B, Hilmer JK. 2010. Probing virus capsids in solution. Royal Society of Chemistry, Cambridge.

18. Rizzuto CD. 1998. A Conserved HIV gp120 Glycoprotein Structure Involved in Chemokine Receptor Binding. Science 280:1949–1953.

19. Levy HC, Bowman VD, Govindasamy L, McKenna R, Nash K, Warrington K, Chen W, Muzyczka N, Yan X, Baker TS, Agbandje-McKenna M. 2009. Heparin binding induces conformational changes in Adeno-associated virus serotype 2. Journal of Structural Biology 165:146.

20. Weiss RA. 2008. HIV receptors and cellular tropism. IUBMB life 53:201–5.

21. Agbandje-McKenna M, Kleinschmidt J. 2011. AAV Capsid Structure and Cell Interactions, p. 47–92. *In* Snyder, RO, Moullier, P (eds.), Methods in Molecular Biology. Humana Press.

22. Cotmore SF, Tattersall P. 2007. Parvoviral host range and cell entry mechanisms. Advances in virus research 70:183–232.

23. Duda RL, Hempel J, Michel H, Shabanowitz J, Hunt D, Hendrix RW. 1995. Structural transitions during bacteriophage HK97 head assembly. Journal of Molecular Biology 247:618–635.

24. Hilmer JK, Zlotnick A, Bothner B. 2008. Conformational Equilibria and Rates of Localized Motion within Hepatitis B Virus Capsids. Journal of Molecular Biology 375:581–94.

25. Gertsman I, Gan L, Guttman M, Lee K, Speir JA, Duda RL, Hendrix RW, Komives EA, Johnson JE. 2009. An unexpected twist in viral capsid maturation. Nature 458:646–50.

26. Gan L, Speir JA, Conway JF, Lander G, Cheng N, Firek BA, Hendrix RW, Duda RL, Liljas L, Johnson JE. 2006. Capsid Conformational Sampling in HK97 Maturation Visualized by X-Ray Crystallography and Cryo-EM. Structure 14:1655–65.

27. Gertsman I, Fu C-Y, Huang R, Komives EA, Johnson JE. 2010. Critical salt bridges guide capsid assembly, stability, and maturation behavior in bacteriophage HK97. Molecular & cellular proteomics : MCP 9:1752–63.

28. Parent KN, Khayat R, Tu LH, Suhanovsky MM, Cortines JR, Teschke CM, Johnson JE, Baker TS. 2010. P22 coat protein structures reveal a novel mechanism for capsid maturation: stability without auxiliary proteins or chemical crosslinks. Structure (London, England : 1993) 18:390–401.

29. Morais MC, Koti JS, Bowman VD, Reyes-Aldrete E, Anderson DL, Rossmann MG. 2008. Defining molecular and domain boundaries in the bacteriophage phi29 DNA packaging motor. Structure (London, England : 1993) 16:1267–74.

30. Ionel A, Velázquez-Muriel JA, Luque D, Cuervo A, Castón JR, Valpuesta JM, Martín-Benito J, Carrascosa JL. 2011. Molecular rearrangements involved in the capsid shell maturation of bacteriophage T7. The Journal of biological chemistry 286:234–42.

31. Helgstrand C, Munshi S, Johnson JE, Liljas L. 2004. The refined structure of Nudaurelia capensis omega virus reveals control elements for a T = 4 capsid maturation. Virology 318:192–203.

32. Munshi S, Liljas L, Cavarelli J, Bomu W, McKinney B, Reddy V, Johnson JE. 1996. The 2.8 A structure of a T = 4 animal virus and its implications for membrane translocation of RNA. Journal of molecular biology 261:1–10.

33. Canady MA, Tihova M, Hanzlik TN, Johnson JE, Yeager M. 2000. Large conformational changes in the maturation of a simple RNA virus, nudaurelia capensis omega virus (NomegaV). Journal of molecular biology 299:573–84.

34. Bothner B, Taylor D, Jun B, Lee KK, Siuzdak G, Schlutz CP, Johnson JE. 2005. Maturation of a tetravirus capsid alters the dynamic properties and creates a metastable complex. Virology 334:17–27.

35. Janshoff A, Bong DT, Steinem C, Johnson JE, Ghadiri MR. 1999. An animal virus-derived peptide switches membrane morphology: possible relevance to nodaviral transfection processes. Biochemistry 38:5328–36.

36. Taylor DJ, Krishna NK, Canady MA, Schneemann A, Johnson JE. 2002. Large-scale, pH-dependent, quaternary structure changes in an RNA virus capsid are reversible in the absence of subunit autoproteolysis. Journal of virology 76:9972–80.

37. Lewis JK, Bothner B, Smith TJ, Siuzdak G. 1998. Antiviral agent blocks breathing of the common cold virus. Proceedings of the National Academy of Sciences 95:6774–6778.

38. Bothner B, Dong XF, Bibbs L, Johnson JE, Siuzdak G. 1998. Evidence of Viral Capsid Dynamics Using Limited Proteolysis and Mass Spectrometry. Journal of Biological Chemistry 273:673–676.

39. Fox MP, Otto MJ, McKinlay MA. 1986. Prevention of rhinovirus and poliovirus uncoating by WIN 51711, a new antiviral drug. Antimicrobial agents and chemotherapy 30:110–6.

40. Rombaut B, Andries K, Boeyé A. 1991. A comparison of WIN 51711 and R 78206 as stabilizers of poliovirus virions and procapsids. The Journal of general virology 72 (Pt 9):2153–7.

41. Gruenberger M, Pevear D, Diana GD, Kuechler E, Blaas D. 1991. Stabilization of human rhinovirus serotype 2 against pH-induced conformational change by antiviral compounds. The Journal of general virology 72 (Pt 2):431–3.

42. Speir JA, Munshi S, Wang G, Baker TS, Johnson JE. 1995. Structures of the native and swollen forms of cowpea chlorotic mottle virus determined by X-ray crystallography and cryo-electron microscopy. Structure (London, England : 1993) 3:63–78.

43. Speir JA, Bothner B, Qu C, Willits DA, Young MJ, Johnson JE. 2006. Enhanced Local Symmetry Interactions Globally Stabilize a Mutant Virus Capsid That Maintains Infectivity and Capsid Dynamics 80:3582–3591.

44. Wang L, Lane LC, Smith DL. 2001. Detecting structural changes in viral capsids by hydrogen exchange and mass spectrometry. Protein science : a publication of the Protein Society 10:1234–43.

45. G Vriend,M.A. Hemminga,B.J.M. Verduin TJS. 1982. Swelling of Cowpea chlorotic mottle virus studied by proton NMR. FEBS Lett. 146:319–321.

46. Krell T, Manin C, Nicolaï M-C, Pierre-Justin C, Bérard Y, Brass O, Gérentes L, Leung-Tack P, Chevalier M. 2005. Characterization of different strains of poliovirus and influenza virus by differential scanning calorimetry. Biotechnology and applied biochemistry 41:241–6.

47. Shnyrov VL, Zhadan GG, Cobaleda C, Sagrera A, Muñoz-Barroso I, Villar E. 1997. A differential scanning calorimetric study of Newcastle disease virus:

identification of proteins involved in thermal transitions. Archives of biochemistry and biophysics 341:89–97.

48. Jeembaeva M, Jönsson B, Castelnovo M, Evilevitch A. 2010. DNA heats up: energetics of genome ejection from phage revealed by isothermal titration calorimetry. Journal of molecular biology 395:1079–87.

49. Zlotnick A, Aldrich R, Johnson JM, Ceres P, Young MJ. 2000. Mechanism of capsid assembly for an icosahedral plant virus. Virology 277:450–6.

50. Yi G, Vaughan RC, Yarbrough I, Dharmaiah S, Kao CC. 2009. RNA binding by the brome mosaic virus capsid protein and the regulation of viral RNA accumulation. Journal of Molecular Biology 391:314–26.

51. Ni P, Wang Z, Ma X, Das NC, Sokol P, Chiu W, Dragnea B, Hagan M, Kao CC. 2012. An examination of the electrostatic interactions between the N-terminal tail of the Brome Mosaic Virus coat protein and encapsidated RNAs. Journal of molecular biology 419:284–300.

52. Ode H, Nakashima M, Kitamura S, Sugiura W, Sato H. 2012. Molecular dynamics simulation in virus research. Frontiers in microbiology 3:258.

53. Kronenberg S, Kleinschmidt J a, Böttcher B, Kronenberg J. A. Kleinschmidt, and B. Bottcher S, Kronenberg S, Kleinschmidt J a, Böttcher B, Kronenberg J. A. Kleinschmidt, and B. Bottcher S. 2001. Electron cryo-microscopy and image reconstruction of adeno-associated virus type 2 empty capsids. EMBO Rep 2:997–1002.

54. Vriend G, Verduin BJ, Hemminga M a. 1986. Role of the N-terminal part of the coat protein in the assembly of cowpea chlorotic mottle virus. A 500 MHz proton nuclear magnetic resonance study and structural calculations. Journal of molecular biology 191:453–60.

55. Byeon I-JL, Meng X, Jung J, Zhao G, Yang R, Ahn J, Shi J, Concel J, Aiken C, Zhang P, Gronenborn AM. 2009. Structural convergence between Cryo-EM and NMR reveals intersubunit interactions critical for HIV-1 capsid function. Cell 139:780–90.

56. Tsutsui Y, Wintrode PL. 2007. Hydrogen/deuterium exchange-mass spectrometry: a powerful tool for probing protein structure, dynamics and interactions. Current medicinal chemistry 14:2344–58.

57. Douglas T, Young M. 1998. Host–guest encapsulation of materials by assembled virus protein cages 393:1996–1999.

58. Wang Q, Lin T, Tang L, Johnson JE, Finn MG. 2002. Icosahedral virus particles as addressable nanoscale building blocks. Angewandte Chemie (International ed. in English) 41:459–62.

59. Singh P, Destito G, Schneemann A, Manchester M. 2006. Canine parvovirus-like particles, a novel nanomaterial for tumor targeting. Journal of nanobiotechnology 4:2.

60. Liepold L, Anderson S, Willits D, Oltrogge L, Frank J a, Douglas T, Young M. 2007. Viral capsids as MRI contrast agents. Magnetic resonance in medicine : official journal of the Society of Magnetic Resonance in Medicine / Society of Magnetic Resonance in Medicine 58:871–9.

61. Miller R a, Presley AD, Francis MB. 2007. Self-assembling light-harvesting systems from synthetically modified tobacco mosaic virus coat proteins. Journal of the American Chemical Society 129:3104–9.

62. Sun J, DuFort C, Daniel M-C, Murali A, Chen C, Gopinath K, Stein B, De M, Rotello VM, Holzenburg A, Kao CC, Dragnea B. 2007. Core-controlled polymorphism in virus-like particles. Proceedings of the National Academy of Sciences of the United States of America 104:1354–9.

63. Klem MT, Young M, Douglas T. 2008. Biomimetic synthesis of β-TiO2 inside a viral capsid. Journal of Materials Chemistry 18:3821.

64. Liu H, Qu C, Johnson JE, Case D a. 2003. Pseudo-atomic models of swollen CCMV from cryo-electron microscopy data. Journal of Structural Biology 142:356–363.

65. Liepold LO, Revis J, Allen M, Oltrogge L, Young M, Douglas T. 2005. Structural transitions in Cowpea chlorotic mottle virus (CCMV). Physical biology 2:S166–72.

66. Uchida M, Klem MT, Allen M, Suci P, Flenniken M, Gillitzer E, Varpness Z, Liepold LO, Young M, Douglas T. 2007. Biological Containers: Protein Cages as Multifunctional Nanoplatforms. Advanced Materials 19:1025–1042.

67. Pettersen EF, Goddard TD, Huang CC, Couch GS, Greenblatt DM, Meng EC, Ferrin TE. 2004. UCSF Chimera—A visualization system for exploratory research and analysis. Journal of Computational Chemistry 25:1605.

68. Lubarsky G V, Davidson MR, Bradley RH. 2007. Hydration-dehydration of adsorbed protein films studied by AFM and QCM-D. Biosensors & bioelectronics 22:1275–81.

69. Mecea VM. 2005. From Quartz Crystal Microbalance to Fundamental Principles of Mass Measurements. Analytical Letters 38:753–767.

70. Dutta AK, Belfort G. 2007. Adsorbed gels versus brushes: viscoelastic differences. Langmuir : the ACS journal of surfaces and colloids 23:3088–94.

71. Michel JP, Ivanovska IL, Gibbons MM, Klug WS, Knobler CM, Wuite GJL, Schmidt CF. 2006. Nanoindentation studies of full and empty viral capsids and the effects of capsid protein mutations.

72. Evilevitch A, Fang LT, Yoffe AM, Castelnovo M, Rau DC, Parsegian VA, Gelbart WM, Knobler CM. 2008. Effects of salt concentrations and bending energy on the extent of ejection of phage genomes. Biophysical journal 94:1110–20.

73. Klug W, Bruinsma R, Michel J-P, Knobler C, Ivanovska I, Schmidt C, Wuite G. 2006. Failure of Viral Shells. Physical Review Letters 97:1–4.

74. Suci P a, Klem MT, Douglas T, Young M. 2005. Influence of electrostatic interactions on the surface adsorption of a viral protein cage. Langmuir : the ACS journal of surfaces and colloids 21:8686–93.

75. Patel AR, Frank CW. 2006. Quantitative analysis of tethered vesicle assemblies by quartz crystal microbalance with dissipation monitoring: Binding dynamics and bound water content. Langmuir : the ACS journal of surfaces and colloids 22:7587–99.

76. Höök F, Kasemo B, Nylander T, Fant C, Sott K, Elwing H. 2001. Variations in Coupled Water, Viscoelastic Properties, and Film Thickness of a Mefp-1 Protein Film during Adsorption and Cross-Linking: A Quartz Crystal Microbalance with Dissipation Monitoring, Ellipsometry, and Surface Plasmon Resonance Study. Analytical Chemistry 73:5796–5804.

77. Ceres P, Zlotnick A. 2002. Articles Weak Protein-Protein Interactions Are Sufficient To Drive Assembly of Hepatitis 4:11525–11531.

78. Ivanovska IL, De Pablo PJ, Ibarra B, Sgalari G, MacKintosh FC, Carrascosa JL, Schmidt CF, Wuite GJL. 2004. Bacteriophage capsids: tough nanoshells with complex elastic properties. Proceedings of the National Academy of Sciences of the United States of America 101:7600–5.

79. Halder S, Ng R, Agbandje-McKenna M. 2012. Parvoviruses: structure and infection. Future Virology 7:253–78.

80. Muzyczka N, Berns KI. 2001. Parvoviridae: The viruses and their replication, p. 2327–60. *In* Howley, DMK and PM (ed.), Fields Virology, 4th ed. Lippincott Williams and Wilkins, New York.

81. Agbandje-McKenna M, Chapman MS. 2006. Correlating structure with function in the viral capsid, p. 125–39. *In* Kerr, JR, Cotmore, SF, Bloom, ME, Linden, R., Parrish, CR (eds.), Parvoviruses. Hodder Arnold Publication.

82. Gao G, Vandenberghe LH, Alvira MR, Lu Y, Calcedo R, Zhou X, Wilson JM. 2004. Clades of Adeno-Associated Viruses Are Widely Disseminated in Human Tissues. Journal of Virology 78:6381–88.

83. Gao G-P, Alvira MR, Wang L, Calcedo R, Johnston J, Wilson JM. 2002. Novel adeno-associated viruses from rhesus monkeys as vectors for human gene therapy. Proceedings of the National Academy of Sciences 99:11854–59.

84. Mori S, Wang L, Takeuchi T, Kanda T. 2004. Two novel adeno-associated viruses from cynomolgus monkey: pseudotyping characterization of capsid protein. Virology 330:375–83.

85. Sanlioglu S, Benson PK, Yang J, Atkinson EM, Reynolds T, Engelhardt JF. 2000. Endocytosis and Nuclear Trafficking of Adeno-Associated Virus Type 2 Are Controlled by Rac1 and Phosphatidylinositol-3 Kinase Activation. Journal of Virology 74:9184–96.

86. Schmidt M, Voutetakis A, Afione S, Zheng C, Mandikian D, Chiorini JA. 2008. Adeno-Associated Virus Type 12 (AAV12): a Novel AAV Serotype with Sialic Acid- and Heparan Sulfate Proteoglycan-Independent Transduction Activity. Journal of Virology 82:1399–1406.

87. Van Vliet KM, Blouin V, Brument N, Agbandje-McKenna M, Snyder RO, Kim M. Van Vliet Nicole Brument, Mavis Agbandje-McKenna, Richard O. Snyder VB. 2008. The role of the adeno-associated virus capsid in gene transfer. Methods in molecular biology (Clifton, N.J.) 437:51–91.

88. Mingozzi F, High KA. 2011. Therapeutic in vivo gene transfer for genetic disease using AAV: progress and challenges. Nature Review, Genetics 12:341–55.

89. Maguire AM, Simonelli F, Pierce EA, Pugh EN, Mingozzi F, Bennicelli J, Banfi S, Marshall KA, Testa F, Surace EM, Rossi S, Lyubarsky A, Arruda VR, Konkle B, Stone E, Sun J, Jacobs J, Dell'Osso L, Hertle R, Ma J, Redmond TM, Zhu X, Hauck B, Zelenaia O, Shindler KS, Maguire MG, Wright JF, Volpe NJ, McDonnell JW, Auricchio A, High KA, Bennett J. 2008. Safety and Efficacy of

Gene Transfer for Leber's Congenital Amaurosis. New England Journal of Medicine 358:2240–48.

90. Chao H, Liu Y, Rabinowitz J, Li C, Samulski RJ, Walsh CE. 2000. Several Log Increase in Therapeutic Transgene Delivery by Distinct Adeno-Associated Viral Serotype Vectors. Molecular Therapy 2:619.

91. Davidson BL, Stein CS, Heth JA, Kotin RM, Derksen TA, Zabner J, Ghodsi A, Chiorini JA, Martins I, Kotin RM, Derksen TA, Zabner J, Ghodsi A, Chiorini JA. 2000. Recombinant adeno-associated virus type 2, 4, and 5 vectors: Transduction of variant cell types and regions in the mammalian central nervous system. Proceedings of the National Academy of Sciences 97:3428–3432.

92. Kern A, Schmidt K, Leder C, Muller OJ, Wobus CE, Bettinger K, Von der Lieth CW, King JA, Kleinschmidt JA. 2003. Identification of a Heparin-Binding Motif on Adeno-Associated Virus Type 2 Capsids. Journal of Virology 77:11072–81.

93. Opie SR, Warrington JKH, Agbandje-McKenna M, Zolotukhin S, Muzyczka N. 2003. Identification of Amino Acid Residues in the Capsid Proteins of Adeno-Associated Virus Type 2 That Contribute to Heparan Sulfate Proteoglycan Binding. Journal of Virology 77:6995–7006.

94. Summerford C, Samulski RJ. 1998. Membrane-Associated Heparan Sulfate Proteoglycan Is a Receptor for Adeno-Associated Virus Type 2 Virions. Journal of Virology 72:1438–45.

95. Akache B, Grimm D, Pandey K, Yant SR, Xu H, Kay MA. 2006. The 37/67-Kilodalton Laminin Receptor Is a Receptor for Adeno-Associated Virus Serotypes 8, 2, 3, and 9. Journal of Virology 80:9831–36.

96. Asokan A, Hamra JB, Govindasamy L, Agbandje-McKenna M, Samulski RJ. 2006. Adeno-Associated Virus Type 2 Contains an Integrin α5β1 Binding Domain Essential for Viral Cell Entry. Journal of Virology 80:8961–69.

97. Kashiwakura Y, Tamayose K, Iwabuchi K, Hirai Y, Shimada T, Matsumoto K, Nakamura T, Watanabe M, Oshimi K, Daida H. 2005. Hepatocyte Growth Factor Receptor Is a Coreceptor for Adeno-Associated Virus Type 2 Infection. Journal of Virology 79:609–14.

98. Qing K, Mah C, Hansen J, Zhou S, Dwarki V, Srivastava A. 1999. Human fibroblast growth factor receptor 1 is a co-receptor for infection by adeno-associated virus 2. Nature Medicine 5:71–7.

99. Seisenberger G, Ried MU, EndreÃŸ T, BÃ¼ning H, Hallek M, BrÃ¤uchle C, Endreβ T, Büning H, Hallek M, Bräuchle C. 2001. Real-Time Single-Molecule Imaging of the Infection Pathway of an Adeno-Associated Virus. Science 294:1929–32.

100. Suikkanen S, Aaltonen T, Nevalainen M, Vālilehto O, Lindholm L, Vuento M, Vihinen-Ranta M. 2003. Exploitation of Microtubule Cytoskeleton and Dynein during Parvoviral Traffic toward the Nucleus. Journal of Virology 77:10270–79.

101. Summerford C, Bartlett JS, Samulski RJ. 1999. αVβ5 integrin: a co-receptor for adeno-associated virus type 2 infection. Nature Medicine 5:78–82.

102. Nonnenmacher M, Weber T. 2011. Adeno-Associated Virus 2 Infection Requires Endocytosis through the CLIC/GEEC Pathway. Cell Host & Microbe 10:563–76.

103. Lerch TF, Xie Q, Chapman MS. 2010. The structure of adeno-associated virus serotype 3B (AAV-3B): Insights into receptor binding and immune evasion. Virology 403:26–36.

104. Blackburn SD, Steadman RA, Johnson FB. 2006. Attachment of adeno-associated virus type 3H to fibroblast growth factor receptor 1. Archives of Virology 151:617.

105. Kaludov N, Brown KE, Walters RW, Zabner J, Chiorini JA. 2001. Adeno-Associated Virus Serotype 4 (AAV4) and AAV5 Both Require Sialic Acid Binding for Hemagglutination and Efficient Transduction but Differ in Sialic Acid Linkage Specificity. Journal of Virology 75:6884–93.

106. Wu Z, Miller E, Agbandje-McKenna M, Samulski RJ. 2006. Alpha2,3 and alpha2,6 N-linked sialic acids facilitate efficient binding and transduction by adeno-associated virus types 1 and 6. Journal of Virology 80:9093–103.

107. Walters RW, Yi SMP, Keshavjee S, Brown KE, Welsh MJ, Chiorini JA, Zabner J. 2001. Binding of Adeno-associated Virus Type 5 to 2,3-Linked Sialic Acid Is Required for Gene Transfer. Journal of Biological Chemistry 276:20610–16.

108. Pasquale G Di, Davidson BL, Stein CS, Martins I, Scudiero D, Monks A, Chiorini JA. 2003. Identification of PDGFR as a receptor for AAV-5 transduction. Nature Medicine 9:1306–12.

109. Shen S, Bryant KD, Brown SM, Randell SH, Asokan A. 2011. Terminal N-linked galactose is the primary receptor for adeno-associated virus 9. The Journal of Biological Chemistry 286:13532–40.

110. Sonntag F, Bleker S, Leuchs B, Fischer R, Kleinschmidt JA. 2006. Adeno-associated virus type 2 capsids with externalized VP1/VP2 trafficking domains are generated prior to passage through the cytoplasm and are maintained until uncoating occurs in the nucleus. Journal of Virology 80:11040–54.

111. Buller RM, Rose JA. 1978. Characterization of adenovirus-associated virus-induced polypeptides in KB cells. Journal of Virology 25:331–8.

112. Rose JA, Maizel J V, Inman JK, Shatkin AJ. 1971. Structural Proteins of Adenovirus-Associated Viruses. Journal of Virology 8:766–70.

113. Chapman MS, Agbandje-McKenna M. 2006. Atomic structure of viral particles, p. 107–23. *In* Kerr, JR, Cotmore, SF, Bloom, ME, Linden, R., Parrish, CR (eds.), Parvoviruses. Edward Arnold Ltd., New York.

114. Salganik M, Venkatakrishnan B, Bennett A, Lins B, Yarbrough J, Muzyczka N, Agbandje-McKenna M, McKenna R. 2012. Evidence for pH-dependent protease activity in the adeno-associated virus capsid. Journal of Virology 86:11877–85.

115. Van Vliet K, Blouin V, Agbandje-McKenna M, Snyder RO. 2006. Proteolytic mapping of the adeno-associated virus capsid. Mol Ther 14:809–21.

116. Popa-Wagner R, Porwal M, Kann M, Reuss M, Weimer M, Florin L, Kleinschmidt JA. 2012. Impact of VP1-specific protein sequence motifs on adeno-associated virus type 2 intracellular trafficking and nuclear entry. Journal of Virology 86:9163–74.

117. Bleker S, Pawlita M, Kleinschmidt JA, Kleinschmidt A. 2006. Impact of Capsid Conformation and Rep-Capsid Interactions on Adeno-Associated Virus Type 2 Genome Packaging Impact of Capsid Conformation and Rep-Capsid Interactions on Adeno-Associated Virus Type 2 Genome Packaging.

118. Govindasamy L, Padron E, McKenna R, Muzyczka N, Kaludov N, Chiorini JA, Agbandje-McKenna M. 2006. Structurally Mapping the Diverse Phenotype of Adeno-Associated Virus Serotype 4. Journal of Virology 80:11556–70.

119. Ng R, Govindasamy L, Gurda BL, McKenna R, Kozyreva OG, Samulski RJ, Parent KN, Baker TS, Agbandje-McKenna M. 2011. Structural Characterization of the Dual Glycan Binding Adeno-Associated Virus Serotype 6. Journal of Virology 84:12945–57.

120. Walters RW, Agbandje-McKenna M, Bowman VD, Moninger TO, Olson NH, Seiler M, Chiorini JA, Baker TS, Zabner J. 2004. Structure of Adeno-Associated Virus Serotype 5. Journal of Virology 78:3361–71.

121. Xie Q, Bu W, Bhatia S, Hare J, Somasundaram T, Azzi A, Chapman MS. 2002. The atomic structure of adeno-associated virus (AAV-2), a vector for human gene therapy. Proceedings of the National Academy of Sciences 99:10405–10.

122. Nam H-J, Lane MD, Padron E, Gurda B, McKenna R, Kohlbrenner E, Aslanidi G, Byrne B, Muzyczka N, Zolotukhin S, Agbandje-McKenna M. 2007. Structure of Adeno-Associated Virus Serotype 8, a Gene Therapy Vector. Journal of Virology 81:12260–71.

123. Wu Z, Asokan A, Samulski RJ. 2006. Adeno-associated virus serotypes: vector toolkit for human gene therapy. Molecular Therapy 14:316–27.

124. McCraw DM, O'Donnell JK, Taylor KA, Stagg SM, Chapman MS. Structure of adeno-associated virus-2 in complex with neutralizing monoclonal antibody A20. Virology 431:40–9.

125. DiMattia M, Govindasamy L, Levy HC, Gurda-Whitaker B, Kalina A, Kohlbrenner E, Chiorini JA, McKenna R, Muzyczka N, Zolotukhin S, Agbandje-McKenna M. 2005. Production, purification, crystallization and preliminary X-ray structural studies of adeno-associated virus serotype 5. Acta Crystallographica Section F 61:917–21.

126. Kohlbrenner E, Aslanidi G, Nash K, Shklyaev S, Campbell-Thompson M, Byrne BJ, Snyder RO, Muzyczka N, Warrington KH, Zolotukhin S. 2005. Successful Production of Pseudotyped rAAV Vectors Using a Modified Baculovirus Expression System. Molecular Therapy 12:1217–25.

127. Lane MD, Nam H-J, Padron E, Gurda-Whitaker B, Kohlbrenner E, Aslanidi G, Byrne B, McKenna R, Muzyczka N, Zolotukhin S, Agbandje-McKenna M. 2005. Production, purification, crystallization and preliminary X-ray analysis of adeno-associated virus serotype 8. Acta Crystallographica Section F 61:558–61.

128. Miller EB, Gurda-Whitaker B, Govindasamy L, McKenna R, Zolotukhin S, Muzyczka N, Agbandje-McKenna M. 2006. Production, purification and preliminary X-ray crystallographic studies of adeno-associated virus serotype 1. Acta Crystallographica Section F 62:1271–74.

129. Mah C, Fraites JTJ, Zolotukhin I, Song S, Flotte TR, Dobson J, Batich C, Byrne BJ. 2002. Improved Method of Recombinant AAV2 Delivery for Systemic Targeted Gene Therapy. Molecular Therapy 6:106–12.

130. Zolotukhin S, Potter M, Zolotukhin I, Sakai Y, Loiler S, Fraites TJ, Chiodo VA, Phillipsberg T, Muzyczka N, Hauswirth WW, Flotte TR, Byrne BJ, Snyder RO.

2002. Production and purification of serotype 1, 2, and 5 recombinant adeno-associated viral vectors. Methods 28:158–67.

131. Yeh AP, McMillan A, Stowell MHB. 2006. Rapid and simple protein-stability screens: application to membrane proteins. Acta Crystallographica Section D 62:451–457.

132. Bothner B, Schneemann A, Marshall D, Reddy V, Johnson JE, Siuzdak G. 1999. Crystallographically identical virus capsids display different properties in solution. Nature Structural & Molecular Biology 6:114–6.

133. Rayaprolu V, Manning BM, Douglas T, Bothner B. 2010. Virus particles as active nanomaterials that can rapidly change their viscoelastic properties in response to dilute solutions. Soft Matter 6:5286–88.

134. Belnap DM, Filman DJ, Trus BL, Cheng N, Booy FP, Conway JF, Curry S, Hiremath CN, Tsang SK, Steven AC, Hogle JM. 2000. Molecular Tectonic Model of Virus Structural Transitions: the Putative Cell Entry States of Poliovirus. Journal of Virology 74:1342–54.

135. Wu P, Xiao WW, Conlon T, Hughes J, Agbandje-McKenna M, Ferkol T, Flotte T, Muzyczka N. 2000. Mutational Analysis of the Adeno-Associated Virus Type 2 (AAV2) Capsid Gene and Construction of AAV2 Vectors with Altered Tropism. Journal of Virology 74:8635–8647.

136. Endres D, Zlotnick A. 2002. Model-Based Analysis of Assembly Kinetics for Virus Capsids or Other Spherical Polymers. Biophysical Journal 83:1217–30.

137. Zlotnick A. 2003. Are weak protein–protein interactions the general rule in capsid assembly? Virology 315:269–74.

138. Ausar SF, Foubert TR, Hudson MH, Vedvick TS, Middaugh CR. 2006. Conformational Stability and Disassembly of Norwalk Virus-like Particles. Journal of Biological Chemistry 281:19478–88.

139. Carrillo-Tripp M, Shepherd CM, Borelli IA, Venkataraman S, Lander G, Natarajan P, Johnson JE, Brooks CL, Reddy VS. 2009. VIPERdb2: an enhanced and web API enabled relational database for structural virology. Nucleic Acids Research 37:D436–42.

140. Park C, Marqusee S. 2004. Probing the High Energy States in Proteins by Proteolysis. Journal of Molecular Biology 343:1467–76.

141. Kronenberg S, Bo B, Lieth CW Von Der, Bleker S, BÃ¶ttcher B, Von der Lieth CW, Kleinschmidt Jã¼A. 2005. A Conformational Change in the Adeno-Associated Virus Type 2 Capsid Leads to the Exposure of Hidden VP1 N Termini. Journal of Virology 79:5296–5303.

142. Akache B, Grimm D, Shen X, Fuess S, Yant SR, Glazer DS, Park J, Kay MA. 2007. A Two-hybrid Screen Identifies Cathepsins B and L as Uncoating Factors for Adeno-associated Virus 2 and 8. Molecular Therapy 15:330–9.

143. Nelson CDS, Minkkinen E, Bergkvist M, Hoelzer K, Fisher M, Bothner B, Parrish CR. 2008. Detecting Small Changes and Additional Peptides in the Canine Parvovirus Capsid Structure. Journal of Virology 82:10397–10407.

144. Fricks CE, Hogle JM. 1990. Cell-induced conformational change in poliovirus: externalization of the amino terminus of VP1 is responsible for liposome binding. Journal of Virology 64:1934–45.

145. Fricks CE, Icenogle JP, Hogle JM. 1985. Trypsin sensitivity of the Sabin strain of type 1 poliovirus: cleavage sites in virions and related particles. Journal of Virology 54:856–59.

146. Golden JS, Harrison SC. 1982. Proteolytic dissection of turnip crinkle virus subunit in solution. Biochemistry 21:3862–6.

147. Johnson JE. 2003. Virus Particle Dynamics. Advances in Protein Chemistry 64:197–218.

148. Kowalski H, Maurer-Fogy I, Vriend G, Casari G, Beyer A, Blaas D. 1989. Trypsin sensitivity of several human rhinovirus serotypes in their low pH-induced conformation. Virology 171:611–4.

149. Horton N, Lewis M. 1992. Calculation of the free energy of association for protein complexes. Protein Science 1:169–81.

150. Vedadi M, Niesen FH, Allali-Hassani A, Fedorov OY, Finerty PJ, Wasney GA, Yeung R, Arrowsmith C, Ball LJ, Berglund H, Hui R, Marsden BD, Nordlund P, Sundstrom M, Weigelt J, Edwards AM. 2006. Chemical screening methods to identify ligands that promote protein stability, protein crystallization, and structure determination. Proceedings of the National Academy of Sciences 103:15835–40.

151. Nam H-J, Gurda BL, McKenna R, Potter M, Byrne B, Salganik M, Muzyczka N, Agbandje-McKenna M. 2011. Structural studies of adeno-associated virus serotype 8 capsid transitions associated with endosomal trafficking. Journal of virology 85:11791–9.

152. Bleker S, Sonntag F, Kleinschmidt A. 2005. Mutational Analysis of Narrow Pores at the Fivefold Symmetry Axes of Adeno-Associated Virus Type 2 Capsids Reveals a Dual Role in Genome Packaging and Activation of Phospholipase A2 Activity 79:2528–2540.

153. Lochrie MA, Tatsuno GP, Christie B, McDonnell JW, Zhou S, Surosky R, Pierce GF, Colosi P. 2006. Mutations on the External Surfaces of Adeno-Associated Virus Type 2 Capsids That Affect Transduction and Neutralization. Journal of Virology 80:821–34.

154. Skehel JJ, Bayley PM, Brown EB, Martin SR, Waterfield MD, White JM, Wilson IA, Wiley DC. 1982. Changes in the conformation of influenza virus hemagglutinin at the pH optimum of virus-mediated membrane fusion. Proceedings of the National Academy of Sciences 79:968–72.

155. Gurda BL, Raupp C, Popa-Wagner R, Naumer M, Olson NH, Ng R, McKenna R, Baker TS, Kleinschmidt JA, Agbandje-McKenna M. 2012. Mapping a Neutralizing Epitope onto the Capsid of Adeno-Associated Virus Serotype 8. Journal of Virology 86:7739–51.

156. Raupp C, Naumer M, Muller OJ, Gurda BL, Agbandje-McKenna M, Kleinschmidt JA. 2012. The threefold protrusions of AAV8 are involved in cell surface targeting as well as post attachment processing. Journal of Virology doi: 10.1128/ JVI.00209–12.

157. Farr GA, Tattersall P. 2004. A conserved leucine that constricts the pore through the capsid fivefold cylinder plays a central role in parvoviral infection. Virology 323:243–56.

158. Zádori Z, Szelei J, Lacoste M-CC, Li Y, Gariépy S, Raymond P, Allaire M, Nabi IR, Tijssen P. 2001. A Viral Phospholipase A2 Is Required for Parvovirus Infectivity. Developmental Cell 1:291–302.

159. Hauck B, Xiao W. 2003. Characterization of Tissue Tropism Determinants of Adeno-Associated Virus Type 1. Journal of Virology 77:2768–74.

160. Bancroft JB, Hills GJ, Markham R. 1967. A study of the self-assembly process in a small spherical virus. Formation of organized structures from protein subunits in vitro. Virology 31:354–79.

161. Burns K, Mukherjee S, Keef T, Johnson JM, Zlotnick A. 2010. Altering the Energy Landscape of Virus Self-Assembly to Generate Kinetically Trapped Nanoparticles 439–442.

162. Comellas-Aragonès M, Engelkamp H, Claessen VI, Sommerdijk NAJM, Rowan AE, Christianen PCM, Maan JC, Verduin BJM, Cornelissen JJLM, Nolte RJM. 2007. A virus-based single-enzyme nanoreactor. Nature nanotechnology 2:635–9.